

AD-A194 974

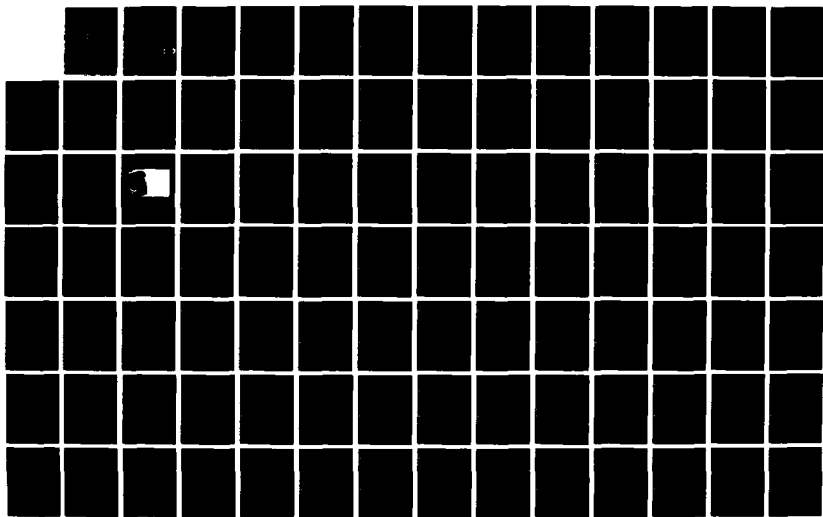
PHOTOINTERCALATING SEMICONDUCTOR/SOLID ELECTROLYTE  
JUNCTIONS FOR STORAGE A (U) ELTRON RESEARCH INC AURORA  
IL A F SAMMELLS 31 MAY 88 N00014-86-C-0128

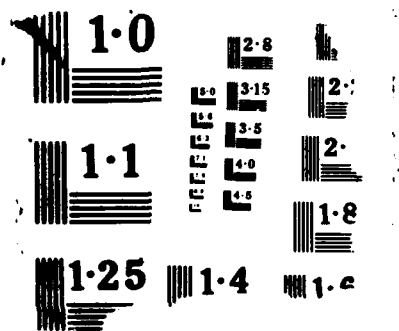
1/2

UNCLASSIFIED

F/G 7/6

NL





AD-A194 974

OFFICE OF NAVAL RESEARCH

FINAL REPORT

FOR

Contract N00014-86-C-0128 (SBIR PHASE II)

PHOTOINTERCALATING SEMICONDUCTOR/SOLID ELECTROLYTE  
JUNCTIONS FOR STORAGE AND CHEMICAL DETECTION

October 1, 1986 through May 31, 1988

Principal Investigator: Anthony F. Sammells

Eltron Research, Inc.  
4260 Westbrook Drive  
Aurora, Illinois 60504

Scientific Officer: Dr. Robert Nowak  
ONR

Reproduction in whole, or in part, is permitted for any purpose of the  
United States Government.

This document has been approved for public release and sale; its  
distribution is unlimited.

ELTRON RESEARCH INC.

DTIC FILE COPY

DTIC  
S JUL 06 1988 D  
H


4

# TABLE OF CONTENTS

	<u>Page</u>
Summary of the Phase II Effort	i
Status of Phase III Commercialization	iii
Publications Resulting From Work Performed During This Program	
Appendix A	Metal Intercalation Characteristics of n-HfS <sub>2</sub> Photoelectrodes in Non-Aqueous Electrolytes
Appendix B	Investigations at the n-HfS <sub>2</sub> /Non-Aqueous Electrolyte Interfacial Region
Appendix C	Impedance and Admittance Measurements at Inter- calated n-HfS <sub>2</sub> /Non-Aqueous Electrolyte Interface
Appendix D	Hafnium Disulfide Photoelectrochemistry in Aqueous Redox Electrolytes
Appendix E	Transient Laser-Induced Photoelectrochemical Measurements at p-InP/Solid Polymer Electrolyte Interface
Appendix F	Organophosphine-Transition Metal Complexes as Selective Surfaces for the Reversible Detection of Sulfur Dioxide on SAW Devices
Appendix G	Reversible SO <sub>2</sub> Detection Using a Multiple Reflecting Optical Waveguide Sensor



Accession For	
NTIS GRA&I	<input checked="" type="checkbox"/>
DTIC TAB	<input type="checkbox"/>
Unannounced	<input type="checkbox"/>
Justification	
By	
Distribution/	
Availability Codes	
Dist	Avail and/or Special
A-1	



## SUMMARY OF THE PHASE II EFFORT

The overall objective of this Phase II effort was to perform a scientific and technical characterization of photointercalating semiconductor/solid electrolyte junctions for photoelectrochemical energy storage, with emphasis being placed upon the Group IV dichalcogenides  $n\text{-HfS}_2$  and  $n\text{-ZrS}_2$  and their interface with solid polymer electrolytes. Also incorporated within the scope of this program was the application of insights gained towards novel approaches for chemical detection. Here, emphasis was placed upon Surface Acoustic Wave (SAW) and multiple-reflecting optical waveguide sensors for the reversible detection of  $\text{SO}_2$ . ←

Specific highlights of this program were as follows:

- Single crystal  $n\text{-HfS}_2$  photoelectrodes prepared by halogen vapor transport were investigated in  $0.1\text{M TBAPF}_6/\text{CH}_3\text{CN}$  electrolyte using both impedance and admittance spectroscopy techniques. The presence of frequency dependent capacitive and resistive elements in the equivalent circuit for  $n\text{-HfS}_2$ /electrolyte interface were evident. Capacitance effects at the interfacial region were found dependent upon the crystal orientation used, with that for defect free van der Waals surfaces being  $10^{-8}\text{F/cm}^2$ ; an order of magnitude lower than for  $n\text{-HfS}_2$  intercalation layers exposed to the electrolyte. High capacitance values were correlated with a high population of surface charges. Admittance spectroscopy analysis suggested the presence of interface states, possibly associated with the presence of resident surface oxides. Open-circuit photovoltages up to  $0.35\text{V}$  under  $100\text{mW/cm}^2$  illumination were observed for van der Waals surfaces, decreasing to  $0.16\text{V}$  as the population intercalating layers exposed to the electrolyte was increased.

- Capacitance, impedance and admittance studies were performed on single crystal  $n\text{-HfS}_2$  before and after copper intercalation from acetonitrile based electrolyte. The  $n\text{-HfS}_2$ /non-aqueous electrolyte interface was modelled by equivalent R-C circuits containing frequency dependent elements. Electrochemical intercalation by copper into  $n\text{-HfS}_2$  introduced Faradaic conductance effects. The composition of copper intercalated  $n\text{-HfS}_2$  in close proximity to the interfacial region was obtained assuming a diffusion coefficient for copper in  $n\text{-HfS}_2$  of  $10^{-8}\text{cm}^2/\text{sec}$ . The photoanode demonstrated apparent degeneracy for  $> 0.1$  moles of intercalated copper, suggesting that progressive electronic population of the  $n\text{-HfS}_2$  conduction band was occurring. This observation

limited the inherent capacity that could be achieved from this group of metal intercalating photoanodes when used at semiconductor/solid polymer electrolyte interface. Capacitance values for intercalated n-HfS<sub>2</sub> were of the order 10<sup>-6</sup> F/cm<sup>2</sup>.

- The van der Waal surface of single crystal n-HfS<sub>2</sub> was subjected to photoelectrochemical (PEC) investigation in aqueous electrolytes containing Fe<sup>3+</sup>/Fe<sup>2+</sup>, Fe(CN)<sub>6</sub><sup>3-</sup>/Fe(CN)<sub>6</sub><sup>4-</sup> and I<sub>3</sub><sup>-</sup>/I<sup>-</sup> redox species. Photoanodic current densities were limited by the number of photogenerated carriers, with highest rates (≈3mA/cm<sup>2</sup>) being found in the presence of Fe<sup>2+</sup> and I<sup>-</sup> ions. Flat-band potentials obtained from Mott-Schottky plots were shifted to negative values by 55.9mV per pH unit over the pH range 0-7, suggesting the possible presence of oxides on the n-HfS<sub>2</sub> surface. Slopes for Mott-Schottky plots were frequency dependent. Electrodes showed low dark oxidation currents.

- Laser-induced photocurrent transient measurements at p-InP/solid polymer electrolyte (SPE) interface were performed as a function of both introduced redox couple within the polymer matrix (methylviologen) and dispersed platinum at the interfacial region. Poly(ethylene oxide)/poly(ethylene glycol) (PEO/PEG) mixtures were used as the SPE in this work. Platinum was found to enhance electron transfer across this interface (τ = 3.57μs for p-InP/Pt vs. 5.12μs for p-InP). However, methylviologen present in the polymer was not found an effective electron acceptor but appeared responsible for introducing recombination sites at the interfacial region. Here, two segment decay curves were observed with only the slower decay rate being dependent upon potential. Results from this work suggest that further improvements in electrocatalysis at this interface will be necessary for promoting efficient minority carrier transfer from the semiconductor to polymer immobilized redox species proximate to the interface.

- Some organotransition metal complexes, Mn(OPPh<sub>3</sub>)<sub>4</sub>I<sub>2</sub>(SO<sub>2</sub>) and Cu(PBz<sub>3</sub>)<sub>2</sub>SPh, were identified as candidate coatings for the detection of sulfur dioxide on piezoelectric crystal sensors. The complex Mn(OPPh<sub>3</sub>)<sub>4</sub>I<sub>2</sub>(SO<sub>2</sub>) binds SO<sub>2</sub> to form Mn(OPPh<sub>3</sub>)<sub>4</sub>I<sub>2</sub>(SO<sub>2</sub>) and can be used as a coating for an integrating piezoelectric sensor. Regeneration of the initial complex can be accomplished by placing the coated piezoelectric sensor under vacuum for 4h. In comparison, the complex, Cu(PBz<sub>3</sub>)<sub>2</sub>SPh, was found to act as a reversible coating for the detection of SO<sub>2</sub> on piezoelectric crystal sensors in the range of 10-1000ppm SO<sub>2</sub>.

- A multiple-reflecting optical waveguide has been investigated for the direct detection and measurement of gaseous  $\text{SO}_2$ . This was achieved by monitoring the variation in light intensity at a silicon photodetector following interaction of multiple-reflected illumination with a  $\text{Cu}(\text{PBz}_3)\text{SPh}$  coating on the surface of a long glass tube. Direct illumination along the tube axis cavity was avoided. Such changes in net transmitted illumination intensity along the tube axis were a consequence of color changes occurring in this complex associated with reversibly binding  $\text{SO}_2$ . This was a result of absorption characteristic changes induced in laterally propagated internally reflected waves within the tube. This as yet unoptimized device, was able to reproducibly and reversibly detect between 100 and 1000ppm  $\text{SO}_2$ .

#### STATUS OF PHASE III COMMERCIALIZATION

The reversible  $\text{SO}_2$  chemical detection technology developed during performance of this program currently appears the most promising area for future commercialization. We are currently evaluating with our Phase III funding commitment source (IEG Venture Management, Inc.) how this detector technology might best be developed into a commercial product. Anticipated future success in this endeavor will be communicated as appropriate to the ONR Scientific Officer.

SECURITY CLASSIFICATION OF THIS PAGE (When Data Entered)

REPORT DOCUMENTATION PAGE		READ INSTRUCTIONS BEFORE COMPLETING FORM
1. REPORT NUMBER 1	2. GOVT ACCESSION NO.	3. RECIPIENT'S CATALOG NUMBER
4. TITLE (and Subtitle) Metal Intercalation Characteristics of n-HfS <sub>2</sub> Photoelectrodes in Non-Aqueous Electrolytes		5. TYPE OF REPORT & PERIOD COVERED Technical Oct. 1986 - May 1987
		6. PERFORMING ORG. REPORT NUMBER
7. AUTHOR(s) K. W. Semkow, N. U. Pujare and A. F. Sammells		8. CONTRACT OR GRANT NUMBER(s) N00014-86-C-0128
9. PERFORMING ORGANIZATION NAME AND ADDRESS Eltron Research, Inc. 4260 Westbrook Drive Aurora, IL 60504		10. PROGRAM ELEMENT, PROJECT, TASK AREA & WORK UNIT NUMBERS
11. CONTROLLING OFFICE NAME AND ADDRESS Office of Naval Research/Chemistry Program Arlington, VA 22217		12. REPORT DATE July 1987
		13. NUMBER OF PAGES 5
14. MONITORING AGENCY NAME & ADDRESS (if different from Controlling Office)  Above		15. SECURITY CLASS. (of this report)  Unclassified
15a. DECLASSIFICATION/DOWNGRADING SCHEDULE		
16. DISTRIBUTION STATEMENT (of this Report)  Approved for public release, distribution unlimited.		
17. DISTRIBUTION STATEMENT (of the abstract entered in Block 20, if different from Report)  Approved for public release, distribution unlimited.		
18. SUPPLEMENTARY NOTES  Presented Electrochemical Society meeting, Philadelphia, May 1987. Abstract #489		
19. KEY WORDS (Continue on reverse side if necessary and identify by block number)  Hafnium disulfide, copper intercalation, capacitance, impedance, photoelectrodes.		
20. ABSTRACT (Continue on reverse side if necessary and identify by block number)  The photoelectrochemical (PEC) performance of single crystal n-HfS <sub>2</sub> was correlated with capacitance and impedance measurements obtained with the photoanode van der Waals layers oriented either parallel or perpendicular to acetonitrile-based non-aqueous electrolytes, with and without CuCl introduced as an intercalating redox species. For van der Waals layers perpendicular to the electrolyte (i.e., available for copper intercalation) space charge capacitance values of respectively 10 <sup>-2</sup> and 1 μF/cm <sup>2</sup> were obtained for the non-intercalated and copper intercalated photoelectrode. The implications of these experimental observations were discussed in relation to		



the application of these intercalating photoelectrodes in both liquid non-aqueous and solid polymer electrolyte PEC storage devices.

METAL INTERCALATION CHARACTERISTICS OF  $n\text{-HfS}_2$   
PHOTOELECTRODES IN NON-AQUEOUS ELECTROLYTES

Krystyna W. Semkow, Nirupama U. Pujare and  
Anthony F. Sammells

Eltron Research, Inc.  
4260 Westbrook Drive  
Aurora, Illinois 60504

Photoelectrodes of the Group IVb transition metal dichalcogenides  $\text{HfS}_2$ ,  $\text{HfSe}_2$ ,  $\text{ZrS}_2$  and  $\text{ZrSe}_2$  (which are all indirect gap materials possessing band gaps of respectively 1.96, 1.13, 1.68 and 1.2eV) have recently been shown compatible for the reversible intercalation of copper and iron species<sup>1,2</sup>. Single crystals of these materials prepared by the halogen ( $\text{I}_2$ ) vapor transport technique were found to be intrinsically n-doped. Intercalation occurs between the weakly bonded van der Waals planes of these materials. The electrochemical intercalation and photoelectrochemical (PEC) deintercalation of redox species at the interfacial region of these layer type photoanodes, with either liquid non-aqueous or solid polymer electrolytes (SPE), could be a viable strategy for PEC storage devices.

The PEC and electrochemical intercalation characteristics for single crystal materials is found highly dependent upon the crystal orientation exposed to the electrolyte of interest.

In work to be discussed here, the PEC performance of n- $\text{HfS}_2$  is correlated with capacitance and impedance measurements obtained with the photoanode van der Waals layers exposed either parallel or perpendicular to the non-aqueous electrolyte. These measurements were performed in acetonitrile/0.1M TBAPF<sub>6</sub> (tetrabutylammonium fluorophosphate) electrolytes with and without 0.1M CuCl present as the intercalating redox species. Ohmic contact to n- $\text{HfS}_2$  was achieved by sparking indium metal to the van der Waals layers, using a 15V DC power supply. Current collection was then accomplished via a nichrome wire attached via silver epoxy and the whole ohmic contact region suitably insulated. In the absence of CuCl, photopotentials for the (defect free) van der Waals surfaces were typically found to be between -220 and -240mV under simulated AMI illumination. For photoelectrodes prepared where the intercalating edge steps were intentionally exposed to the non-aqueous electrolyte, somewhat smaller photopotentials between -80 and -160mV were found. Impedance and capacitance measurements taken over the frequency range 500Hz to 20kHz for the van der Waals surfaces indicated the presence of frequency dependent capacitance (Figure 1 from Mott-Schottky data) and resistive elements in parallel to the photoanode's space charge capacitance. An equivalent circuit rationalizing this interfacial region was addressed using circuit analysis techniques previously discussed by others<sup>4,5</sup>. The corresponding equivalent circuits obtained for both n- $\text{HfS}_2$  crystal orientations are summarized in Figure 2.

Frequency independent capacitance data were obtained by initially measuring

the total frequency dependent capacitance, conductance and impedance of the photoanode/electrolyte interfacial region. From this, the impedance frequency dependence was obtained and used to eliminate the influence of the frequency dependent capacitance and resistance from the interfacial admittance. Space charge capacitance at the van der Waals surface, obtained using this approach, was found to be  $10^{-2} \mu\text{F}/\text{cm}^2$  at open-circuit potential. Order of magnitude higher space charge capacitance values were found for materials whose van der Waals layers were exposed to the electrolyte. Here, frequency independent Mott-Schottky data obtained (Figure 3) for  $\text{n-HfS}_2$  gave  $V_{\text{FB}} = -0.51\text{V}$  vs. SCE and  $N_{\text{D}} = 7.1 \times 10^{17} \text{ cm}^{-3}$ .

The initial photopotentials of  $\text{n-HfS}_2$  in acetonitrile containing  $\text{CuCl}$  were found to possess values of  $-50\text{mV}$  which decreased steadily during the potentiostatic intercalation of copper. Space charge capacitance at the same time was found to increase to  $1 \mu\text{F}/\text{cm}^2$ .

The electrochemical deintercalation of copper could be achieved in the dark implying that the initially intercalated copper occupies energy levels close to the conduction band rather than in the forbidden gap close to the valence band.

The implications of these experimental observations will be discussed in relation to the application of these intercalating photoelectrodes in both liquid non-aqueous and SPE, PEC storage devices.

#### ACKNOWLEDGEMENT

This work was supported in part by the Office of Naval Research.

#### REFERENCES

1. B. G. Yacobi, F. W. Baswell and J. M. Corbett, J. Phys. C., 12, 2189 (1979).
2. H. Tributsch, Structure and Bonding, 49, 127 (1982).
3. H. Tributsch, Solar Energy Matls., 1, 705 (1979).
4. J. F. McCann, S. P. S. Badwal and J. Pezy, J. Electroanal. Chem., 118, 115 (1981).
5. J. F. McCann and S. P. S. Badwal, J. Electrochem. Soc., 129, 5551 (1982).

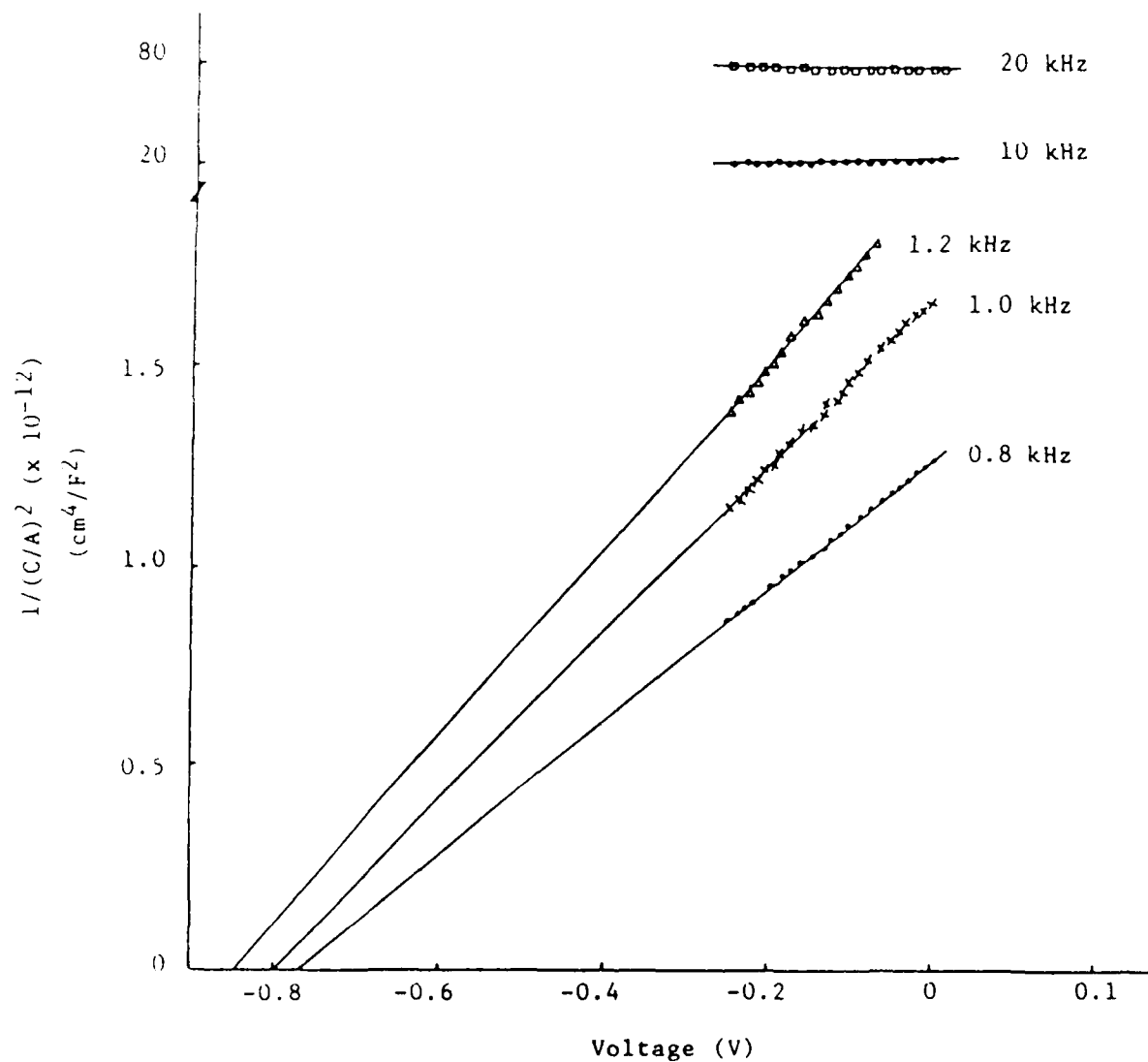


Figure 1. Frequency dependent Mott-Schottky plot for n-HfS<sub>2</sub> in 0.1M TBAPF<sub>6</sub> in CH<sub>3</sub>CN oriented perpendicular to van der Waal layer in CH<sub>3</sub>CN/0.1M TBAPF<sub>6</sub> electrolyte.

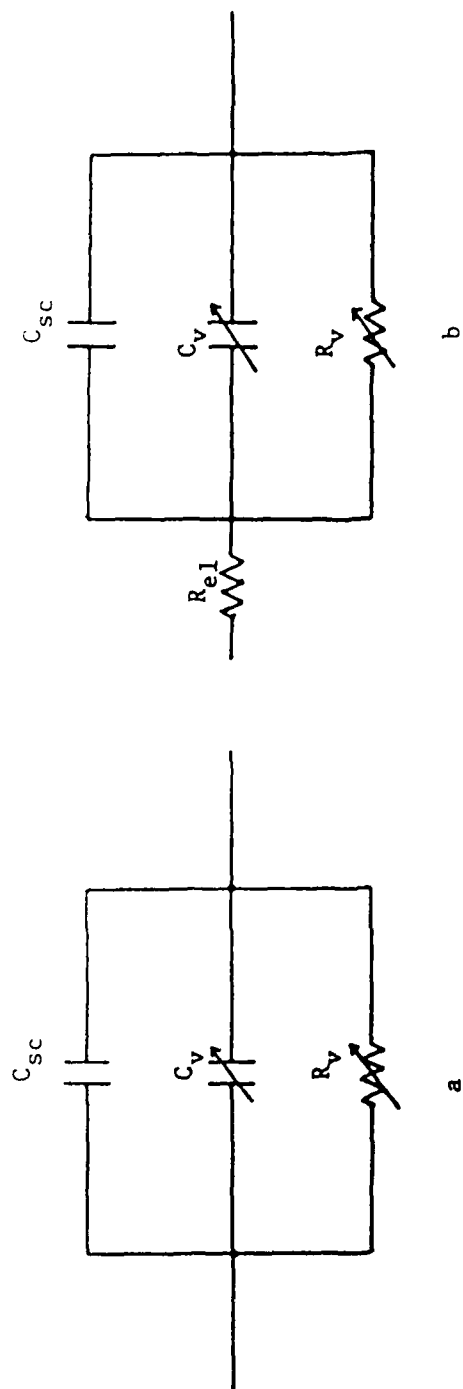


Figure 2. Equivalent circuits for n-HfS<sub>2</sub>/CH<sub>3</sub>CN interfacial region.  
 a) n-HfS<sub>2</sub> perpendicular to van der Waals layers (i.e. intercalating edges exposed to electrolyte).  
 b) n-HfS<sub>2</sub> parallel to van der Waals layer.

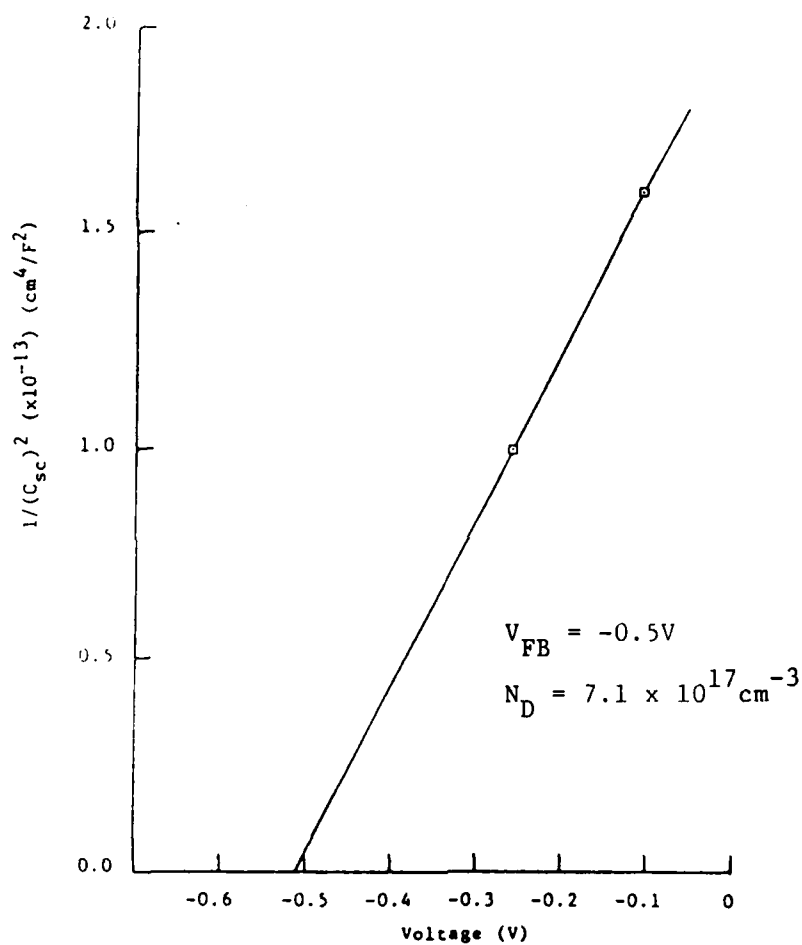


Figure 3. Frequency independent Mott-Schottky plot for n-HfS<sub>2</sub>/CH<sub>3</sub>CN interface oriented perpendicular to van der Waals layer.

SECURITY CLASSIFICATION OF THIS PAGE (When Data Entered)

REPORT DOCUMENTATION PAGE		READ INSTRUCTIONS BEFORE COMPLETING FORM
1. REPORT NUMBER 2	2. GOVT ACCESSION NO.	3. RECIPIENT'S CATALOG NUMBER
4. TITLE (and Subtitle) Investigations at the n-HfS <sub>2</sub> /Non-Aqueous Electrolyte Interfacial Region		5. TYPE OF REPORT & PERIOD COVERED Technical Oct. 1986 - July 1987
7. AUTHOR(s) K. W. Semkow, N. U. Pujare and A. F. Sammells		6. PERFORMING ORG. REPORT NUMBER
9. PERFORMING ORGANIZATION NAME AND ADDRESS Eltron Research, Inc. 4260 Westbrook Drive Aurora, IL 60504		8. CONTRACT OR GRANT NUMBER(s) N00014-86-C-0128
11. CONTROLLING OFFICE NAME AND ADDRESS Office of Naval Research/Chemistry Program Arlington, VA 22217		10. PROGRAM ELEMENT, PROJECT, TASK AREA & WORK UNIT NUMBERS
14. MONITORING AGENCY NAME & ADDRESS (if different from Controlling Office) Above		12. REPORT DATE July 1987
		13. NUMBER OF PAGES 26
		15. SECURITY CLASS. (of this report) Unclassified
		15a. DECLASSIFICATION/DOWNGRADING SCHEDULE
16. DISTRIBUTION STATEMENT (of this Report) Approved for public release, distribution unlimited.		
17. DISTRIBUTION STATEMENT (of the abstract entered in Block 20, if different from Report) Approved for public release, distribution unlimited.		
18. SUPPLEMENTARY NOTES Published: Journal of the Electrochemical Society, 135, 1142 (1988)		
19. KEY WORDS (Continue on reverse side if necessary and identify by block number) Hafnium disulfide, admittance spectroscopy, van der Waals surfaces, photoelectrodes.		
20. ABSTRACT (Continue on reverse side if necessary and identify by block number) Single crystal n-HfS <sub>2</sub> photoelectrodes prepared by halogen vapor transport were investigated in 0.1M TBAPF <sub>6</sub> /CH <sub>3</sub> CN electrolyte using both impedance and admittance spectroscopy techniques. The presence of frequency dependent capacitive and resistive elements in the equivalent circuit for n-HfS <sub>2</sub> /electrolyte interface were evident. Measured capacitance effects at the interfacial region were found dependent upon the crystal orientation used, with that for defect free van der Waals surfaces being 10 <sup>-8</sup> F/cm <sup>2</sup> ; an order of magnitude lower than for n-HfS <sub>2</sub> intercalation layers exposed to the electrolyte. High capacitance values were correlated with a high population		



of surface charges. Admittance spectroscopy analysis suggested the presence of surface states associated with surface adsorption processes. Open-circuit photovoltages up to 0.35V under  $100\text{mW}/\text{cm}^2$  illumination were observed for van der Waals surfaces, decreasing to 0.16V as the population intercalating layers exposed to the electrolyte was increased.

## INVESTIGATIONS AT THE n-HfS<sub>2</sub>/NON-AQUEOUS ELECTROLYTE INTERFACIAL REGION

Krystyna W. Semkow\*, Nirupama U. Pujare and Anthony F. Sammells\*

Eltron Research, Inc.  
Aurora, Illinois 60504

### ABSTRACT

Single crystal n-HfS<sub>2</sub> photoelectrodes prepared by halogen vapor transport were investigated in 0.1M TBAPF<sub>6</sub>/CH<sub>3</sub>CN electrolyte using both impedance and admittance spectroscopy techniques. The presence of frequency dependent capacitive and resistive elements in the equivalent circuit for n-HfS<sub>2</sub>/electrolyte interface were evident. Capacitance effects at the interfacial region were found dependent upon the crystal orientation used, with that for defect free van der Waals surfaces being 10<sup>-8</sup>F/cm<sup>2</sup>; an order of magnitude lower than for n-HfS<sub>2</sub> intercalation layers exposed to the electrolyte. High capacitance values were correlated with a high population of surface charges. Admittance spectroscopy analysis suggested the presence of interface states, possibly associated with the presence of resident surface oxides. Open-circuit photovoltages up to 0.35V under 100mW/cm<sup>2</sup> illumination were observed for van der Waals surfaces, decreasing to 0.16V as the population intercalating layers exposed to the electrolyte was increased.

\*Electrochemical Society Active Member

Key Words: interfacial capacitance, impedance, admittance spectroscopy, intercalating compounds

Considerable work has already been reported<sup>(1-10)</sup>, directed towards investigating the photoelectrochemical (PEC) properties of transition metal dichalcogenides (TMDs) belonging to the periodic groups IV, VI and VIII. These materials all possess a layer type structure between the transition metal and chalcogenide, held together by relatively weak van der Waals forces. The electronic structure of these materials and corresponding PEC characteristics are dependent in part, upon whether the dichalcogenide possesses an octahedral or trigonal prismatic type structure.

For group IVB TMDs ( $\text{HfS}_2$ ,  $\text{HfSe}_2$ ,  $\text{ZrS}_2$  and  $\text{ZrSe}_2$ ) which possess an octahedral structure, electron photoexcitation within the semiconductor band gap proceeds from energy bands derived from bonding sulfur p-orbitals into metal d-orbitals ( $t_{2g}$ )<sup>(11-18)</sup>. By comparison group VIB TMDs ( $\text{MoS}_2$ ,  $\text{WSe}_2$ ) possess a trigonal prismatic symmetry which result in a splitting of the  $t_{2g}$  d-orbitals into lower ( $d_{z^2}$ ) and upper ( $d_{xy}$  and  $d_{x^2-y^2}$ ) states. In this latter case photoelectron excitation will occur between these TMD split non-bonding d-orbitals<sup>2,11,12</sup>. All of these semiconductors possess indirect band gaps, although their absorption coefficients are quite high, with most photons becoming captured within  $1000\text{\AA}$  from the interfacial region<sup>12</sup>. Group VIB based photoelectrodes have previously been investigated by us in both regenerative<sup>19</sup> and ex situ storage PEC cells<sup>20</sup> where they have demonstrated good stability against photoanodic corrosion.

One alternative strategy for the storage of incident PEC energy would be to exploit the reversible intercalation of redox metal species within layer type photoelectrodes themselves. In the case of molybdenum and tungsten dichalcogenides their van der Waals layers are incompatible for the reversible intercalation of reduced transition metal species. Group IVB dichalcogenides by comparison have the potential ability to function both as photoelectrodes and as the substrate electrode for subsequent reversible intercalation of reduced transition metal species<sup>11,21-28</sup>. It has already been reported<sup>24</sup> that p- $\text{ZrS}_2$  is capable of maintaining its semiconducting properties after partial intercalation by either Cu or Fe to form  $\text{ZrM}_y\text{S}_2$  while the degree of intercalation will vary as,  $0 < y < 0.22$ , although these photoelectrodes will become progressively more degenerate during intercalation, due to an increasing conduction band population.

We have recently become interested in the group IVB TMDs, with particular emphasis being placed upon n- $\text{HfS}_2$  (band gap 1.96eV) because of the encouraging

photopotential observed by us from this material (up to -350mV in acetonitrile based electrolytes). This has resulted in the preparation and the on going investigation of solid-state two photoelectrode storage PEC cells possessing the general configuration:



The van der Waals layers available in single crystal n-HfS<sub>2</sub> for the intercalation of metal species resident in close proximity to the interfacial region during electrochemical discharge of the above cell, are shown in Figure 1. During electrochemical discharge interfacial Cu<sup>+</sup> species become reduced followed by their subsequent intercalation within the n-HfS<sub>2</sub> van der Waals layer. PEC charge of the photoanode interfacial region will occur via the promotion of photoexcited electron holes from the n-HfS<sub>2</sub> valence band leading to the photodeintercalation of copper and formation of cuprous ions. The performance that might be realized from such solid-state PEC storage devices will be determined in part by the population of exposed van der Waals layers resident at the interfacial region. Too high a population of exposed intercalation layers will inhibit PEC performance via recombination of photogenerated carriers, whereas too low a population will limit the Faradaic capacity of this intercalating photoelectrode.

As a consequence of the above discussion it is evident that there is a clear incentive to perform some characterization of the n-HfS<sub>2</sub>/electrolyte interfacial region as a function of crystal orientation. This has been addressed here by the application of impedance and admittance techniques to investigate the n-HfS<sub>2</sub>/electrolyte interfacial region initially in the absence of interfering intercalating metal species. For experimental convenience this study was performed in acetonitrile based liquid electrolytes. Measurements were performed as a function of whether the n-HfS<sub>2</sub> photoelectrode was oriented perpendicular to the c-lattice vector (⊥-c), where a relatively defect-free van der Waals surface was exposed to the electrolyte, or parallel to the c-lattice vector (∥-c) where a high population of interstitial sites would be exposed to the non-aqueous electrolyte.

#### EXPERIMENTAL

Single crystals of n-HfS<sub>2</sub> were prepared by the halogen (I<sub>2</sub>) vapor trans-

port technique (Northwestern University). Initial solid-state chemical reaction between Hf (99.5%) and S (99.999%) was accomplished by heating an intimate mixture together with 5mg I<sub>2</sub>/ml of the quartz transport tube volume. This was performed in a three temperature zone furnace. Typical thermal gradients used were between 375°C and 800°C. Crystal growth occurred over 25 days. In all cases the relatively large crystals obtained were intrinsically n-type. Ohmic contact to n-HfS<sub>2</sub> was accomplished by sparking indium onto one side of the crystal using a 15 volt DC power supply. This was performed using a fine indium wire as a cathode with the other pole of the power supply clamped to the n-HfS<sub>2</sub> single crystal. When the indium wire was within 1mm of the crystal, a transient spark could be observed. This resulted in the ion implantation of indium into the ohmic contact region. Current collection was performed with a nichrome wire attached with silver epoxy and cured at 120°C for 1h. Photoelectrodes were then appropriately isolated from later contact with the electrolyte by epoxy (Norton Chemplast), so that only the single crystal front face of interest was exposed. Typical photoelectrode areas for l-c oriented crystals was 0.04cm<sup>2</sup> and 0.06cm<sup>2</sup> for ||-c surfaces.

Measurements were performed in a standard glass H-cell arrangement using a platinum counter electrode. SCE was used as a reference to the working electrode compartment via a salt bridge. Photoelectrode potentials were controlled by a Stonehard Associates BC 1200 potentiostat. Impedance, conductance and capacitance measurements were performed using a Hewlett-Packard 4276A digital LCZ meter over the frequency range 20kHz - 100Hz.

### RESULTS AND DISCUSSION

Work performed was directed towards investigating the interfacial characteristics of single crystal n-HfS<sub>2</sub> as a function of crystal orientation in liquid non-aqueous electrolyte (acetonitrile containing 0.1M tetrabutylammonium fluorophosphate (TBAPF<sub>6</sub>)) as the supporting electrolyte in the absence of potentially intercalating transition metal species. This investigation emphasizes the application of capacitance, impedance and admittance measurement techniques towards such a goal.

Mott-Schottky(MS) type measurements were performed on the cell n-HfS<sub>2</sub>/0.1M TBAPF<sub>6</sub>,CH<sub>3</sub>CN/Pt for both l-c and ||-c single crystal orientations over the frequency range 800Hz to 20kHz. Capacitance measurements at frequencies between 10 and 20kHz showed little dependency upon applied electrode potential.

This indicated small changes in potential drop across the semiconductor depletion layer with the majority of applied potential being present in the electrolyte Helmholtz layer. At lower frequencies (800-1200Hz) MS data showed some frequency dependence as shown respectively in Figures 2 and 3 for l-c and c-c oriented n-HfS<sub>2</sub> electrode. Table 1 summarizes flat band potential ( $V_{FB}$ ) and carrier density ( $N_D$ ) values obtained from the MS relationship at 1kHz as a function of crystal orientation. A dielectric constant of 5 was used in these calculations and assumed as a first approximation to be independent of surface orientation. In general, more negative  $V_{FB}$  and larger  $N_D$  values were obtained for the c-c oriented n-HfS<sub>2</sub> crystal face compared to the l-c surface.

The observed frequency dependency of capacitance when lower measurement frequencies were used implied that the n-HfS<sub>2</sub>/acetonitrile interfacial region could not be represented by a simple equivalent circuit model consisting of frequency independent capacitors and resistors. As a consequence, an equivalent circuit analysis model of this interface was performed using methodology previously discussed by others<sup>29,30</sup>. In this approach the semiconductor/liquid junction was represented by a continuous distribution of individual elements comprising series resistances and capacitances, resulting in a large number of relaxation times. These individual elements can originate from a variety of charge accumulation modes, such as surface states, inhomogeneous doping and surface crystal defects. For a large distribution of elements, the equivalent circuit could be represented by a frequency dependent resistor,  $R_v$ , in parallel with a frequency dependent capacitor,  $C_v$ , and a frequency independent capacitor,  $C_{sc}$ , representative of the space charge layer capacitance. The model may also incorporate electrolyte resistance and double layer capacitance, if appropriate. Expressions for the total admittance  $Y$ , impedance  $Z$ , conductance  $G$ , and susceptance  $B$ , for an equivalent circuit consisting of a large number of R-C elements, could be represented by the following relationships:

$$Y = a\omega^n + kb\omega^n \quad (1)$$

$$Z = A\omega^{-n} - jB\omega^{-n} \quad (2)$$

$$G = a\omega^n \quad (3)$$

$$B = b\omega^n \quad (4)$$

where  $A$ ,  $B$ ,  $a$ ,  $b$  and  $n$  are characteristic circuit constants and  $\omega$  is the angular frequency.

In order to determine the equivalent circuit for the n-HfS<sub>2</sub>/acetonitrile interface, capacitance, impedance and conductance responses were taken over the frequency range 20kHz - 100Hz at the dark photoelectrode. Figures 4 and 5 summarize respectively impedance and admittance responses for l-c oriented n-HfS<sub>2</sub> at the two electrode potentials -0.022 and -0.172V vs. SCE. As can be seen, all of this data was linear and went through the origin. Thus, no influence by either the electrolyte resistance or double layer capacitance was evident. The equivalent circuit for the cell could therefore be represented by the space charge capacitance, C<sub>sc</sub>, at the n-HfS<sub>2</sub> surface being in parallel to the frequency dependent components R<sub>v</sub> and C<sub>v</sub><sup>29,30</sup>, as shown in Figure 6a.

The impedance and admittance responses for ||-c oriented n-HfS<sub>2</sub> in acetonitrile at -0.103 and -0.253V vs. SCE are summarized in Figures 7 and 8 respectively. Linear dependencies were found between real and imaginary parts of the measured cell impedance. Extrapolation to infinite frequency indicated cell electrolyte resistance to be 200Ω (Figure 7A). Similar electrolyte resistance values were obtained upon analysis of high frequency impedance data at -0.253V vs. SCE (Figure 7B). In this latter case however, impedance data obtained in the lower frequency region (below 6kHz) possesses a somewhat different slope. This may have reflected the presence of additional surface states other than those associated with exposed van der Waals layer edges at the semiconductor surface. The admittance responses shown in Figure 8 possessed radii between 2.3-2.5 x 10<sup>-3</sup> 1/Ω, close to the reciprocal of the electrolyte resistance. The equivalent circuit used here for ||-c oriented n-HfS<sub>2</sub> is shown in Figure 6b.

The high frequency region of the impedance/admittance response data was used to determine the n-HfS<sub>2</sub> space charge capacitance. The magnitude of C<sub>sc</sub> was usually relatively small compared to C<sub>v</sub> and in the low frequency range its contribution can often be neglected<sup>33,34</sup>. The relationship between log G and log ω, where G represents the total conductance of the cell corrected for electrolyte resistance, are summarized in Figure 9a-d for both l-c and ||-c oriented n-HfS<sub>2</sub>. From the slopes obtained here the parameter characterizing an exponential dependency between cell conductance and frequency, n, (eq. 3) could be obtained and used in extracting frequency independent capacitance at the semiconductor/electrolyte junction. As can be seen, n values were usually found between 0.7 and 0.8. An n value of 1 would have suggested the

absence of frequency dependent capacitance effects at the n-HfS<sub>2</sub>/electrolyte interface as implied from relationships 5 and 6<sup>29,30</sup>:

$$B = \omega C_V \quad (5)$$

$$C_V = b\omega^{n-1} \quad (6)$$

The frequency dependence of measured cell capacitance at two electrode potentials, are summarized in Figure 10 for both n-HfS<sub>2</sub> orientations. For  $\parallel$ -c oriented n-HfS<sub>2</sub> in order to calculate capacitance, the cell susceptance value (B) was initially corrected for electrolyte resistance. Extrapolating the capacitance curves to infinite frequency eliminated the frequency dependent capacitance  $C_V$ , thereby permitting frequency independent capacitance values to be obtained. A comparison is made in Table 1 between capacitance data obtained at 1kHz and capacitance data obtained using the frequency-independent analysis of the electrode capacitance. It should be noted that from frequency independent data, capacitance values of  $10^{-8}$ F/cm<sup>2</sup> (at E = -0.022V) were obtained from  $\perp$ -c oriented n-HfS<sub>2</sub> which compares to an order of magnitude higher values ( $2.5 \times 10^{-7}$ F/cm<sup>2</sup>) for  $\parallel$ -c oriented material (at E = -0.103V). Such differences may be attributed to a higher population of surface states for  $\parallel$ -c oriented n-HfS<sub>2</sub>. For very high frequency measurements, many surface states are not able to follow the applied AC voltage<sup>35,36</sup>. This was not a case here where the cumulative capacitance of both surface states and the van der Waals layer ( $\perp$ -c) exposed to the electrolyte was apparently monitored. Thus, the  $C_{SC}$  element shown in Figure 6a represents space charge capacitance on  $\perp$ -c oriented van der Waals n-HfS<sub>2</sub> surfaces, while the  $C_{SC}$  element in Figure 6b represents predominating capacitance on  $\parallel$ -c oriented surfaces.

The frequency independent capacitance values obtained above were used to plot frequency independent MS data (Figure 11). The number of charges on  $\perp$ -c oriented n-HfS<sub>2</sub> was found to be about three orders of magnitude higher than found on the van der Waals layer (Table 1). Such an observation supports previous results on d-band semiconductors, which suggested that accumulation of positive charges occurs at exposed  $\parallel$ -c oriented layer type surfaces<sup>12,23</sup>. The presence of a high density of charged species in the proximity of such edge sites could in part explain the higher conductivity values found through rather than across the van der Waals layers<sup>13</sup>. The frequency independent MS data (Figure 11A) for  $\perp$ -c oriented n-HfS<sub>2</sub> gave similar  $V_{FB}$  values to that obtained at 1kHz (-0.4 vs. -0.26, Table 1). Differences between frequency



Table 1. Mott-Schottky parameters determined for single crystal n-HfS<sub>2</sub> at ||-c and ⊥-c orientations in CH<sub>3</sub>CN containing 0.1M TBAPF<sub>6</sub>.

⊥-c Oriented n-HfS<sub>2</sub> Photoanode, OCP +0.44V

	Mott-Schottky Relation, 1kHz	Frequency Independent Mott-Schottky Relation
C <sub>sc</sub> (F/cm <sup>2</sup> ) at -0.022V	6.1x10 <sup>-8</sup>	1x10 <sup>-8</sup>
V <sub>FB</sub> (V)	-0.40	-0.26
N <sub>D</sub> ( $\frac{1}{\text{cm}^3}$ )	5.3x10 <sup>16</sup>	3.4x10 <sup>14</sup>

||-c Oriented n-HfS<sub>2</sub> Photoanode, OCP -0.103V

	Mott-Schottky Relation, 1kHz	Frequency Independent Mott-Schottky Relation
C <sub>sc</sub> (F/cm <sup>2</sup> ) at -0.103V	1.1x10 <sup>-6</sup>	2.5x10 <sup>-7</sup>
V <sub>FB</sub> (V)	-0.80	-0.51
N <sub>D</sub> ( $\frac{1}{\text{cm}^3}$ )	1.3x10 <sup>19</sup>	7.1x10 <sup>17</sup>

independent MS and conventional MS data becomes greater for  $\parallel$ -c oriented material, probably a consequence of the higher population of surface states on this latter orientation<sup>37</sup>. Energy level diagrams for  $\perp$ -c and  $\parallel$ -c oriented n-HfS<sub>2</sub> are shown respectively in Figure 12 and are based upon charge density and flat band potential data obtained for n-HfS<sub>2</sub> as determined from frequency independent MS data. A value of  $2.5 \times 10^{19} \text{cm}^{-3}$  for the effective density of states in the conduction band was used in this calculation. The n-HfS<sub>2</sub> surface barrier for  $\perp$ -c oriented material was found  $\approx 0.4\text{V}$  and for  $\parallel$ -c  $\approx 0.3\text{V}$ . The consequent lower degree of band bending found for  $\parallel$ -c oriented n-HfS<sub>2</sub> photoelectrodes was reflected in the generally lower photopotentials found for this material (80-160mV compared to 240-350mV for  $\perp$ -c n-HfS<sub>2</sub> surfaces).

The impedance and admittance responses obtained from both  $\perp$ -c and  $\parallel$ -c oriented n-HfS<sub>2</sub> indicated some instability at lower frequencies (usually below 800Hz), suggesting the possible presence of surface state related redox electrochemistry. Some variations were observed in the initial dark n-HfS<sub>2</sub> open-circuit potential, which were typically found to vary between -0.1 and -0.3V vs. SCE for  $\parallel$ -c oriented electrodes and between 0.25 and 0.45V for  $\perp$ -c oriented electrodes. Such observations suggested the possible presence of surface oxides on the n-HfS<sub>2</sub> electrode. From Mott-Schottky type measurements  $V_{\text{FB}}$  values obtained for n-HfS<sub>2</sub> single crystal electrodes in aqueous electrolyte were found to change by 55.9mV for a unit change in pH between 0 and 7. Although pH dependent  $V_{\text{FB}}$  values do not unequivocally prove or disprove the presence of surface oxides on this n-HfS<sub>2</sub> electrode, other workers<sup>25</sup> investigating the related layer type material n-ZrS<sub>2</sub> in similar aqueous electrolytes, showed the presence of surface oxides using XPS measurements. The source of possible surface oxides in our case may have been associated with procedures used during fabrication, when the electrode was heated to 120°C for 1h. In order to detect interface states at both  $\perp$ -c and  $\parallel$ -c oriented n-HfS<sub>2</sub>, together with comparing frequency independent impedance-admittance parameters with those obtained using more conventional MS measurement techniques, admittance spectroscopy analysis techniques were used<sup>31,32</sup>.

In the simplest case the n-HfS<sub>2</sub>/electrolyte interface was assumed to consist of the space charge capacitance,  $C_{\text{SC}}$ , connected in series with a bulk conductance  $G_{\text{el}}$ . By comparing real and imaginary parts of the admittance equation for such an equivalent circuit, with the appropriate in-phase admittance components being obtained experimentally, the following relationship

can be obtained:

$$G/\omega = \frac{\omega C_{sc}^2 G_{el}}{G_B^2 + (\omega C_{sc})^2} \quad (7)$$

where  $G$  represents the measured in-phase cell conductance. By plotting  $G/\omega$  vs.  $\omega$  a maximum will be given at

$$G/\omega_{max} = C_{sc}/2 \quad (8)$$

from which the space charge capacitance could be determined. If interface states are present on the n-HfS<sub>2</sub> surface, additional peaks will be observed possessing a different characteristic frequency  $\omega'_{max}$  similar to relationship (8) above. Figure 13 compares plotting  $\log G/\omega$  vs.  $\log \omega$  for n-HfS<sub>2</sub> oriented both  $\perp$ -c (curves A) and  $\parallel$ -c (curves B). For  $\perp$ -c oriented material no space charge capacitance peak was evident at higher frequencies. A small value of  $C_{sc}$ , expected based upon previous impedance measurements (Figure 11 and Table 1), suggests that frequency maximum relating to space charge layer might occur at frequencies above 20kHz<sup>31,32</sup>. The small peak observed at  $\log \omega \approx 4.1$  suggested the presence of interface state effects. Such effects can be represented by frequency dependent components  $C_v$  and  $R_v$  in the equivalent circuit diagram given in Figure 6a. For  $\perp$ -c oriented material, increasing  $G/\omega$  values were observed at lower frequencies, indicating the presence of a Faradaic cell resistance component. Extrapolating  $\log G/\omega$  to zero  $\log \omega$  indicated a Faradaic resistance of  $10^7 \Omega$  suggesting a high degree of polarizability and low exchange current densities at the n-HfS<sub>2</sub> electrode surface, as might be expected since no electroactive species were intentionally added to the non-aqueous electrolyte. For  $\parallel$ -c oriented material (curves B) the high frequency peak observed was associated with the semiconductor space charge capacitance giving a value of  $4.8 \times 10^{-7} \text{F/cm}^2$ . In comparison a capacitance value of  $2.5 \times 10^{-7} \text{F/cm}^2$  was obtained from frequency independent impedance studies. Since the population of electrolyte exposed van der Waals layers was probably subtly different between these two experiments, these two capacitance values are in relatively good agreement. The peak observed at  $\log \omega \approx 3.7$  was again probably associated with surface oxide interface states at the van der Waals surface as represented by  $C_v$  and  $R_v$  components in the equivalent circuit diagram given in Figure 6a and b.

A frequency independent method of analyzing impedance and admittance spectroscopy data for n-HfS<sub>2</sub> electrodes in acetonitrile has been discussed. These frequency independent studies on n-HfS<sub>2</sub> indicated that capacitance

for the  $\perp$ -c surface was about an order of magnitude lower than that for the  $\parallel$ -c surface. The high capacitance of  $\parallel$ -c oriented n-HfS<sub>2</sub> electrode was explained by a high population of surface states (surface edges) accumulating about three orders of magnitude more charges than the  $\perp$ -c face. Those surface edges capable of intercalation act as effective recombination centers permitting only smaller photopotentials to be realized. The presence of interface states other than those assigned to intercalating edges were observed by admittance spectroscopy measurements. These were most probably associated with surface oxides resident on the n-HfS<sub>2</sub>.

#### ACKNOWLEDGEMENT

This work was supported in part by the Office of Naval Research.

#### REFERENCES

1. H. Tributsch and J. C. Bennett, J. Electroanalyt. Chem., 81, 97 (1977).
2. H. Tributsch, Z. Naturforsch., 32a, 972 (1977).
3. H. Tributsch, Ber. Bunsenges. Phys. Chem., 81, 361 (1977).
4. H. Tributsch, Ber. Bunsenges. Phys. Chem., 82, 169 (1978).
5. H. Tributsch, J. Electrochem. Soc., 125, 1086 (1978).
6. J. Gobrecht, H. Gerischer and H. Tributsch, Ber. Bunsenges. Phys. Chem., 82, 1331 (1978).
7. J. Gobrecht, H. Gerischer and H. Tributsch, J. Electrochem. Soc., 125, 2085 (1978).
8. S. M. Ahmed and H. Gerischer, Electrochim. Acta., 24, 705 (1979).
9. H. Tributsch, Solar Energy Materials, 1, 705 (1979).
10. H. Tributsch, H. Gerischer, C. Clemen and E. Bucher, Ber. Bunsenges. Phys. Chem., 83, 655 (1979).
11. H. Tributsch, J. Electrochem. Soc., 128, 1261 (1981).
12. H. Tributsch, Structure and Bonding, 49, 127 (1982).
13. J. A. Wilson and A. D. Yoffe, Adv. Phys., 18, 193 (1969).
14. A. R. Beal, J. C. Knights, and W. Y. Liang, J. Phys. C. Solid State Phys., 5, 5531 (1972).
15. H. P. Hughes and W. Y. Liang, ibid., 10, 1079 (1977).
16. E. R. Shepherd and P. M. Williams, J. Phys. C. Solid State Phys., 7, 4416 (1974).
17. R. B. Murray, R. A. Bromley, and A. D. Yoffe, ibid., 5, 746 (1972).
18. L. F. Mattheiss, Phys. Rev., B8, 3719 (1973).
19. P. G. P. Ang and A. F. Sammells, J. Electrochem. Soc., 129, 233 (1982).

20. P. G. P. Ang, C. J. Liu, A. A. Rossignuolo, A. J. Tiller and A. F. Sammells, Measurement Techniques for Photoelectrochemical Solar Cells, Eds. W. L. Wallace, A. G. Nozik, S. K. Deb and R. H. Wilson, Proc. Electrochem. Soc., 697-703, 1981.
21. M. S. Whittingham, Science, 192, 1126 (1976).
22. H. Tributsch, Appl. Phys., 23, 61 (1980).
23. W. Kautek, H. Gerischer and H. Tributsch, Ber. Bunsenges. Phys. Chem., 83, 1000 (1979).
24. B. G. Yacobi, F. W. Boswell and J. M. Corbett, J. Phys. C. Solid State Phys., 12, 2189 (1979).
25. N. Chandra, J. K. Leland and A. J. Bard, J. Electrochem. Soc., 134, 76 (1987).
26. G. V. Subbor Rao and J. C. Tsang, Mater. Res. Bull., 9, 921 (1974).
27. M. S. Whittingham, U.S. Pat. 4,040,917 (1977).
28. A. R. Beal and W. Y. Liang, Phil. Mag., 27, 1397 (1973).
29. J. F. McCann, S. P. S. Badwal and J. Pezy, J. Electroanal. Chem., 118, 115 (1981).
30. J. F. McCann and S. P. S. Badwal, J. Electrochem. Soc., 129, 551 (1982).
31. Peter A. Smith, "Electrical Characterization of Polycrystalline and Photochemical Solar Cells," M. S. Thesis, Colorado State University, Ft. Collins, 1980.
32. J. Dubow and R. Krishnar, "Novel Concepts in Electrochemical Solar Cells," SERI Final Report, Contract No. XS-0-9272-1 (October, 1981).
33. S. P. S. Badwal and H. J. de Bruin, Phys. Status Solidi., A, 54, 261 (1979).
34. I. D. Raistrick, Chun Ho and R. A. Huggins, J. Electrochem. Soc., 123, 1469 (1976).
35. A. Goetzberger, E. Klansman and M. J. Schulz, CRC Int. Rev. Solid State Sci., 6, 1 (1976).
36. K. W. Frese, Jr. and S. R. Morrison, J. Electrochem. Soc., 126, 1235 (1979).
37. S. R. Morrison, Electrochemistry at Semiconductor and Oxidized Metal Electrodes, Plenum Press, New York, 1980.

## FIGURE CAPTIONS

- Figure 1. X20 photograph of single crystal n-HfS<sub>2</sub> grown by halogen vapor transport showing van der Waals layers available for the electrochemical intercalation of metal species.
- Figure 2. Frequency dependence of Mott-Schottky relation for a n-HfS<sub>2</sub> electrode at  $\perp$ -c orientation in 0.1M TBAPF<sub>6</sub> in CH<sub>3</sub>CN.
- Figure 3. Frequency dependence of Mott-Schottky relation for n-HfS<sub>2</sub> electrode at  $\parallel$ -c orientation in 0.1M TBAPF<sub>6</sub> in CH<sub>3</sub>CN.
- Figure 4. Impedance responses for an n-HfS<sub>2</sub> electrode at  $\perp$ -c orientation in contact with 0.1M TBAPF<sub>6</sub> in CH<sub>3</sub>CN at -0.022V (A) and -0.172V (B) vs. SCE. Counter electrode Pt.
- Figure 5. Admittance responses for  $\perp$ -c oriented n-HfS<sub>2</sub> in CH<sub>3</sub>CN/0.1M TBAPF<sub>6</sub> electrolyte at A) -0.022V and, B) -0.172V vs. SCE. Counter electrode Pt.
- Figure 6. Equivalent circuits used in this work for rationalizing the cell n-HfS<sub>2</sub>/CH<sub>3</sub>CN/Pt as a function of crystal orientation.
- Figure 7. Impedance responses for  $\parallel$ -c oriented n-HfS<sub>2</sub> in CH<sub>3</sub>CN (0.1M TBAPF<sub>6</sub>) at A) -0.103V (OCP) and, B) -0.253V vs. SCE. Counter electrode Pt.
- Figure 8. Admittance responses for  $\parallel$ -c oriented n-HfS<sub>2</sub> electrode in CH<sub>3</sub>CN (0.1M TBAPF<sub>6</sub>) at A) -0.103V (OCP) and, B) -0.253V vs. SCE. Counter electrode Pt.
- Figure 9. Conductance frequency response for n-HfS<sub>2</sub> in CH<sub>3</sub>CN (0.1M TBAPF<sub>6</sub>) A)  $\perp$ -c orientation at -0.022V, and B)  $\perp$ -c orientation at -0.172V, C)  $\parallel$ -c orientation at -0.103V (OCP), and D)  $\parallel$ -c orientation at -0.253V, all versus SCE.
- Figure 10. Capacitance frequency dependence for the cell n-HfS<sub>2</sub>/0.1M TBAPF<sub>6</sub>, CH<sub>3</sub>CN/Pt A)  $\perp$ -c oriented n-HfS<sub>2</sub> at -0.022V and -0.172V, B)  $\parallel$ -c oriented n-HfS<sub>2</sub> at -0.103V and -0.253V. SCE used as reference electrode.
- Figure 11. Frequency independent Mott-Schottky plot for n-HfS<sub>2</sub> in CH<sub>3</sub>CN (0.1M TBAPF<sub>6</sub>) A)  $\perp$ -c oriented, B)  $\parallel$ -c oriented.
- Figure 12. Energy schemes for n-HfS<sub>2</sub> electrode in 0.1M TBAPF<sub>6</sub>/CH<sub>3</sub>CN. Flat band potentials are based on frequency-independent results.
- Figure 13. Frequency dependence of G/ $\omega$  values for n-HfS<sub>2</sub> electrode in CH<sub>3</sub>CN (0.1M TBAPF<sub>6</sub>). A)  $\perp$ -c oriented, B)  $\parallel$ -c oriented. Electrode potential (vs. SCE) is shown next to the curves.



Figure 1. X20 photograph of single crystal n-HfS<sub>2</sub> grown by halogen vapor transport showing van der Waals layers available for the electrochemical intercalation of metal species.

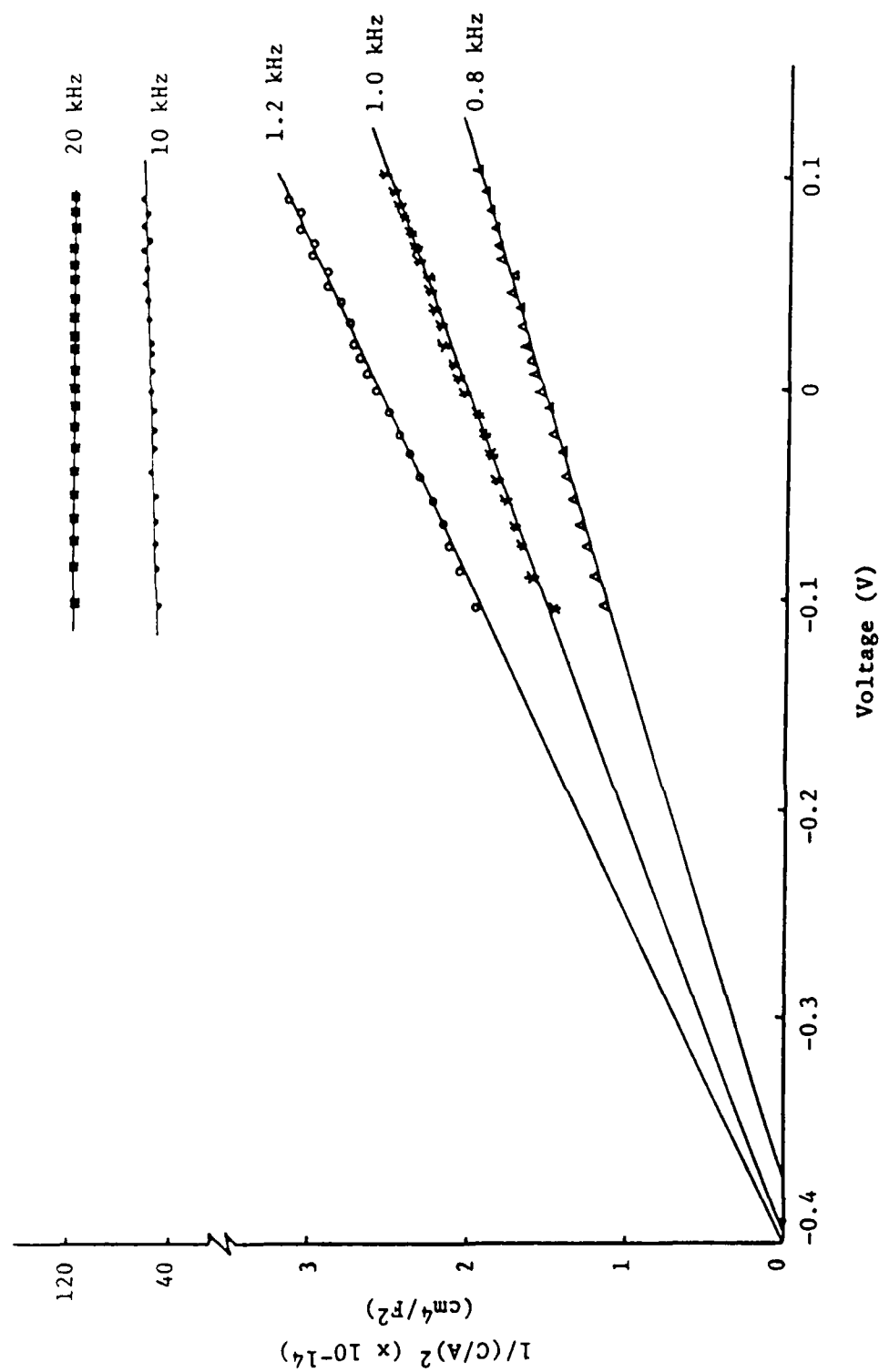


Figure 2. Frequency dependence of Mott-Schottky relation for a n-HfS<sub>2</sub> electrode at l-c orientation in 0.1M TBAPF<sub>6</sub> in CH<sub>3</sub>CN.



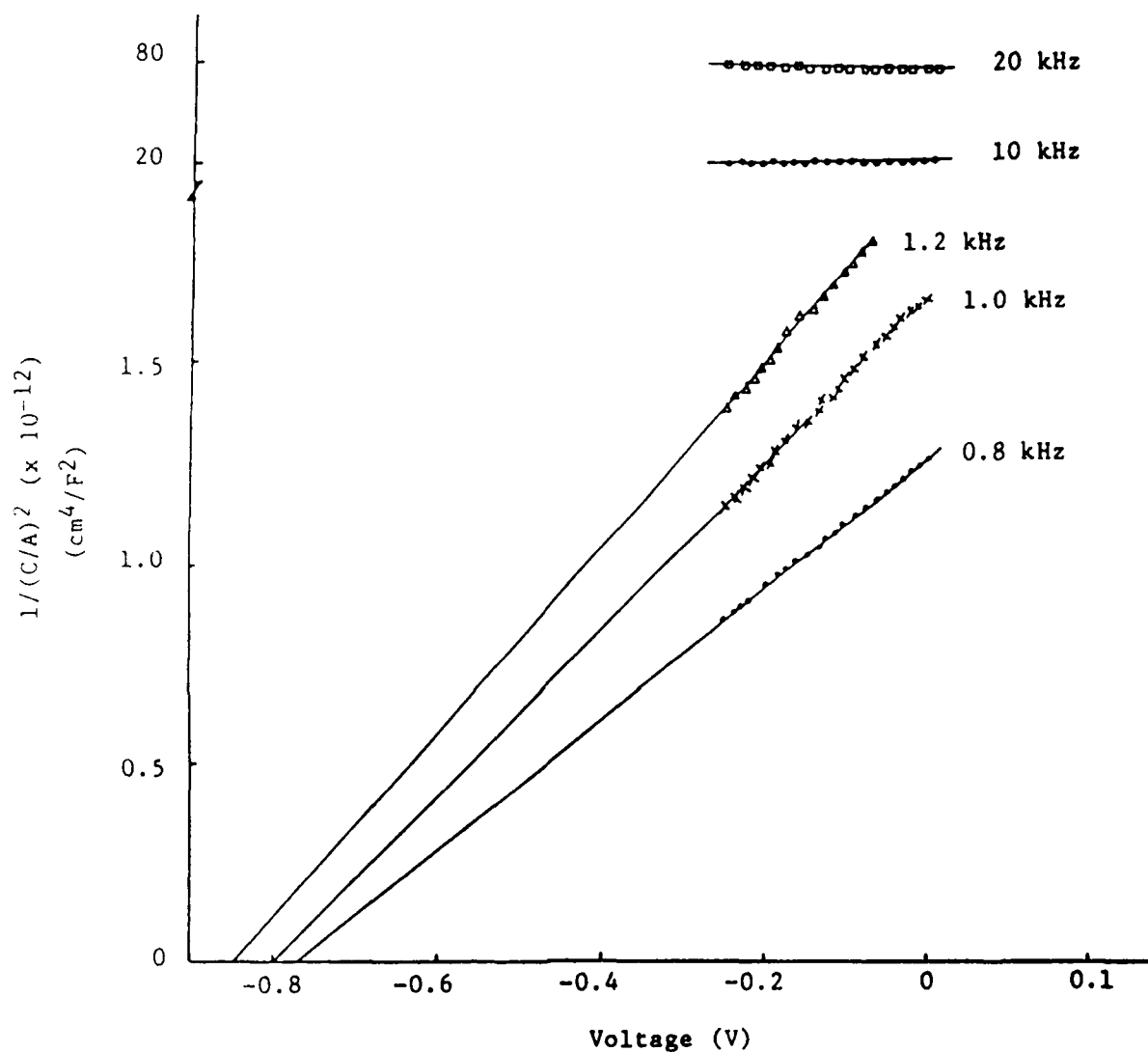


Figure 3. Frequency dependence of Mott-Schottky relation for n-HfS<sub>2</sub> electrode at ||-c orientation in 0.1M TBAPF<sub>6</sub> in CH<sub>3</sub>CN.

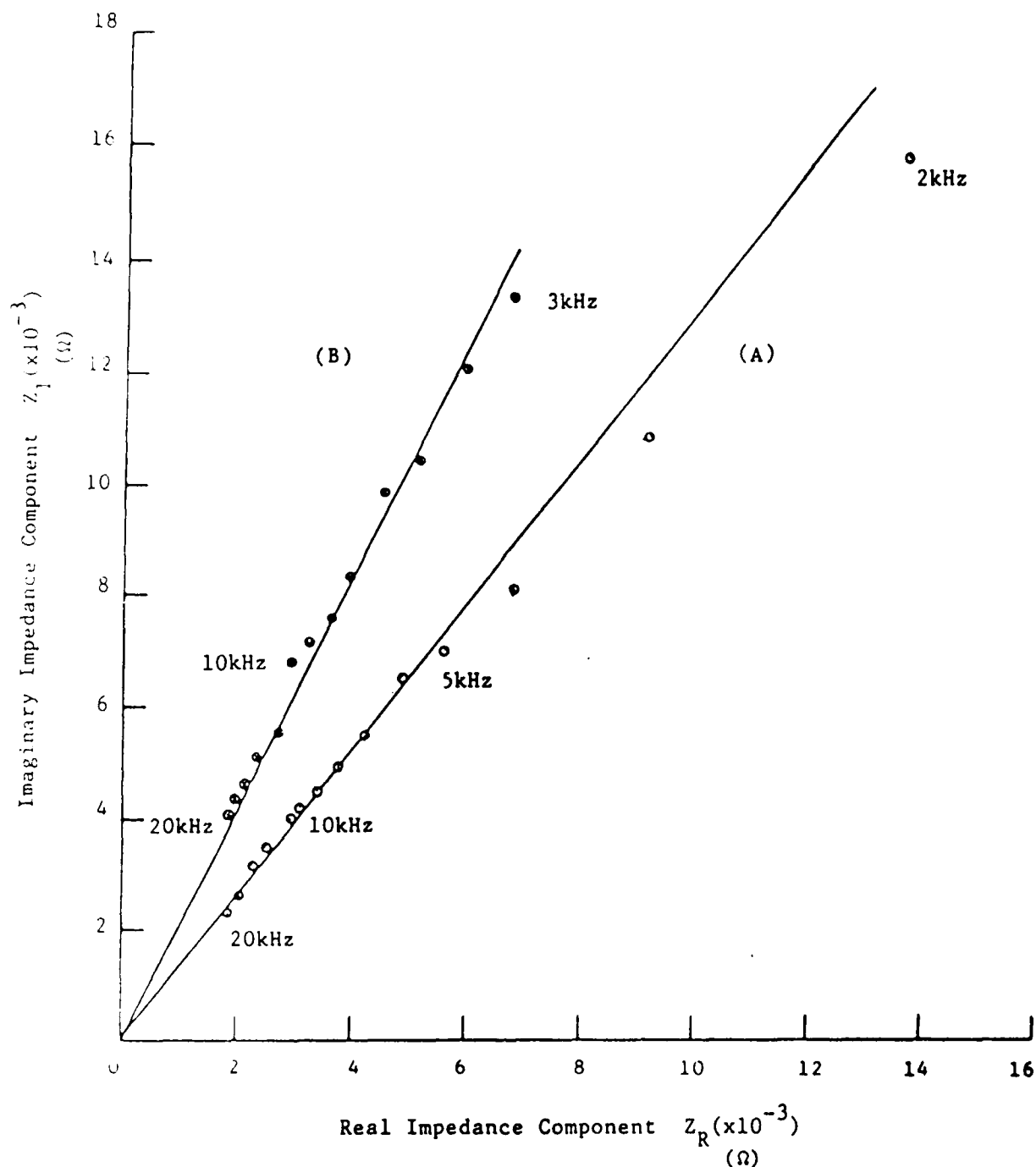


Figure 4. Impedance responses for an n-HfS<sub>2</sub> electrode at 1-c orientation in contact with 0.1M TBAPF<sub>6</sub> in CH<sub>3</sub>CN at -0.022V (A) and -0.172V (B) vs SCE. Counter electrode, Pt.

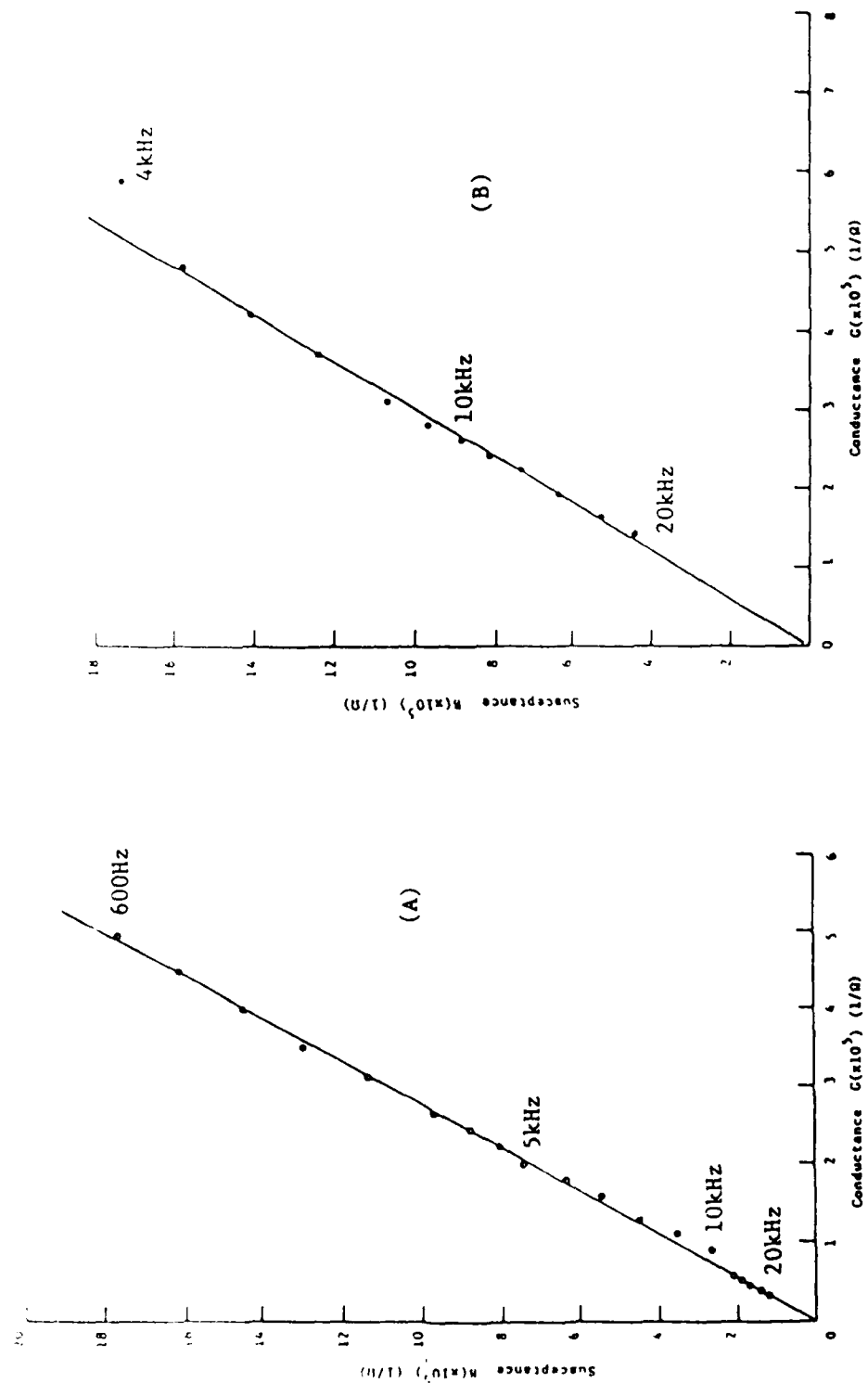
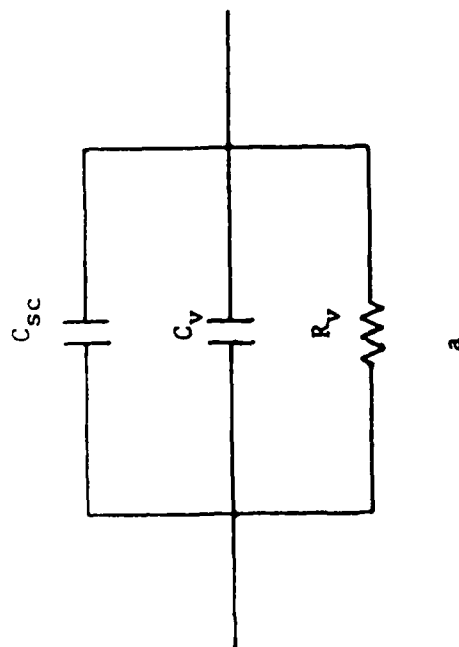


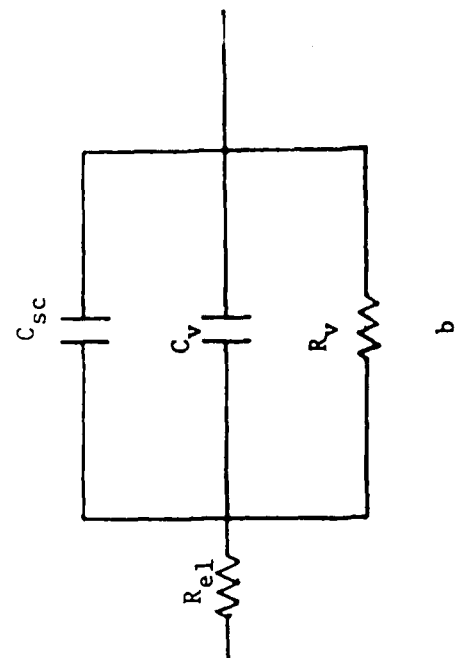
Figure 5. Admittance responses for L-c oriented n-HfS<sub>2</sub> in CH<sub>3</sub>CN/0.1M TBAPF<sub>6</sub> electrolyte at A) -0.022V and, B) -0.172V vs. SCE. Counter electrode Pt.

⊥-c Oriented n-HfS<sub>2</sub>



a

||-c Oriented n-HfS<sub>2</sub>



b

Figure 6. Equivalent circuits used in this work for rationalizing the cell n-HfS<sub>2</sub>/CH<sub>3</sub>CN/Pt as a function of crystal orientation.

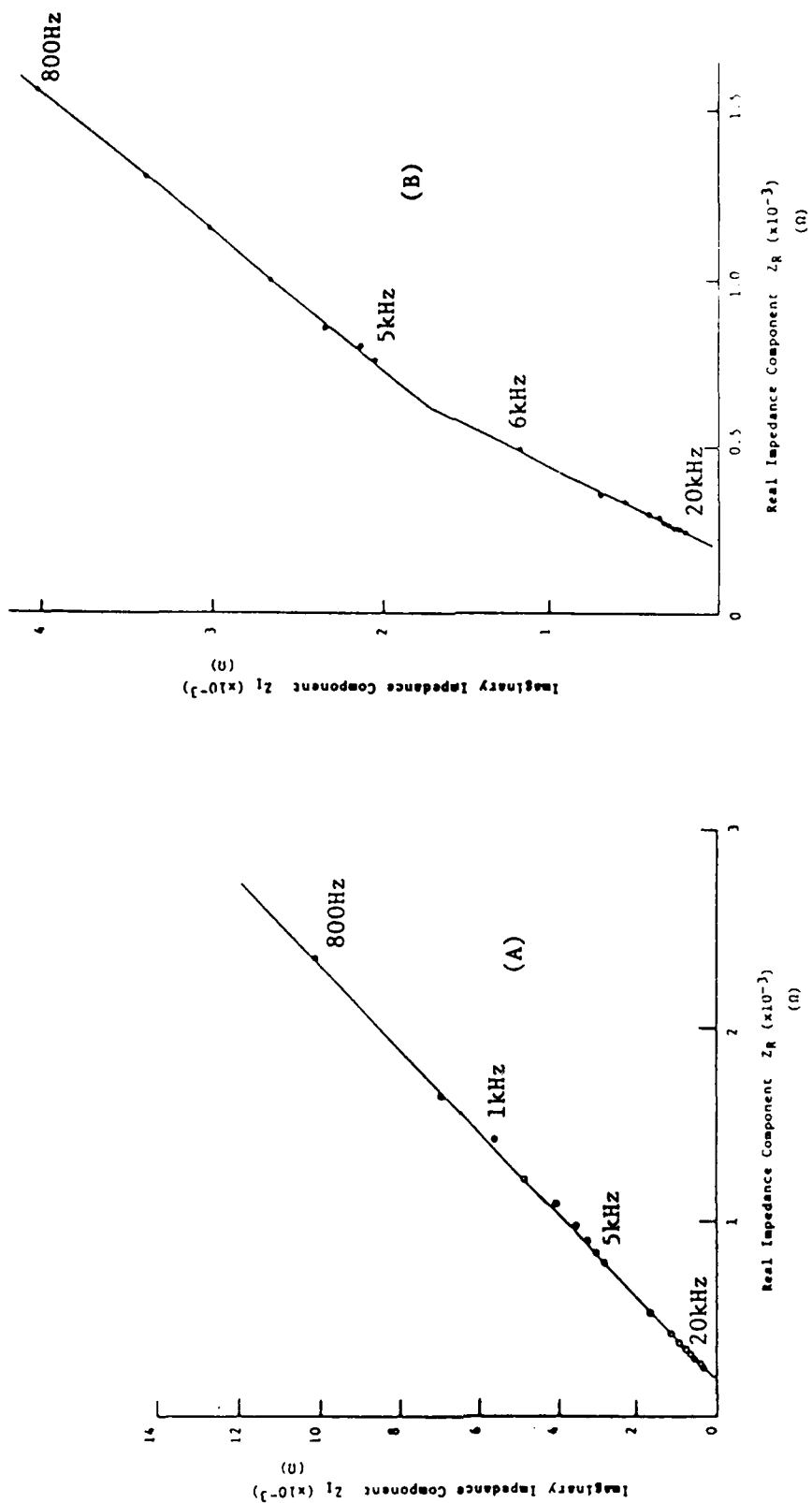


Figure 7. Impedance responses for ||-c oriented n-HfS<sub>2</sub> in CH<sub>3</sub>CN(0.1M TBAPF<sub>6</sub>) at A) -0.253V(SCE) and, B) -0.103V vs. SCE. Counter electrode Pt.

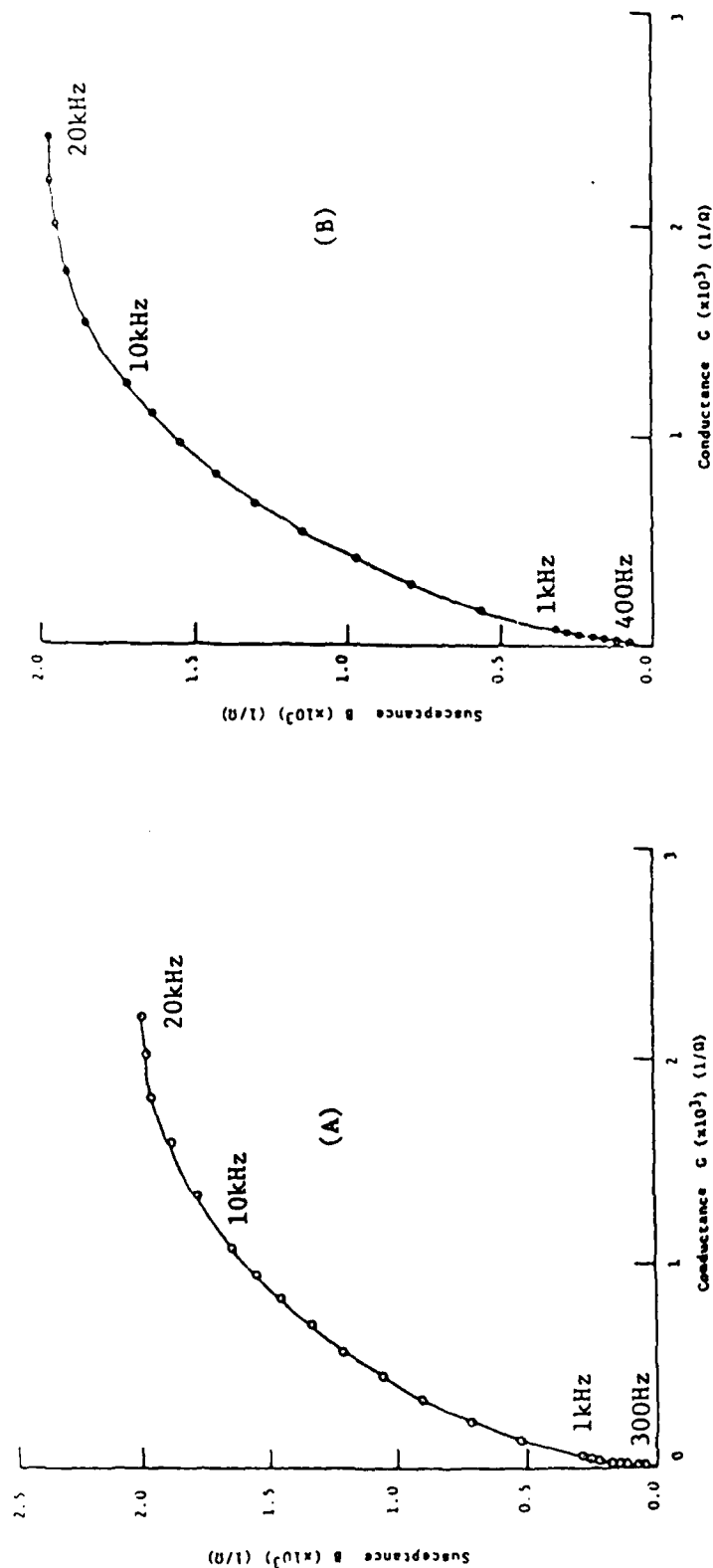


Figure 8. Admittance responses for 11-c oriented n-HfS<sub>2</sub> electrode in CH<sub>3</sub>CN(0.1M TBAPF<sub>6</sub>) at A) -0.103V(OCP) and, B) -0.253V vs. SCE. Counter electrode Pt.

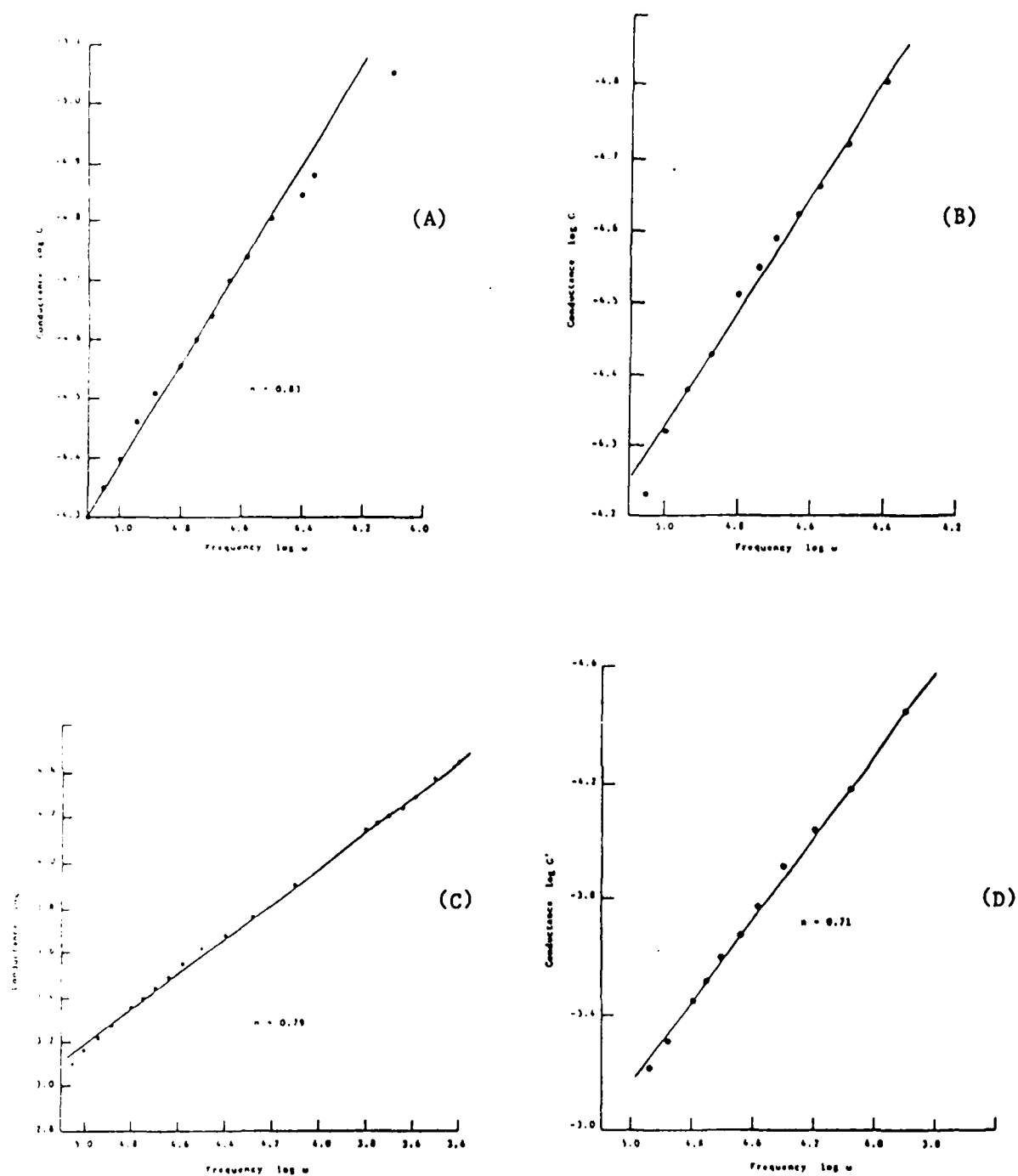


Figure 9. Conductance frequency response for n-HfS<sub>2</sub> in CH<sub>3</sub>CN (0.1M TBAPF<sub>6</sub>) A)  $\perp$ -c orientation at -0.022V; and B)  $\perp$ -c orientation at -0.172V; C)  $\parallel$ -c orientation at -0.103V(OCP), and D)  $\parallel$ -c orientation at -0.253V, all versus SCE.

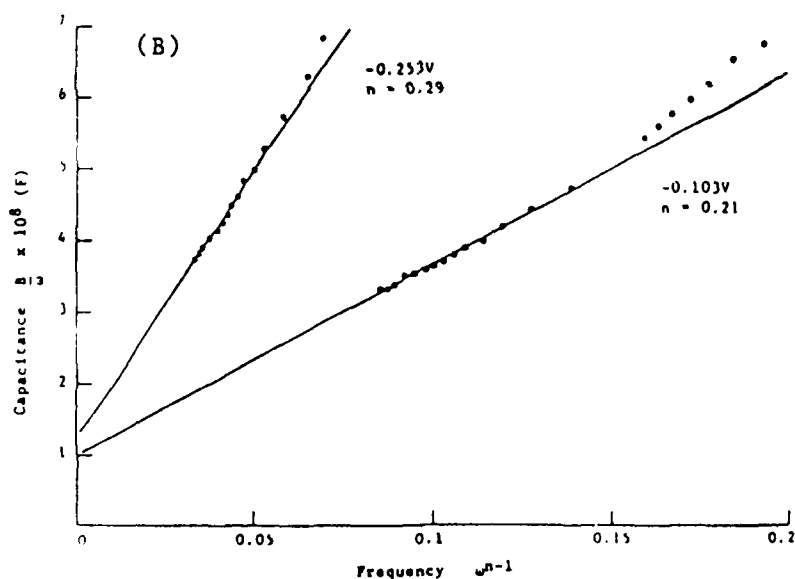
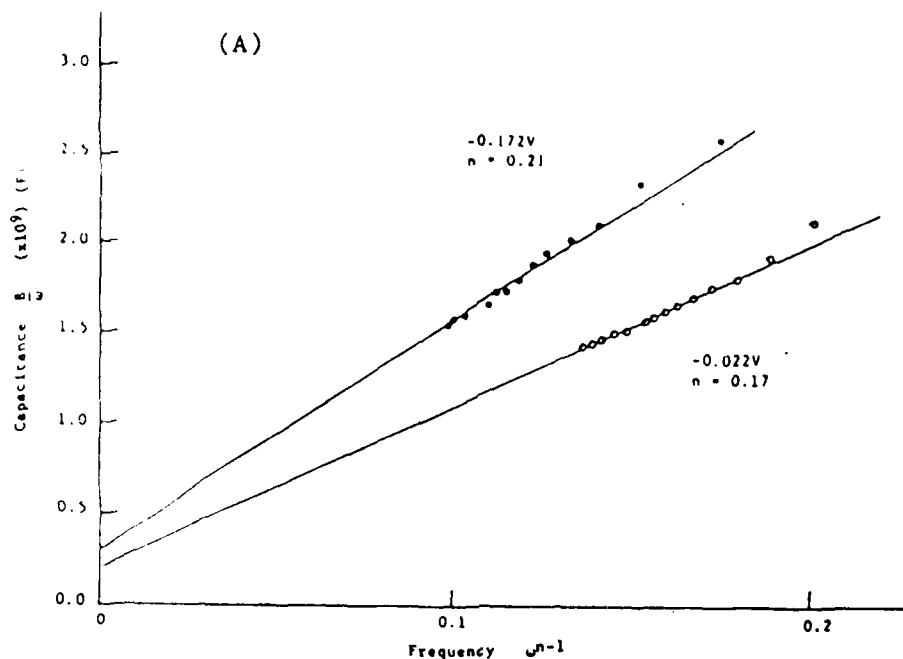


Figure 10. Capacitance frequency dependence for the cell  $n\text{-HfS}_2 / 0.1\text{M TBAPF}_6, \text{CH}_3\text{CN/Pt}$  A)  $\perp$ -c oriented  $n\text{-HfS}_2$  at  $-0.022\text{V}$  and  $-0.172\text{V}$ , B)  $\parallel$ -c oriented  $n\text{-HfS}_2$  at  $-0.103\text{V}$  and  $-0.253\text{V}$ . SCE used as reference electrode.



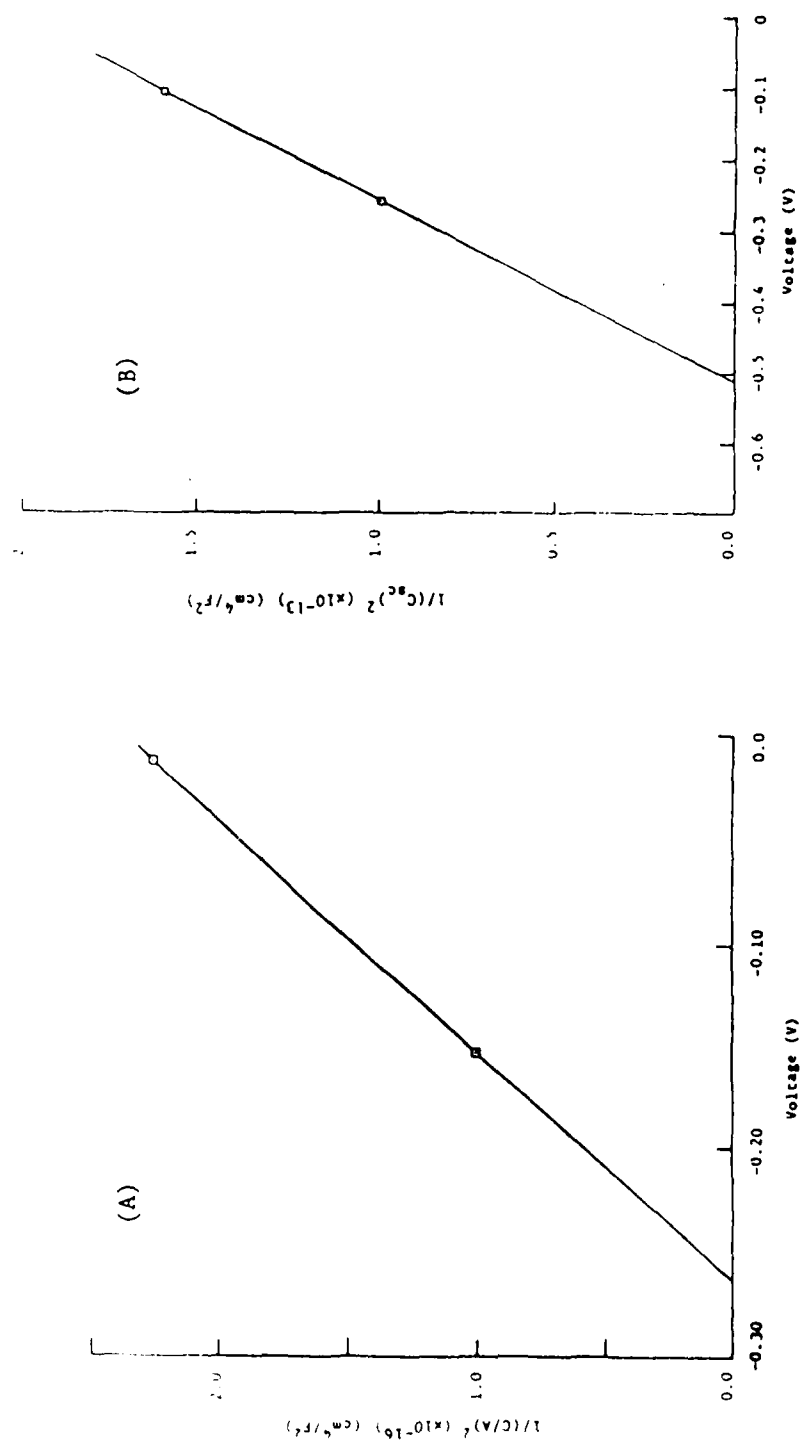


Figure 11. Frequency independent Mott-Schottky plot for n-HfS<sub>2</sub> in CH<sub>3</sub>CN(0.1M TBAPF<sub>6</sub>)  
 A) 1-c oriented, B) 11-c oriented.

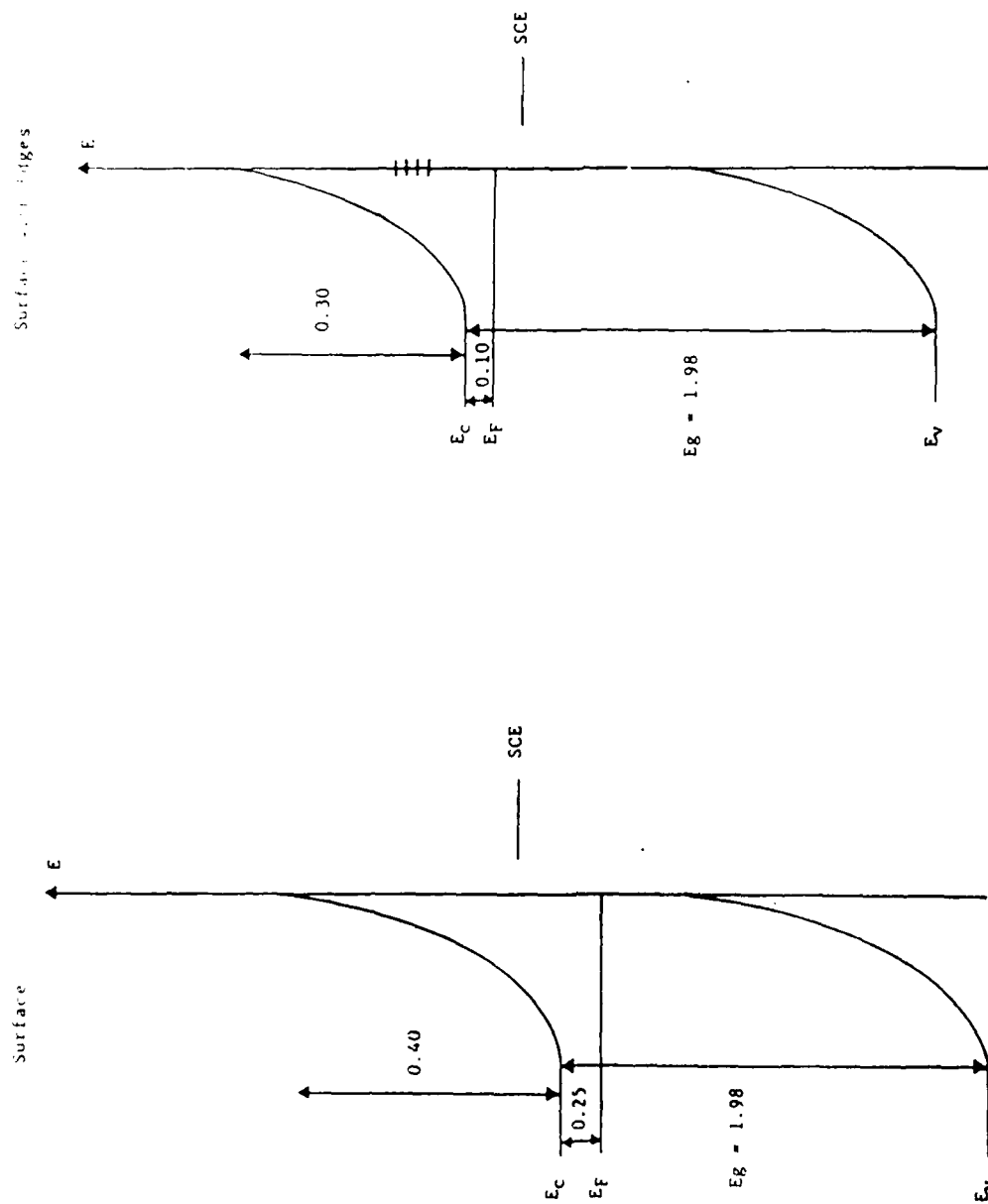


Figure 12. Energy schemes for n-HfS<sub>2</sub> electrode in 0.1M TBAPF<sub>6</sub>/CH<sub>3</sub>CN. Flat band potentials are based on frequency-independent results.

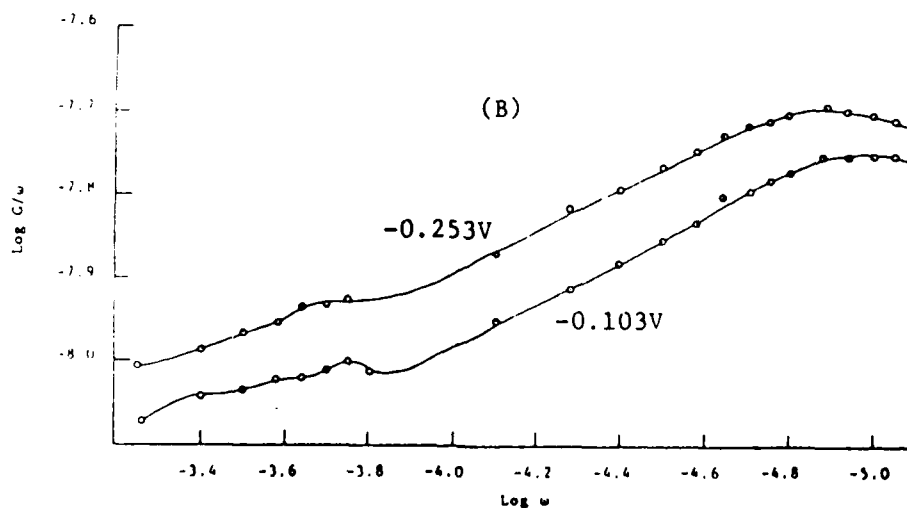
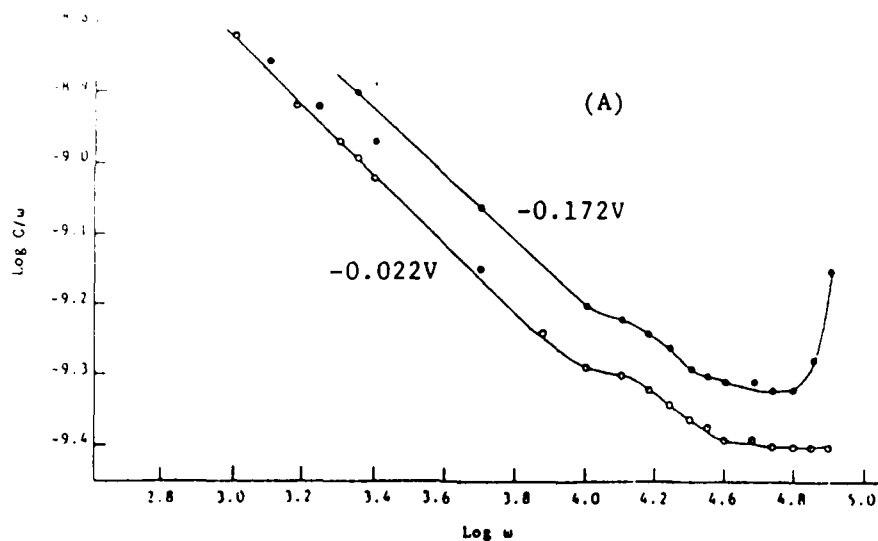


Figure 13. Frequency dependence of  $G/\omega$  values for  $n\text{-HfS}_2$  electrode in  $\text{CH}_3\text{CN}$  (0.1M  $\text{TBAPF}_6$ ). A) 1-c oriented, B) 11-c oriented. Electrode potential (vs. SCE) is shown next to the curves.

SECURITY CLASSIFICATION OF THIS PAGE (When Data Entered)

REPORT DOCUMENTATION PAGE		READ INSTRUCTIONS BEFORE COMPLETING FORM
1. REPORT NUMBER 3	2. GOVT ACCESSION NO.	3. RECIPIENT'S CATALOG NUMBER
4. TITLE (and Subtitle) Impedance and Admittance Measurements at Inter- calated n-HfS <sub>2</sub> /Non-Aqueous Electrolyte Interface		5. TYPE OF REPORT & PERIOD COVERED Technical Oct. 1986 - July 1987
		6. PERFORMING ORG. REPORT NUMBER
7. AUTHOR(s) K. W. Semkow, N. U. Pujare and A. F. Sammells		8. CONTRACT OR GRANT NUMBER(s) N00014-86-C-0128
9. PERFORMING ORGANIZATION NAME AND ADDRESS Eltron Research, Inc. 4260 Westbrook Drive Aurora, IL 60504		10. PROGRAM ELEMENT, PROJECT, TASK AREA & WORK UNIT NUMBERS
11. CONTROLLING OFFICE NAME AND ADDRESS Office of Naval Research/Chemistry Program Arlington, VA 22217		12. REPORT DATE July 1987
		13. NUMBER OF PAGES 22
14. MONITORING AGENCY NAME & ADDRESS (if different from Controlling Office) Above		15. SECURITY CLASS. (of this report) Unclassified
		15a. DECLASSIFICATION/DOWNGRADING SCHEDULE
16. DISTRIBUTION STATEMENT (of this Report) Approved for public release, distribution unlimited.		
17. DISTRIBUTION STATEMENT (of the abstract entered in Block 20, if different from Report) Approved for public release, distribution unlimited.		
18. SUPPLEMENTARY NOTES Published: Journal of the Electrochemistry Society, <u>135</u> , 327 (1988)		
19. KEY WORDS (Continue on reverse side if necessary and identify by block number) Hafnium disulfide, capacitance, impedance, admittance spectroscopy, copper intercalation.		
20. ABSTRACT (Continue on reverse side if necessary and identify by block number) Capacitance, impedance and admittance studies were performed on single crystal n-HfS <sub>2</sub> before and after copper intercalation from acetonitrile based electrolyte. The n-HfS <sub>2</sub> /non-aqueous electrolyte interface was modelled by equivalent R-C circuits containing frequency dependent elements. Electrochemical intercalation by copper into n-HfS <sub>2</sub> introduced Faradaic conductance effects. The composition of copper intercalated n-HfS <sub>2</sub> in close proximity to the interfacial region was obtained assuming a diffusion coefficient for copper in n-HfS <sub>2</sub> of 10 <sup>-8</sup> cm <sup>2</sup> /sec. The photo-anode demonstrated apparent degeneracy for > 0.1 moles of intercalated copper,		

suggesting that progressive electronic population of the n-HfS<sub>2</sub> conduction band was occurring. Capacitance values for intercalated n-HfS<sub>2</sub> were of the order 10<sup>-6</sup>F/cm<sup>2</sup>.

IMPEDANCE AND ADMITTANCE MEASUREMENTS AT INTERCALATED

n-HfS<sub>2</sub>/NON-AQUEOUS ELECTROLYTE INTERFACE

Krystyna W. Semkow\*, Nirupama U. Pujare and Anthony F. Sammells\*

Eltron Research, Inc.  
Aurora, Illinois 60504

ABSTRACT

Capacitance, impedance and admittance studies were performed on single crystal n-HfS<sub>2</sub> before and after copper intercalation from acetonitrile based electrolyte. The n-HfS<sub>2</sub>/non-aqueous electrolyte interface was modelled by equivalent R-C circuits containing frequency dependent elements. Electrochemical intercalation by copper into n-HfS<sub>2</sub> introduced Faradaic conductance effects. The composition of copper intercalated n-HfS<sub>2</sub> in close proximity to the interfacial region was obtained assuming a diffusion coefficient for copper in n-HfS<sub>2</sub> of 10<sup>-8</sup>cm<sup>2</sup>/sec. The photoanode demonstrated apparent degeneracy for > 0.1 moles of intercalated copper, suggesting that progressive electronic population of the n-HfS<sub>2</sub> conduction band was occurring. Capacitance values for intercalated n-HfS<sub>2</sub> were of the order 10<sup>-6</sup>F/cm<sup>2</sup>.

\*Electrochemical Society Active Member

Key Words: hafnium disulfide, copper intercalation, impedance, capacitance, admittance measurements

Group IVB transition metal dichalcogenides (TMDs) comprising  $\text{HfS}_2$ ,  $\text{HfSe}_2$ ,  $\text{ZrS}_2$  and  $\text{ZrSe}_2$  are interesting materials for photoelectrochemical (PEC) study since they can in principle function as both a photoelectrode and simultaneously as the substrate electroactive material for the reversible intercalation of transition metal species<sup>1-13</sup>. For example, it has already been reported that  $\text{ZrS}_2$  and  $\text{HfS}_2$  are capable of maintaining their semiconducting properties after partial electrochemical intercalation by either Cu or Fe to form  $\text{ZrM}_y\text{S}_2$  and  $\text{HfM}_y\text{S}_2$  over the compositional range  $0 < y < 0.22$ <sup>13</sup>. Such intercalation does however result in a decrease of the band gap width. The group IVB TMDs have also been shown susceptible to cathodic intercalation by alkali and alkaline earth metals and organic species<sup>7-12</sup>. As expected, intercalation into these materials results in a widening of the van der Waals layers<sup>14</sup>. Group IVB TMDs possess an octahedral structure with electron photoexcitation within the semiconductor band gap proceeding from energy bands derived from bonding sulfur p-orbitals into metal  $t_{2g}$  d-orbitals<sup>6</sup>. These photoelectrodes possess indirect band gaps with high absorption coefficients, since most incident photons become captured within  $1000\text{\AA}$  from the interfacial region<sup>15</sup>.

Insight gained relating the dependency of photoelectrode properties for these materials on the presence or absence of intercalated metal species, will be of value for identifying conditions where they might be incorporated into PEC cells possessing in situ electrochemical energy storage. Work reported here applies impedance and admittance measurement techniques to single crystal n- $\text{HfS}_2$  materials in non-aqueous electrolyte, oriented parallel to the c-lattice vector ( $\parallel$ -c) where a high population of intercalation sites would be exposed. Measurements were performed on this photoanode before and after electrochemical intercalation by copper which allowed us to preliminarily model the interfacial region. From such information liquid non-aqueous electrolyte and solid polymer electrolyte PEC storage cells using this photoanode might be more systematically prepared.

#### EXPERIMENTAL

Single crystals of n- $\text{HfS}_2$  were prepared by the halogen ( $\text{I}_2$ ) vapor transport technique (Northwestern University). Initial solid-state chemical reaction between Hf (99.5%) and S (99.999%) was accomplished by heating an intimate mixture together with 5mg  $\text{I}_2$ /ml of the quartz transport tube volume. This was performed in a three temperature zone furnace. Typical thermal gradients used

were between 875°C and 800°C. Crystal growth occurred over 25 days. In all cases the relatively large crystals obtained were intrinsically n-type. Ohmic contact to n-HfS<sub>2</sub> was accomplished by sparking indium onto one side of the crystal using a 15 volt DC power supply. This was performed using a fine indium wire as a cathode with the other pole of the power supply clamped to the n-HfS<sub>2</sub> single crystal. When the indium wire was within ≈1mm of the crystal, a transient spark could be observed. This resulted in ion implantation of indium into the ohmic contact region. Current collection was performed with a nichrome wire attached with silver epoxy and cured at 120°C for 1h. Photoelectrodes were then appropriately isolated from later contact with the electrolyte by epoxy (Norton Chemplast), so that only the single crystal front face of interest was exposed. Typical photoelectrode areas for H-c oriented crystals were 0.06cm<sup>2</sup>.

Measurements were performed in a standard glass H-cell arrangement using a platinum counter electrode. SCE was used as a reference to the working electrode compartment via a salt bridge. Photoelectrode potentials were controlled by a Stonehart Associates BC 1200 potentiostat. Impedance, conductance and capacitance measurements were performed using a Hewlett-Packard 4276A digital LCZ meter over the frequency range 20kHz-100Hz.

### RESULTS AND DISCUSSION

Work performed was directed towards investigating the interfacial characteristics of single crystal n-HfS<sub>2</sub> in liquid non-aqueous electrolyte (acetonitrile containing 0.1M tetrabutylammonium hexafluorophosphate (TBAPF<sub>6</sub>) as the supporting electrolyte) in the presence of 0.001M CuCl, both with and without copper intercalation. From capacitance, impedance and admittance measurements the n-HfS<sub>2</sub>/liquid junction could be modelled by an equivalent circuit which incorporated frequency dependent resistances,  $R_v$ , capacitances,  $C_v$ , together with the n-HfS<sub>2</sub> space charge capacitance,  $C_{sc}$  and the cell resistance  $R_{el}$ . The presence of frequency dependent elements may originate from a variety of charge accumulation modes such as surface states caused by adsorption, inhomogeneous doping and crystal defects. Expressions for the total admittance  $Y$ , impedance  $Z$ , conductance  $G$ , and susceptance  $B$ , for an equivalent circuit consisting of a large number of R-C elements, could be represented by the following relationships<sup>16,17</sup>:



$$Y = a\omega^n + kb\omega^n \quad (1)$$

$$Z = A\omega^{-n} - jB\omega^{-n} \quad (2)$$

$$G = a\omega^n \quad (3)$$

$$B = b\omega^n \quad (4)$$

where A, B, a, b and n are characteristic circuit constants and  $\omega$  is the angular frequency.

Impedance and admittance responses for ||-c oriented n-HfS<sub>2</sub>/acetonitrile interface were performed over the frequency range 20kHz to 100Hz in the dark. The impedance and admittance results for this interfacial region in the absence of any copper intercalation within the n-HfS<sub>2</sub> or copper present in the electrolyte are shown respectively in Figures 1 and 2. The dark photoelectrode possessed an initial open-circuit potential (OCP) of -0.295V vs. SCE. The impedance data (Figure 1) could be approximated by two linear regions corresponding to high and low frequencies. From our previously reported work<sup>18</sup> on ||-c oriented n-HfS<sub>2</sub>, linear dependencies were found between real and imaginary impedance over this whole frequency range for dark photoelectrode possessing an OCP of -0.103V, however at -0.253V two linear regions were observed, analogous to the result obtained here. A change in dependence between real and imaginary parts of the cell impedance with frequency, as in Figure 1, suggested a complex equivalent circuit for the interfacial region in which the impedance response of one part predominates at low and another part at higher frequencies. From this data the cell resistance ( $R_{e1}$ ) was obtained by extrapolating the high frequency impedance data to infinite frequency giving  $R_{e1} = 165\Omega$ .

The admittance data shown in Figure 2 gave a semicircular plot. The intercept of the semicircle to the G-axis gave  $1/R_{e1}$ . No additional semicircular regions were observed indicating a different frequency dependence of admittance at high and low frequencies. Therefore, if the n-HfS<sub>2</sub> interfacial region could be represented by one general equivalent circuit acting as two separate circuits responsive to respectively high and low frequency regions, their time constants must be similar<sup>19,20</sup>. Impedance and admittance responses for the ||-c oriented n-HfS<sub>2</sub> interface can be explained by the equivalent circuits shown in Figure 3a. In this figure  $C_{sc}$  represents a frequency independent capacitance attributed to the photoanode space charge capacitance while  $C_v$  and  $R_v$  represent the frequency dependent capacitance and resistance, respectively, operating in high

and low frequency regions. The magnitude of  $C_{SC}$  is usually relatively small compared to  $C_V$  and in the low frequency region its contribution can be neglected<sup>19,20</sup>. The network operating at higher frequencies (A) accounts for the linear impedance response observed above 1kHz, crossing the real impedance axis at  $R_{e1}$  (Figure 1) as well as for a semicircular admittance response of radius  $1/R_{e1}$  (Figure 2). Another network (B) accounts for a change in impedance slope at frequencies below 1kHz and appears to possess a semicircular response analogous to that found at high frequencies. Upon introducing 0.001M CuCl into the above cell, the dark n-HfS<sub>2</sub> OCP changed from -0.295V to -0.11V vs. SCE. Copper intercalation proceeded into the n-HfS<sub>2</sub> by potentiostating the electrode at -0.26V vs. SCE when a steady-state cathodic current of the order of  $\approx 10\mu A$  occurred. The cathodic electrochemical intercalation of n-HfS<sub>2</sub> by copper could proceed in the dark since the necessary electrons are present as majority carriers. Impedance and admittance data were obtained after respectively 42 min. and 129 min. after initiating intercalation (Figures 4 to 7). Assuming a diffusion coefficient for copper intercalation of  $D = 10^{-8} \text{ cm}^2/\text{sec}$ , then a mean intercalation depth  $X$  given by equation (5) can be calculated:

$$X = \sqrt{2Dt} \quad (5)$$

and the respective degree of intercalation to this depth  $X$  after 42 and 129 min. would correspond to the stoichiometries  $\text{HfCu}_{0.18}\text{S}_2$  and  $\text{HfCu}_{0.3}\text{S}_2$ . The impedance data obtained (Figures 4 and 6) approximated a linear relationship between real and imaginary parts in the low frequency region with a circular dependence being observed at higher frequencies. This latter observation suggested an additional resistive element in parallel to the variable resistance in the network operating in the high frequency region shown in Figure 3a. A value for this new resistance  $R_0$  was estimated on the basis of the semicircular radius drawn through experimental data in this high frequency region. For n-HfS<sub>2</sub> copper intercalated for 42 min.  $R_0$  was found to be of the order  $\approx 200\Omega$ . Such resistance was not found in the absence of copper intercalation suggesting that  $R_0$  may represent resistance for reversible intercalation by copper in n-HfS<sub>2</sub>.

At measurement frequencies below 1kHz the imaginary part of the cell impedance was found to decrease by an order of magnitude after initial copper intercalation and progressively decreased upon further intercalation as shown by reference to Figures 1, 4 and 6. This observation suggested an increased capacitive cell response in the low frequency region attributable to the presence of intercalated

copper. Similar conclusions could also be drawn from the admittance data shown in Figures 2, 5 and 7. For measurement frequencies below  $\approx 1$  kHz copper intercalated n-HfS<sub>2</sub> showed higher susceptance values (Figures 5, 7) compared to when copper was absent (Figure 2). This suggests the presence of a capacitive element associated with Faradaic copper intercalation  $C_0$ , in series with  $R_0$  in this lower frequency range.

Admittance data obtained after respectively 42 and 129 min. of copper intercalation demonstrated a semicircular response in both the low and high frequency region as shown respectively in Figure 5 and 7. This observation may be attributable to differences in time constants for predominant circuit elements operating in high and low frequency ranges for copper intercalated n-HfS<sub>2</sub>. The overall impedance and admittance response experimentally observed for copper intercalated n-HfS<sub>2</sub> in acetonitrile could be modelled by the equivalent circuits shown in Figure 3b. This circuit combines all the network elements explaining experimental observations in the high and low frequency regions. In these equivalent circuits the capacitance element  $C_0$  associated with reversible copper intercalation may be omitted in the high frequency region, whereas n-HfS<sub>2</sub> space charge capacitance  $C_{sc}$  may be eliminated at lower frequencies.

To investigate the influence of intercalated copper on n-HfS<sub>2</sub>  $C_{sc}$  in acetonitrile, impedance and admittance responses were analyzed as previously described by others<sup>16,17</sup>.  $C_{sc}$  for  $\parallel$ -c oriented n-HfS<sub>2</sub> in acetonitrile was obtained by subtracting susceptance values associated with cell resistance,  $R_{el}$ , from measured susceptance and by extrapolating capacitance data to infinite frequency (Figure 8). A value for  $C_{sc}$  of  $\approx 3.2 \times 10^{-7}$  F/cm<sup>2</sup> at -0.295V vs. SCE was obtained, higher than  $2.5 \times 10^{-7}$  F/cm<sup>2</sup> at -0.103V vs. SCE determined in a previous study<sup>18</sup> by us using similar single crystal material, as expected at the more negative electrode potential used here. The dark  $C_{sc}$  for n-HfS<sub>2</sub> increased to  $1.4 \times 10^{-6}$  F/cm<sup>2</sup> after intercalating copper at -0.26V vs. SCE and remained essentially constant during the intervening (129 min.) intercalation (Figure 9). The potential of the dark n-HfS<sub>2</sub> electrode after 10-129 min. intercalation was relatively constant and remained at  $\approx -0.1$ V vs. SCE during 129 min. of intercalation. This suggested an equilibrium concentration of intercalated copper present after about 10 min. with further intercalation resulting in deeper copper incorporation into the crystal structure. For longer copper deposition times than 129 min. unit activity copper was evident on the n-HfS<sub>2</sub> surface after which the OCP became -0.4V vs. SCE. Cyclic

voltammograms for copper intercalated n-HfS<sub>2</sub> in acetonitrile are shown in Figure 10. The current peak corresponding to the reversible intercalation of copper was found to increase somewhat with time as the degree of copper intercalation was increased. Again this suggested that the semiconductor surface came relatively quickly to equilibrium (within  $\approx 10$  min.) in the concentration of intercalated copper. For single crystal n-HfS<sub>2</sub> used in this work the initial photopotential obtained prior to intercalation was 217mV under 100mW/cm<sup>2</sup> ELH illumination, but was found to decrease to 55mV upon initial copper intercalation, 36mV after 5 min. at  $\approx 10\mu\text{A}$  and 18mV after 10 min. No photopotential was observed after 42 min.

To gain further insight into the influence of intercalated copper on the behavior of n-HfS<sub>2</sub> admittance spectroscopy analysis of the admittance data was performed<sup>21,22</sup>. Results of this analysis are summarized in Figure 11. In the simplest case the n-HfS<sub>2</sub>/electrolyte interface was assumed to consist of the space charge capacitance,  $C_{sc}$ , connected in series with a bulk conductance  $G_{el}$ . By comparing real and imaginary parts of the admittance equation for such an equivalent circuit, with the appropriate in-phase admittance components being obtained experimentally, the following relationship can be obtained:

$$G/\omega = \frac{\omega C_{sc}^2 G_{el}}{G_B^2 + (\omega C_{sc})^2} \quad (6)$$

where  $G$  represents the measured in-phase cell conductance. By plotting  $G/\omega$  vs.  $\omega$  a maximum was given at

$$G/\omega_{\max} = C_{sc}/2 \quad (7)$$

from which the space charge capacitance was determined. The peak  $G/\omega$  (where  $G$  corresponds to the total cell conductance) was identified with the n-HfS<sub>2</sub> space charge capacitance (curve A). Upon introducing CuCl into the electrolyte (curves B-D) evidence for an additional parameter in the equivalent circuit became evident. This was interpreted as corresponding to a Faradaic conductance in parallel to  $C_{sc}$  as shown by a linear  $\log G/\omega$  vs.  $\log \omega$  relationship<sup>21,22</sup>. At sufficiently low frequencies the measured conductance became equal to the Faradaic conductance. Thus, increased conductance in the low/middle frequency region for copper intercalated HfS<sub>2</sub> gave evidence for the Faradaic intercalation-deintercalation reaction of copper. Unfortunately, increased conductance by the cell due to electron transfer at the interface

overshadows effects from the space charge capacitance. Deposition of copper onto the n-HfS<sub>2</sub> surface (curve E) shifted the conductance associated with the Faradaic reaction to even higher values. This suggested a higher exchange current density for this copper compared to that intercalated within the n-HfS<sub>2</sub>.

It has been suggested that metals intercalated into group IVB TMDs result in the formation of energy levels within the band gap<sup>7</sup>. Copper deintercalation from voltammetric experiments occur even in the absence of any measurable photopotential suggesting the formation of energy levels close to the conduction band during intercalation. A similar explanation has been postulated<sup>23</sup> for cyclopropylamine intercalated HfSe<sub>2</sub>. Intercalation by copper or iron into ZrS<sub>2</sub> and HfS<sub>2</sub> by others<sup>13</sup> has indicated that the electrode remains semiconducting at intercalation levels below HfCu<sub>0.22</sub>S<sub>2</sub>. It is probable that in work discussed here the degree of copper intercalation may have been higher than calculated using the diffusion coefficient 10<sup>-8</sup>cm<sup>2</sup>/sec. To preserve n-HfS<sub>2</sub> semiconducting properties the total charge passed during copper intercalation should be lower than 0.3C per 1cm<sup>2</sup> for  $\parallel$ -c oriented material. Such intercalating photoelectrodes may eventually be of interest in liquid non-aqueous or solid polymer electrolyte cells. In the latter cells the deintercalated transition metal ions would be stored in close proximity to the electrode/solid electrolyte interfacial region.

#### CONCLUSION

The  $\parallel$ -c oriented n-HfS<sub>2</sub>/non-aqueous electrolyte interface can be modelled by equivalent circuits consisting of space charge capacitance, cell resistance and frequency dependent R-C elements. In the presence of intercalated copper in n-HfS<sub>2</sub> increased Faradaic conduction became evident related to intercalation-deintercalation at the interfacial region. The space charge capacitance of n-HfS<sub>2</sub> in acetonitrile was obtained by eliminating the capacitive response of frequency dependent elements and was found to be of the order 10<sup>-7</sup> F/cm<sup>2</sup>. This increased to 10<sup>-6</sup> F/cm<sup>2</sup> after intercalating > 18m/o copper into this semiconductor. Electrochemical copper deintercalation proceeded in the dark suggesting that the semiconductor became degenerate at this degree of intercalation with a high population of electrons being localized close to the n-HfS<sub>2</sub> conduction band.

#### ACKNOWLEDGEMENT

This work was supported in part by the Office of Naval Research.

## REFERENCES

1. J. A. Wilson and A. D. Yoffee, *Adv. Phys.*, 18, 193 (1969).
2. E. Mooser, Ed., Physics and Chemistry of Materials with Layered Structures, Reidel, Dordrecht, Boston, MA, 1976.
3. R. B. Murray, R. A. Bromley and A. D. Yoffee, *J. Phys. C. Solid State Phys.*, 5, 746 (1972).
4. L. F. Mattheiss, *Phys. Rev.*, B8, 3719 (1973).
5. H. Tributsch, *J. Electrochem. Soc.*, 128, 1261 (1981).
6. H. Tributsch, *Faraday Discuss. Chem. Soc.*, 70, 190 (1981).
7. M. Abramovich, H. Tributsch and O. Gorochoy, *J. Electroanal. Chem.*, 153, 115 (1983).
8. M. Abramovich and H. Tributsch, *J. Electroanal. Chem.*, 138, 121 (1982).
9. H. Tributsch, *Appl. Phys.*, 23, 61 (1980).
10. F. R. Gamble and T. H. Geballe, Treatise on Solid State Chemistry, Vol 3, Plenum Press, New York, 1976.
11. G. V. Subbarao and J. C. Tsang, *Mater. Res. Bull.*, 9, 921 (1974).
12. M. S. Whittingham, U.S. Patent 4,040,917 (1977).
13. B. G. Yacobi, F. W. Boswell and J. M. Corbett, *J. Phys. C. Solid State Phys.*, 12, 2189 (1979).
14. W. Kantele, H. Gerischer and H. Tributsch, *Ber. Bunsenges Phys. Chem.*, 83, 1000 (1979).
15. H. Tributsch, *Structure and Bonding*, 49, 128 (1982).
16. J. F. McCann, S. P. S. Badwal and J. Pezy, *J. Electroanal. Chem.*, 118, 115 (1981).
17. J. F. McCann and S. P. S. Badwal, *J. Electrochem. Soc.*, 129, 551 (1982).
18. K. W. Semkow, N. U. Pujare and A. F. Sammells, *J. Electrochem. Soc.*, (submitted).
19. S. P. S. Badwal and H. J. de Bruin, *Phys. Status Solidi A*, 54, 261 (1979).
20. I. D. Raistrick, C. Ho and R. A. Huggins, *J. Electrochem. Soc.*, 123, 1469 (1976).
21. P. A. Smith, "Electrical Characterization of Polycrystalline and Photo-electrochemical Solar Cells", M. S. Thesis, Colorado State University, Ft. Collins, CO (1980).
22. J. Dubow and R. Krishnar, "Novel Concepts in Electrochemical Solar Cells", SERI Final Report, Contract No. XS-0-9272-1 (October 1981).
23. A. R. Beal and W. Y. Liang, *Phil. Mag.*, 27, 1397 (1973).

# FIGURE CAPTIONS

- Figure 1. Impedance response for  $\parallel$ -c oriented n-HfS<sub>2</sub> in CH<sub>3</sub>CN (0.1M TBAPF<sub>6</sub>) at OCP (-0.295V).
- Figure 2. Admittance response for  $\parallel$ -c oriented n-HfS<sub>2</sub> in CH<sub>3</sub>CN (0.1M TBAPF<sub>6</sub>) at OCP (-0.295V).
- Figure 3a. Equivalent circuits for  $\parallel$ -c oriented n-HfS<sub>2</sub> in CH<sub>3</sub>CN (0.1M TBAPF<sub>6</sub>) at high (A) and low (B) frequencies.
- Figure 3b. Equivalent circuit for copper intercalated  $\parallel$ -c oriented n-HfS<sub>2</sub> in CH<sub>3</sub>CN (0.1M TBAPF<sub>6</sub> + 0.001M CuCl) at high (A) and low (B) frequencies.
- Figure 4. Impedance response for  $\parallel$ -c oriented n-HfS<sub>2</sub> in CH<sub>3</sub>CN (0.1M TBAPF<sub>6</sub> + 0.001M CuCl) after 42 minutes copper intercalation ( $\approx 10\mu\text{A}$ ) at -0.26V vs. SCE.
- Figure 5. Admittance response for  $\parallel$ -c oriented n-HfS<sub>2</sub> in CH<sub>3</sub>CN (0.1M TBAPF<sub>6</sub> + 0.001M CuCl) after 42 minutes copper intercalation ( $\approx 10\mu\text{A}$ ) at -0.26V vs. SCE.
- Figure 6. Impedance response for  $\parallel$ -c oriented n-HfS<sub>2</sub> in CH<sub>3</sub>CN (0.1M TBAPF<sub>6</sub> + 0.001M CuCl) after 129 minutes copper intercalation ( $\approx 10\mu\text{A}$ ) at -0.26V vs. SCE.
- Figure 7. Admittance response for  $\parallel$ -c oriented n-HfS<sub>2</sub> in CH<sub>3</sub>CN (0.1M TBAPF<sub>6</sub> + 0.001M CuCl) after 129 minutes copper intercalation ( $\approx 10\mu\text{A}$ ) at -0.26V vs. SCE.
- Figure 8. Frequency dependent capacitance for  $\parallel$ -c oriented n-HfS<sub>2</sub> in CH<sub>3</sub>CN (0.1M TBAPF<sub>6</sub>) at OCP (-0.295 vs. SCE). Geometric electrode area 0.06cm<sup>2</sup>.
- Figure 9. Frequency dependent capacitance for  $\parallel$ -c oriented n-HfS<sub>2</sub> in CH<sub>3</sub>CN (0.1M TBAPF<sub>6</sub> + 0.001M CuCl) after copper intercalation at -0.26V vs. SCE ( $\approx 10\mu\text{A}$ ) for 10 minutes (curve A), 42 minutes (curve B) and 129 minutes (curve C). Geometric electrode area 0.06cm<sup>2</sup>.
- Figure 10. Cyclic voltammograms for  $\parallel$ -c oriented n-HfS<sub>2</sub> in CH<sub>3</sub>CN (0.1M TBAPF<sub>6</sub> + 0.001M CuCl) after copper intercalation of -0.26V ( $\approx 10\mu\text{A}$ ) for A) 2 min., B) 5 min., and C) 10 min. Scan rate: 20mV/sec.
- Figure 11. Relationship between  $G/\omega$  and  $\omega$  for  $\parallel$ -c oriented n-HfS<sub>2</sub> in CH<sub>3</sub>CN (0.1M TBAPF<sub>6</sub>) without (curve A) and with (curves B-E) 0.001M CuCl. Curve A at OCP -0.295V vs. SCE. Curves B, C and D after 10, 42 and 129 minutes respectively copper intercalation at -0.26V ( $\approx 10\mu\text{A}$ ) (OCP -0.1V); E after 130 minutes when copper deposition on the n-HfS<sub>2</sub> surface became evident (OCP -0.4V vs. SCE).

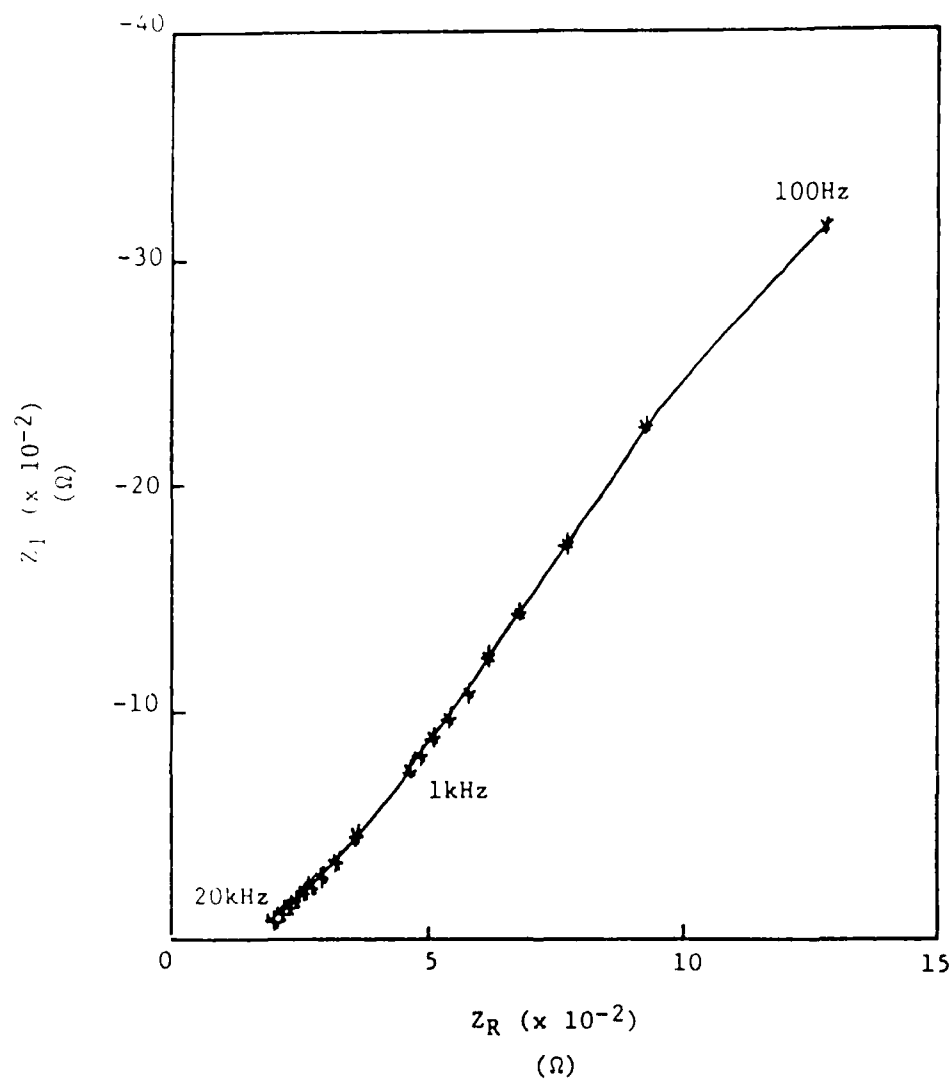


Figure 1. Impedance response for ||-c oriented n-HfS<sub>2</sub> in CH<sub>3</sub>CN (0.1M TBAPF<sub>6</sub>) at OCP (-0.295V).



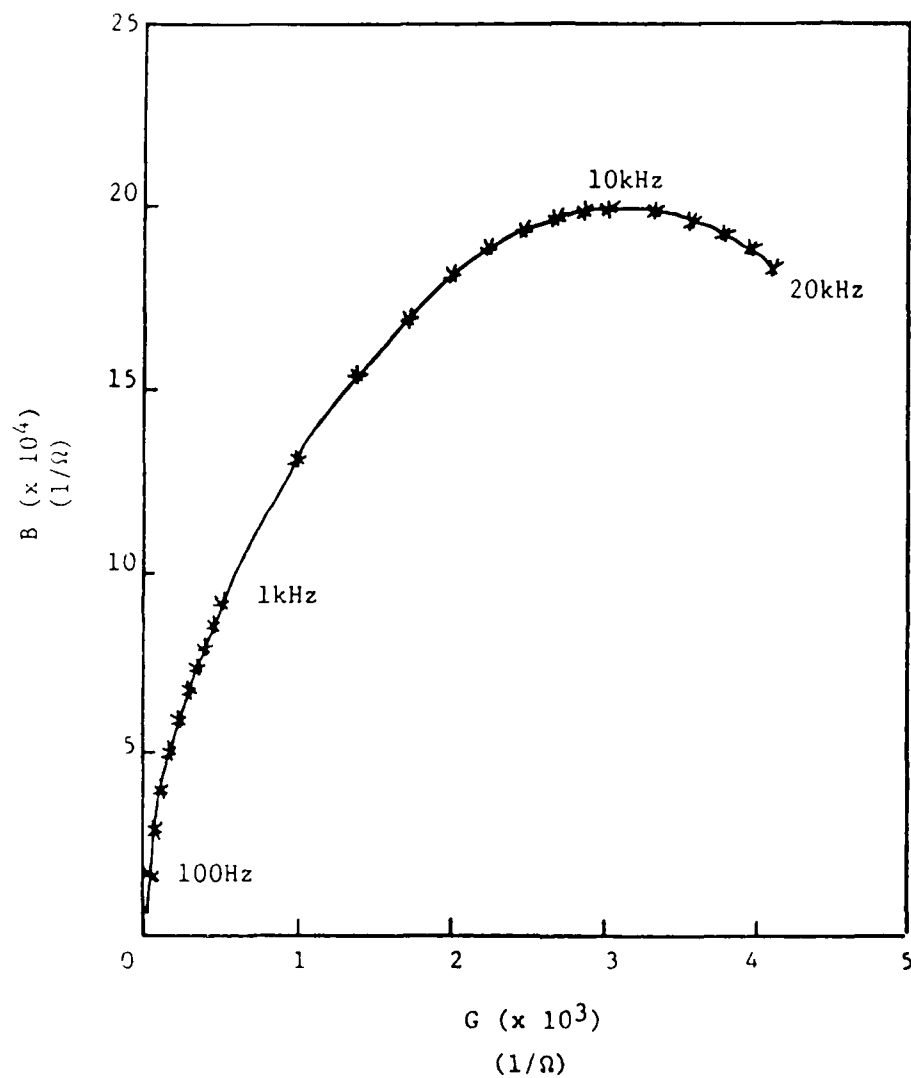


Figure 2. Admittance response for ||-c oriented n-HfS<sub>2</sub> in CH<sub>3</sub>CN (0.1M TBAPF<sub>6</sub>) at OCP (-0.295V).

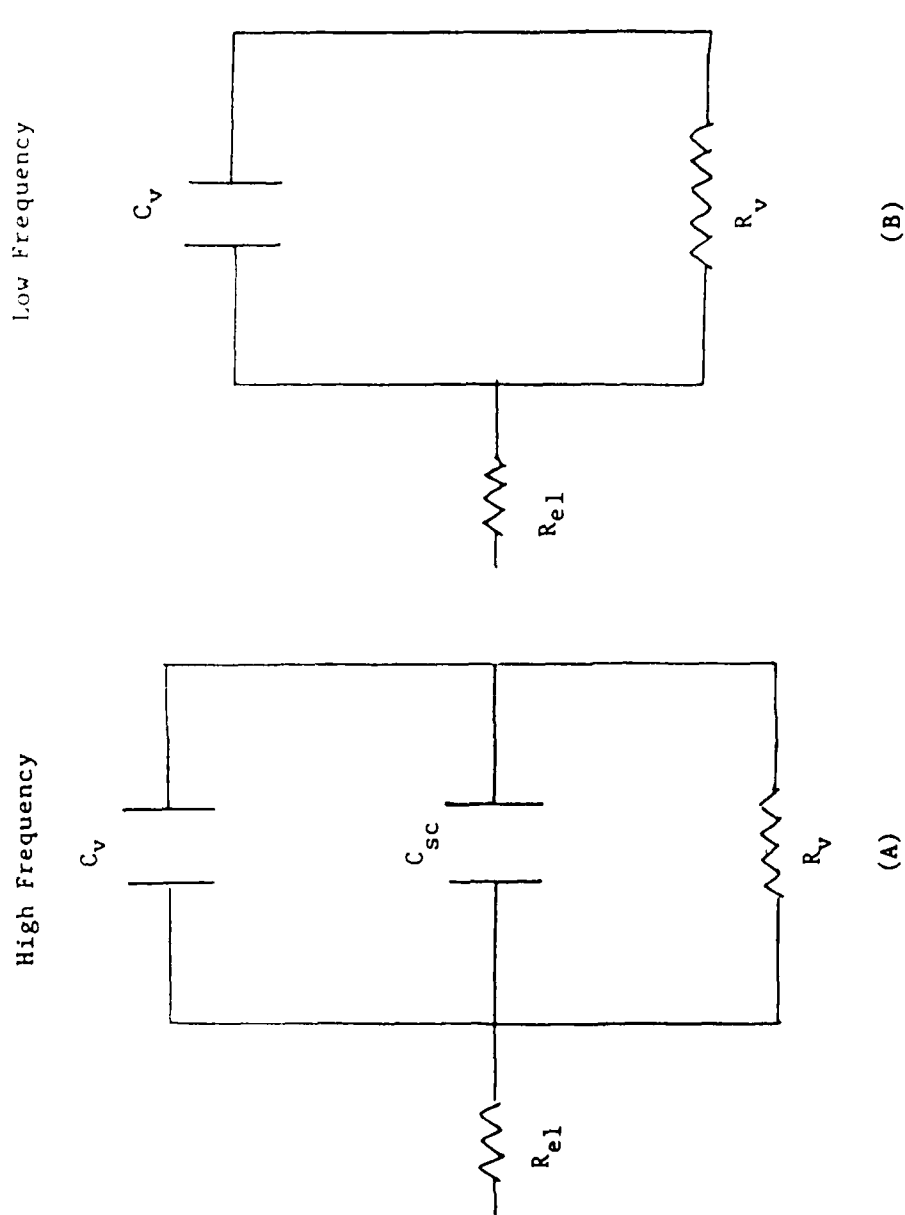


Figure 3a. Equivalent circuits for ||-c oriented n-HfS<sub>2</sub> in CH<sub>3</sub>CN (0.1M TBAPF<sub>6</sub>) at high (A) and low (B) frequencies.

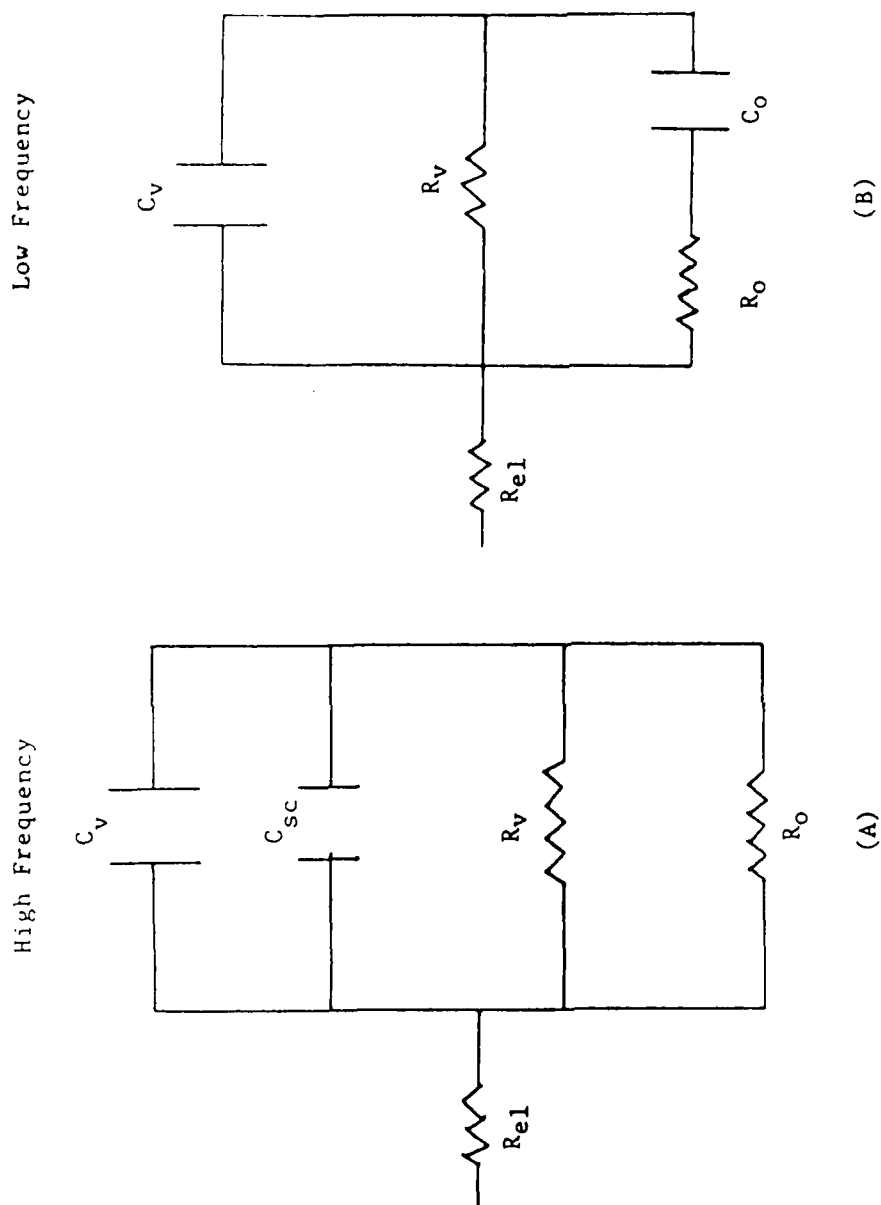


Figure 3b. Equivalent circuit for copper intercalated Il-c oriented n-HfS<sub>2</sub> in CH<sub>3</sub>CN (0.1M TBAPF<sub>6</sub> + 0.001M CuCl) at high (A) and low (B) frequencies.

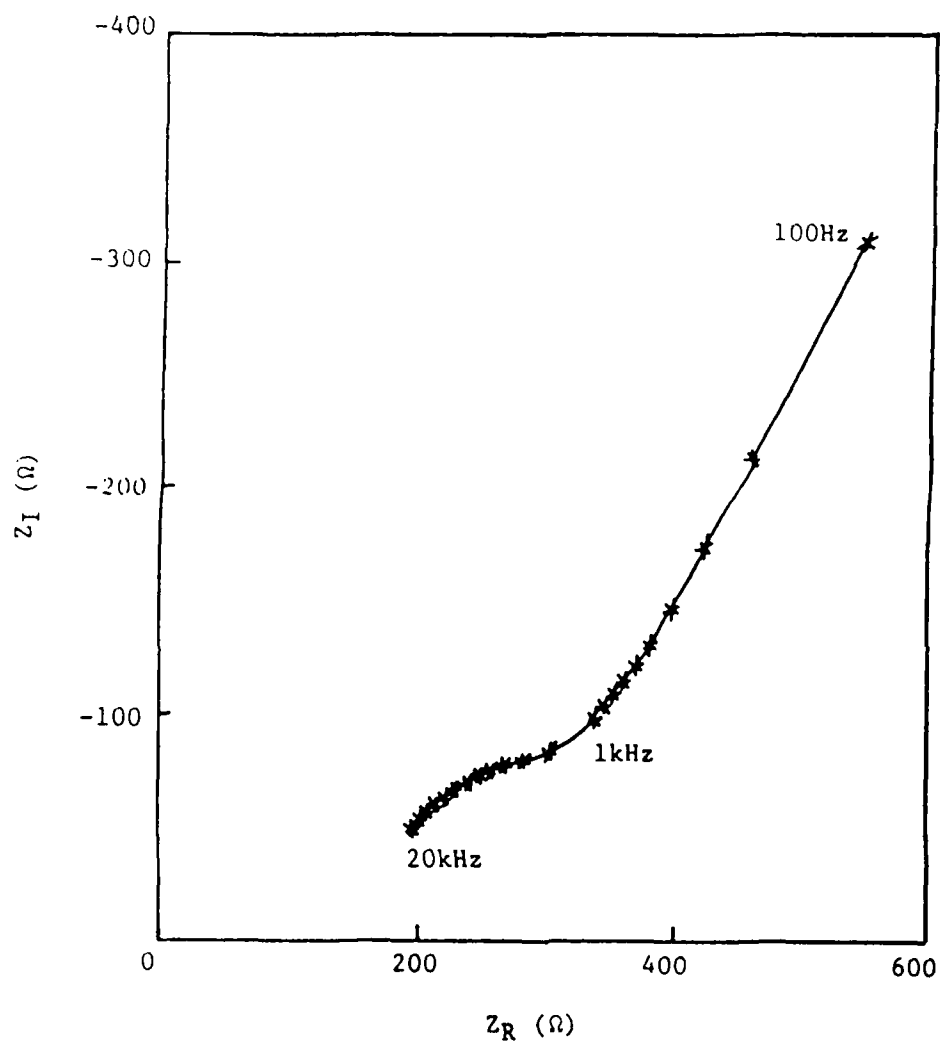


Figure 4. Impedance response for H-c oriented n-HfS<sub>2</sub> in CH<sub>3</sub>CN (0.1M TBAPF<sub>6</sub> + 0.001M CuCl) after 42 minutes copper intercalation (±10 $\mu$ A) at -0.26V vs. SCE.

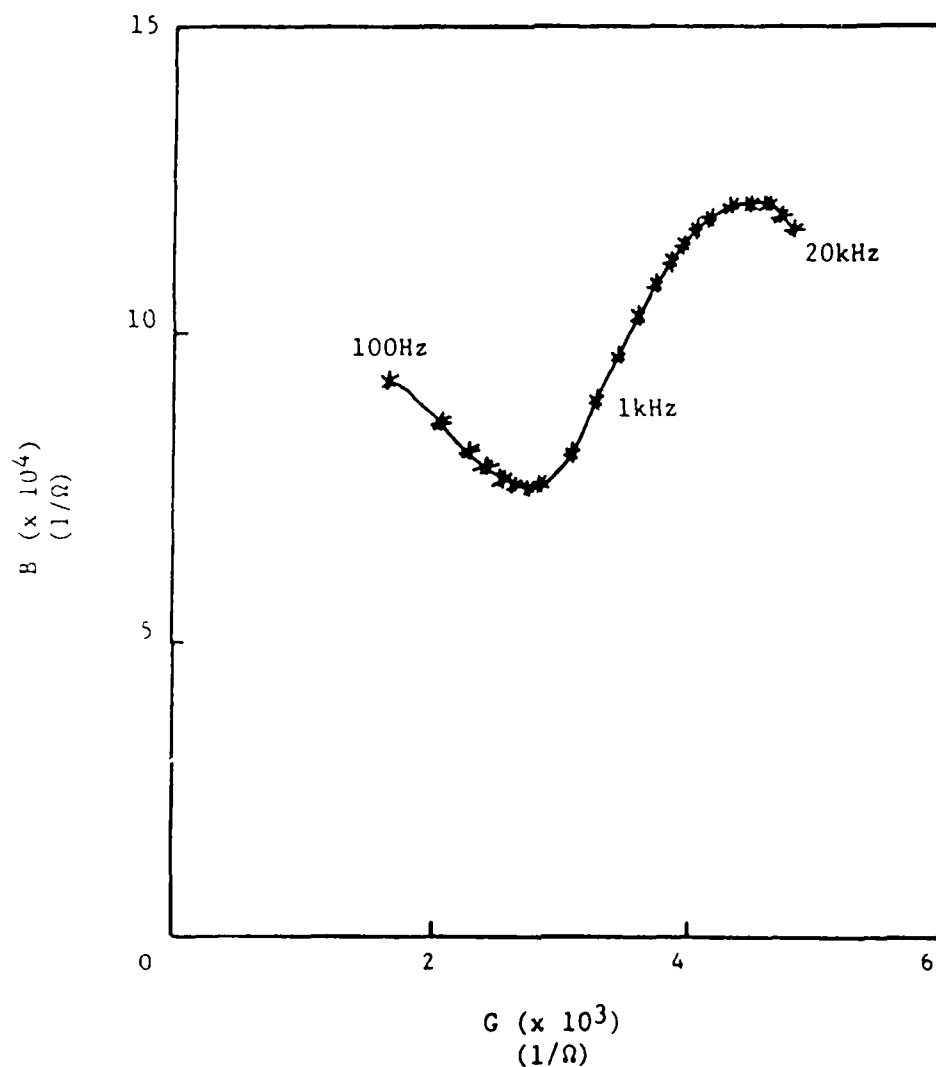


Figure 5. Admittance response for H-c oriented n-HfS<sub>2</sub> in CH<sub>3</sub>CN (0.1M TBAPF<sub>6</sub> + 0.001M CuCl) after 42 minutes copper intercalation (≈10μA) at -0.26V vs. SCE.

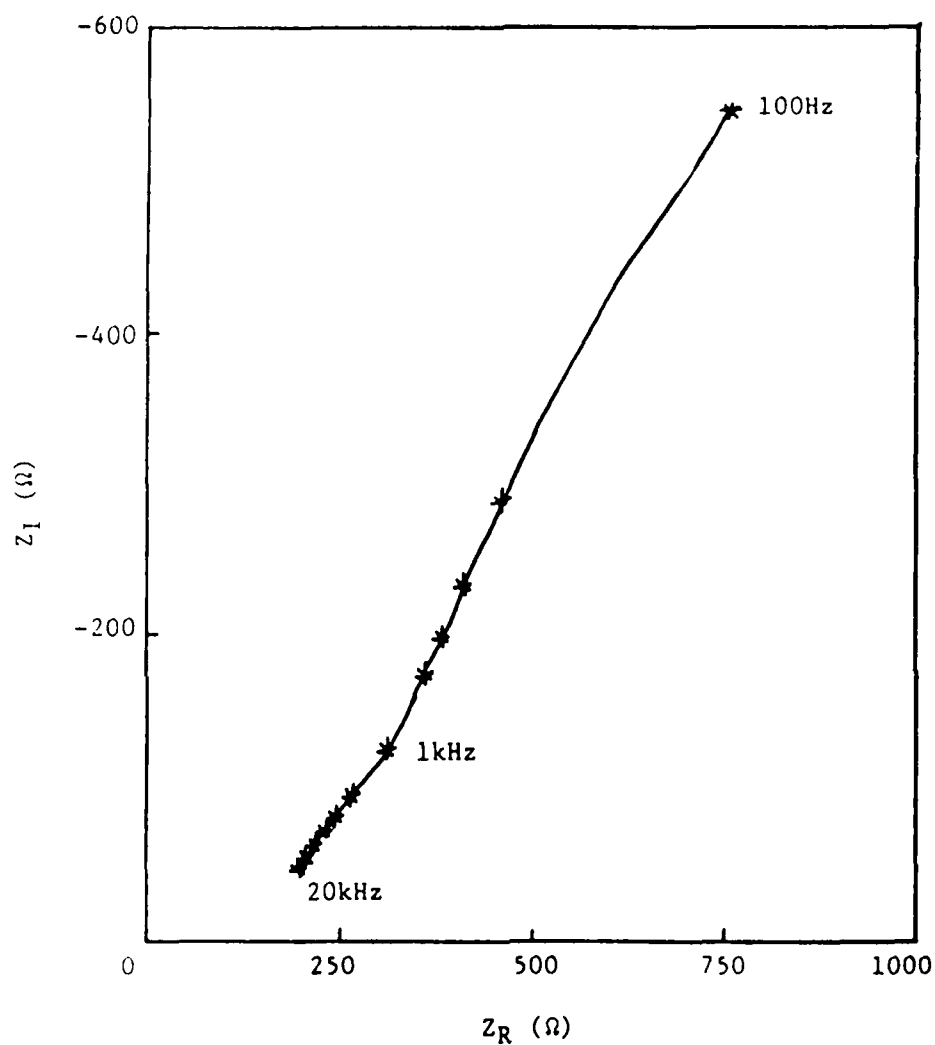


Figure 6. Impedance response for H-c oriented n-HfS<sub>2</sub> in CH<sub>3</sub>CN (0.1M TBAPF<sub>6</sub> + 0.001M CuCl) after 129 minutes copper intercalation ( $\approx 10\mu\text{A}$ ) at -0.26V vs. SCE.

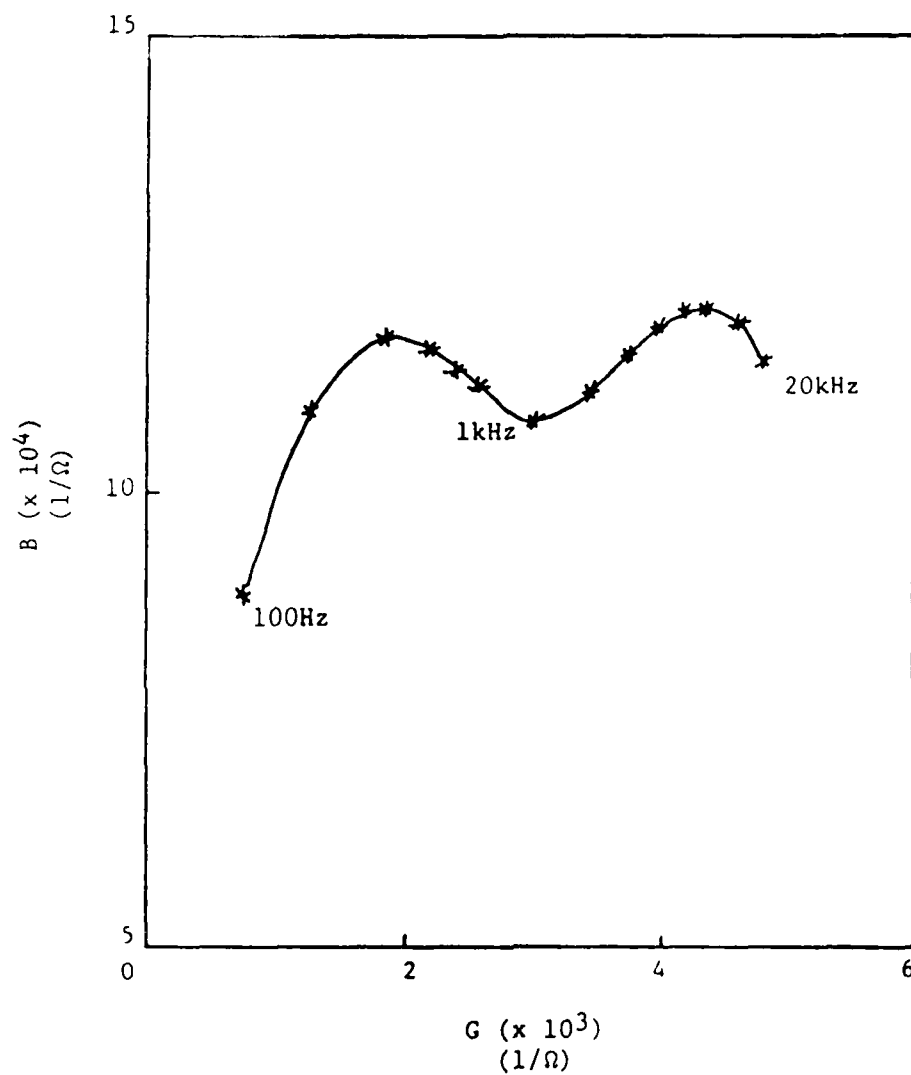


Figure 7. Admittance response for H-c oriented n-HfS<sub>2</sub> in CH<sub>3</sub>CN (0.1M TBAPF<sub>6</sub> + 0.001M CuCl) after 129 minutes copper intercalation (≈10μA) at -0.26V vs. SCE.

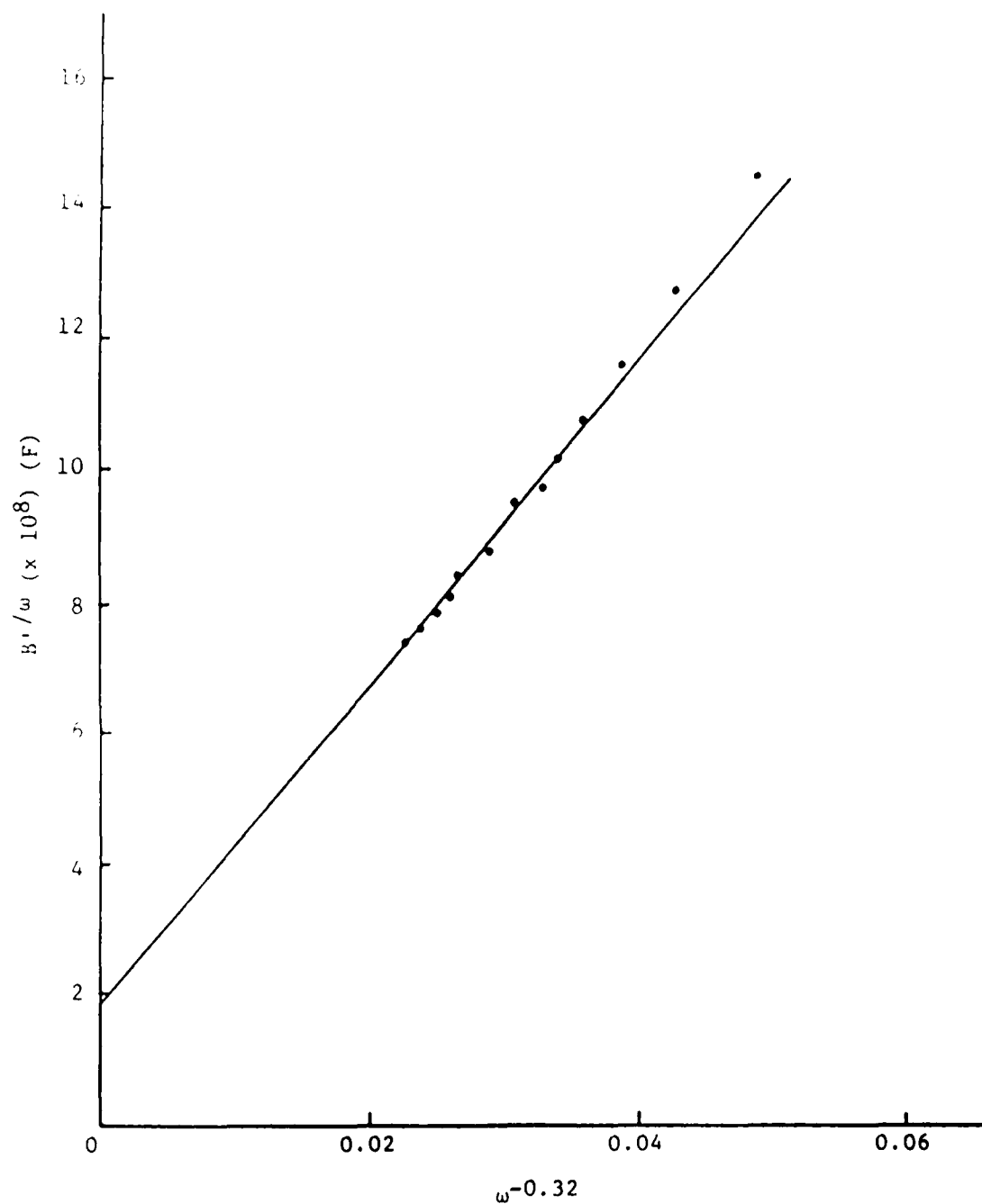


Figure 8. Frequency dependent capacitance for  $\parallel$ -c oriented n-HfS<sub>2</sub> in CH<sub>3</sub>CN (0.1M TBAPF<sub>6</sub>) at OCP (-0.295 vs. SCE). Geometric electrode area 0.06cm<sup>2</sup>.



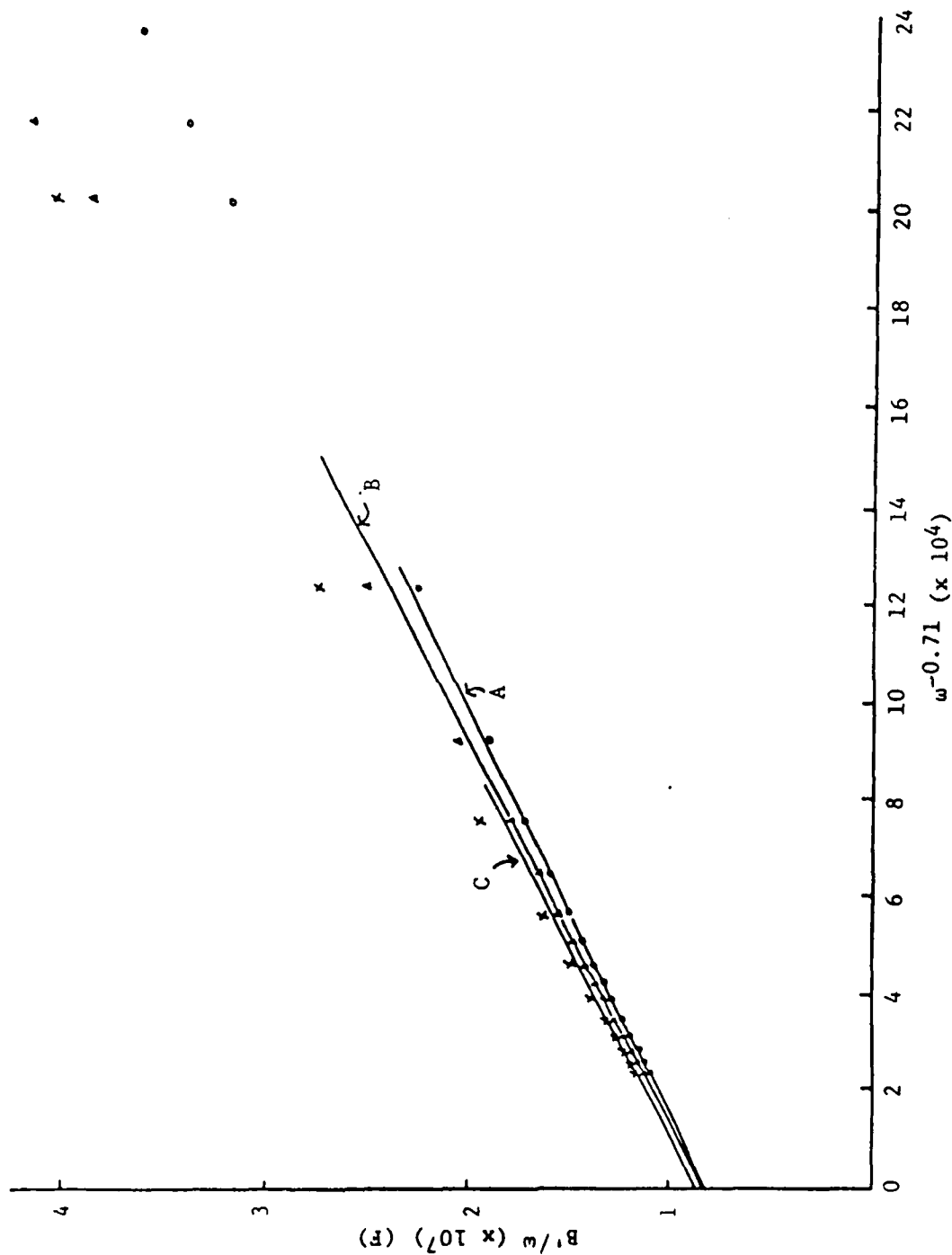


Figure 9. Frequency dependent capacitance for  $\parallel$ -c oriented n-HfS<sub>2</sub> in CH<sub>3</sub>CN (0.1M TBAPF<sub>6</sub> + 0.001M CuCl) after copper intercalation at -0.26V vs. SCE ( $\approx 10\mu$ A) for 10 minutes (curve A), 42 minutes (curve B) and 129 minutes (curve C). Geometric electrode area 0.06cm<sup>2</sup>.

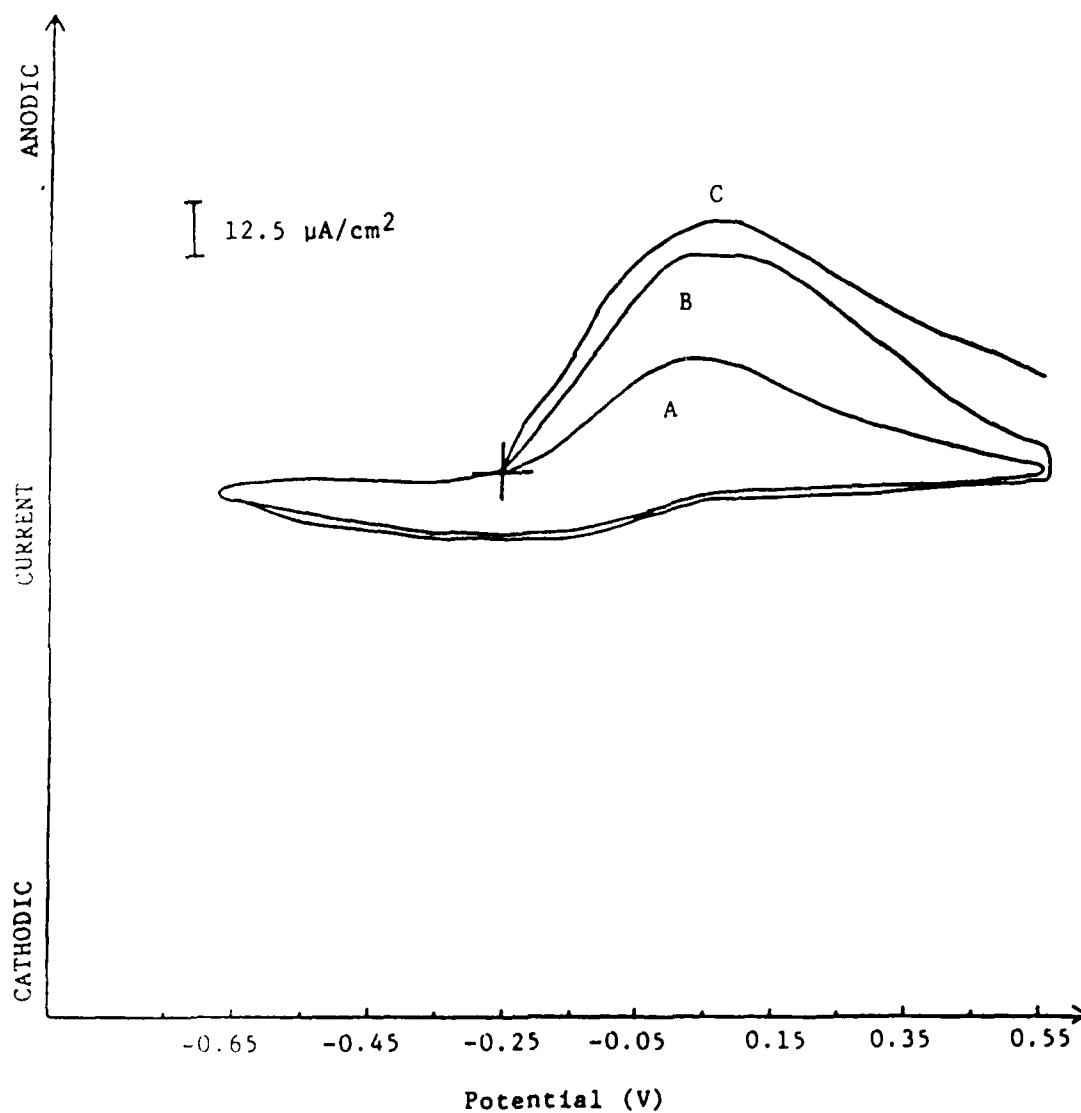


Figure 10. Cyclic voltammograms for H-c oriented n-HfS<sub>2</sub> in CH<sub>3</sub>CN (0.1M TBAPF<sub>6</sub> + 0.001M CuCl) after copper intercalation of -0.26V ( $\approx 10\mu\text{A}$ ) for A) 2 min., B) 5 min., and C) 10 min. Scan rate: 20mV/sec.

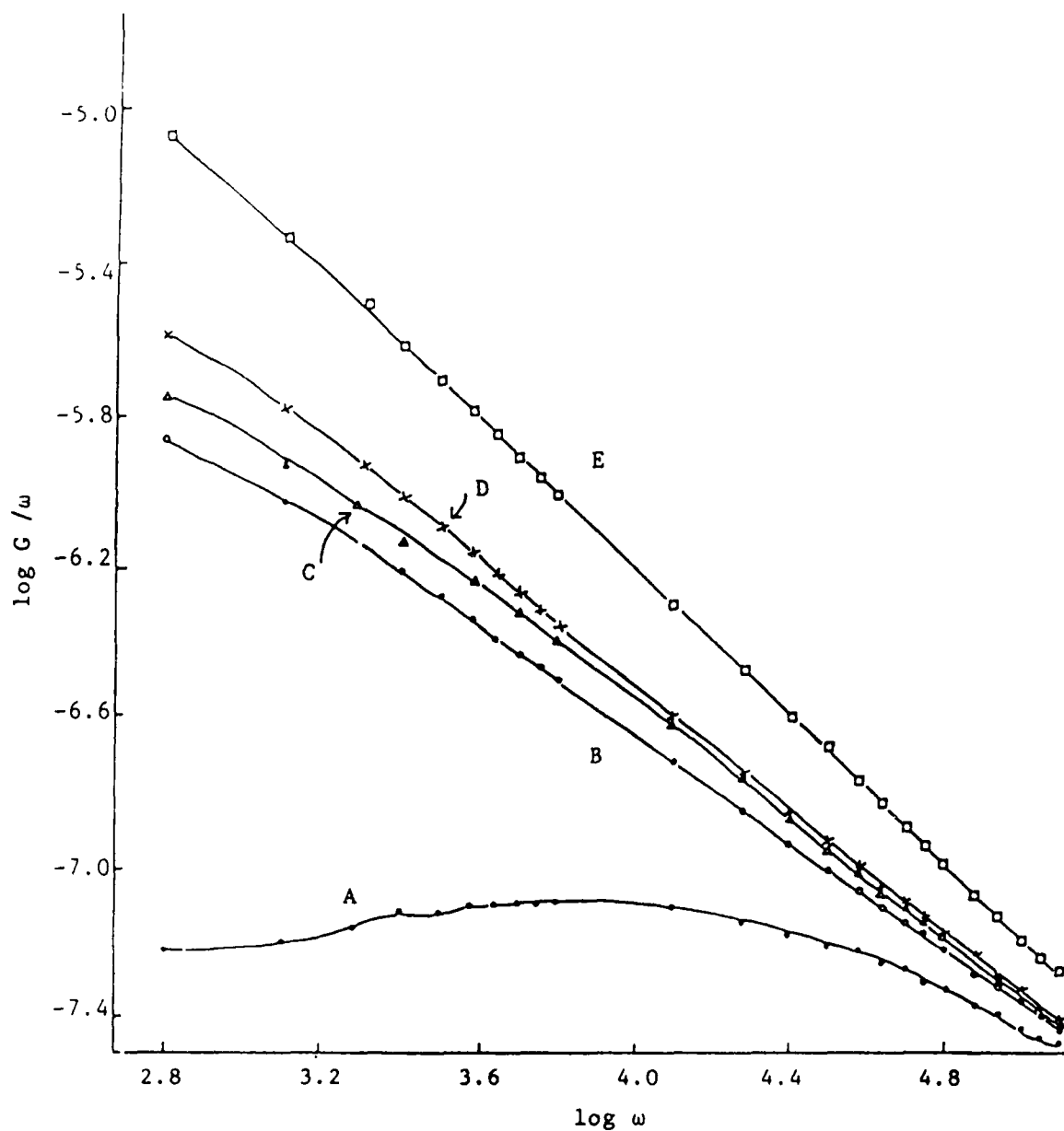


Figure 11. Relationship between  $G/\omega$  and  $\omega$  for H-c oriented n-HfS<sub>2</sub> in CH<sub>3</sub>CN (0.1M TBAPF<sub>6</sub>) without (curve A) and with (curves B-E) 0.001M CuCl. Curve A at OCP -0.295V vs. SCE. Curves B, C and D after 10, 42 and 129 minutes respectively copper intercalation at -0.26V ( $\approx 10\mu\text{A}$ ) (OCP -0.1V); E after 130 minutes when copper deposition on the n-HfS<sub>2</sub> surface became evident (OCP -0.4V vs. SCE).

SECURITY CLASSIFICATION OF THIS PAGE (When Data Entered)

REPORT DOCUMENTATION PAGE		READ INSTRUCTIONS BEFORE COMPLETING FORM
1. REPORT NUMBER	2. GOVT ACCESSION NO.	3. RECIPIENT'S CATALOG NUMBER
4		
4. TITLE (and Subtitle)		5. TYPE OF REPORT & PERIOD COVERED
Hafnium Disulfide Photoelectrochemistry in Aqueous Redox Electrolytes		Technical Aug. 1987 - May 1988
		6. PERFORMING ORG. REPORT NUMBER
7. AUTHOR(s)		8. CONTRACT OR GRANT NUMBER(s)
Nirupama U. Pujare, Krystyna W. Semkow and Anthony F. Sammells		N00014-86-C-0128
9. PERFORMING ORGANIZATION NAME AND ADDRESS		10. PROGRAM ELEMENT, PROJECT, TASK AREA & WORK UNIT NUMBERS
Eltron Research, Inc. 4260 Westbrook Drive Aurora, IL 60504		
11. CONTROLLING OFFICE NAME AND ADDRESS		12. REPORT DATE
Office of Naval Research/Chemistry Program Arlington, VA 22217		May 1988
		13. NUMBER OF PAGES
		17
14. MONITORING AGENCY NAME & ADDRESS (if different from Controlling Office)		15. SECURITY CLASS. (of this report)
Above		Unclassified
		15a. DECLASSIFICATION/DOWNGRADING SCHEDULE
16. DISTRIBUTION STATEMENT (of this Report)		
Approved for public release, distribution unlimited.		
17. DISTRIBUTION STATEMENT (of the abstract entered in Block 20, if different from Report)		
Approved for public release, distribution unlimited.		
18. SUPPLEMENTARY NOTES		
Submitted: Journal of the Electrochemical Society		
19. KEY WORDS (Continue on reverse side if necessary and identify by block number)		
aqueous redox electrolytes, hafnium disulfide, photoelectrochemistry		
20. ABSTRACT (Continue on reverse side if necessary and identify by block number)		
<p>The van der Waal surface of single crystal n-HfS<sub>2</sub> was subjected to photoelectrochemical (PEC) investigation in aqueous electrolytes containing Fe<sup>3+</sup>/Fe<sup>2+</sup>, Fe(CN)<sub>6</sub><sup>3-</sup>/Fe(CN)<sub>6</sub><sup>4-</sup> and I<sub>3</sub><sup>-</sup>/I<sup>-</sup> redox species. Photoanodic current densities were limited by the number of photogenerated carriers, with highest rates (≈3mA/cm<sup>2</sup>) being found in the presence of Fe<sup>2+</sup> and I<sup>-</sup> ions. Flat-band potentials obtained from Mott-Schottky plots were shifted to negative values by 55.9mV per pH unit over the pH range 0-7, suggesting the possible presence of oxides on the n-HfS<sub>2</sub> surface. Slopes for Mott-Schottky plots were frequency dependent. Electrodes showed low dark oxidation currents.</p>		

DD FORM 1 JAN 73 1473

EDITION OF 1 NOV 65 IS OBSOLETE  
S/N 0107-UR 014-6601

trodes showed low dark oxidation currents.

Unclassified

SECURITY CLASSIFICATION OF THIS PAGE (When Data Entered)

HAFNIUM DISULFIDE PHOTOELECTROCHEMISTRY  
IN AQUEOUS REDOX ELECTROLYTES

Nirupama U. Pujare, Krystyna W. Semkow\*  
and Anthony F. Sammells\*

Eltron Research, Inc.  
Aurora, Illinois 60504

The van der Waal surface of single crystal n-HfS<sub>2</sub> was subjected to photoelectrochemical (PEC) investigation in aqueous electrolytes containing Fe<sup>3+</sup>/Fe<sup>2+</sup>, Fe(CN)<sub>6</sub><sup>3-</sup>/Fe(CN)<sub>6</sub><sup>4-</sup> and I<sub>3</sub><sup>-</sup>/I<sup>-</sup> redox species. Photoanodic current densities were limited by the number of photogenerated carriers, with highest rates ( $\approx 3\text{mA/cm}^2$ ) being found in the presence of Fe<sup>2+</sup> and I<sup>-</sup> ions. Flat-band potentials obtained from Mott-Schottky plots were shifted to negative values by 55.9mV per pH unit over the pH range 0-7, suggesting the possible presence of oxides on the n-HfS<sub>2</sub> surface. Slopes for Mott-Schottky plots were frequency dependent. Electrodes showed low dark oxidation currents.

\*Electrochemical Society Active Member

Key Words: aqueous redox electrolytes, hafnium disulfide, photoelectrochemistry

## INTRODUCTION

Group IVB transition metal dichalcogenides (TMDs) typified by  $\text{HfS}_2$  (band gap 1.9eV) are unique layer type materials for photoelectrochemical (PEC) study since they can, in principle, act as both a photoelectrode and as a substrate for the reversible intercalation of transition metal species<sup>1-13</sup>.  $\text{HfS}_2$  has been shown<sup>14</sup> capable of maintaining its semiconducting properties after partial electrochemical intercalation by either Cu or Fe to give  $\text{ZrMyS}_2$  over the compositional range  $0 < y < 0.22$ . Such intercalation would be expected to result in decreasing the semiconductor band gap width. Recent work performed in our laboratory using impedance and admittance measurement techniques at n- $\text{HfS}_2$ /non-aqueous electrolyte interface<sup>14,15</sup> have suggested that n- $\text{HfS}_2$  becomes degenerate for  $>0.1$  moles intercalated copper. Capacitance values at these interfacial regions were found on the order  $10^{-6}\text{F/cm}^2$ .

TMDs can also be cathodically intercalated by alkali/alkaline earth metals and larger organic molecules<sup>7-12</sup> resulting, in all cases, in a widening of the van der Waals layer. Group IVB TMDs possess an octahedral structure with electron photoexcitation within the semiconductor band gap proceeding from energy bands derived from bonding sulfur p-orbitals into metal  $t_{2g}$  d-orbitals<sup>6</sup>. They are, as a result, susceptible to photocorrosion, which in the case of n-doped materials, can lead to a layer of sulfur being formed on the photoelectrode surface<sup>5</sup>.

The relatively low degree of intercalation that can be achieved by these photoelectrodes before degeneration occurs, motivated us to investigate the photoelectrochemistry of n- $\text{HfS}_2$  in aqueous electrolyte using the non-intercalating 1-c oriented surface. Redox electrolytes of iodide,  $\text{Fe}^{3+}/\text{Fe}^{2+}$  and  $\text{Fe}(\text{CN})_6^{3-}/\text{Fe}(\text{CN})_6^{4-}$  were investigated. A related study has recently been reported using single crystal n- $\text{ZrS}_2$  photoelectrodes<sup>16</sup>. Mott-Schottky measurements on n- $\text{HfS}_2$  in these aqueous redox electrolytes permitted the dependency of pH on extrapolated flat-band potential to be determined. The presence of some frequency dependent capacitance values did not permit doping densities to be reliably determined.

## EXPERIMENTAL

Single crystals of n- $\text{HfS}_2$  were prepared by the halogen ( $\text{I}_2$ ) vapor transport technique (Northwestern University). Initial solid-state chemical reactions between Hf (99.5%) and S (99.999%) were accomplished by heating an intimate mix-

ture together with 5mg  $I_2$ /ml of the quartz transport tube volume. This was performed in a three temperature zone furnace. Typical thermal gradients used were between 875°C and 800°C. Crystal growth occurred over 25 days. In all cases the relatively large crystals obtained were intrinsically n-type. Ohmic contact to n-HfS<sub>2</sub> was accomplished by sparking indium onto one side of the crystal using a 15 volt DC power supply. This was performed using a fine indium wire as a cathode with the other pole of the power supply clamped to the n-HfS<sub>2</sub> single crystal. When the indium wire was within  $\approx 1$ mm of the crystal, a transient spark could be observed. This resulted in the ion implantation of indium into the ohmic contact region. Current collection was performed with a nichrome wire attached with silver epoxy and cured at 120°C for 1h. Photoelectrodes were then appropriately isolated from later contact with the electrolyte by epoxy (Norton Chemplast), so that only the single crystal front face of interest was exposed. Typical photoelectrode areas for  $\perp$ -c oriented crystals were 0.04cm<sup>2</sup>.

Measurements were performed in a standard glass H-cell arrangement using a platinum counter electrode. SCE was used as a reference to the working electrode compartment via a salt bridge. Photoelectrode potentials were controlled by a Stonehart Associates BC 1200 potentiostat. Capacitance measurements were performed using a Hewlett-Packard 4276A digital LCZ meter over the frequency range 20kHz - 100Hz.

## RESULTS AND DISCUSSION

Mott-Schottky capacitance-potential measurements were performed on single crystal  $\perp$ -c oriented n-HfS<sub>2</sub> over the aqueous electrolyte pH range 0 to 7. Electrolyte pH was systematically adjusted between 0 and 5 by titrating appropriate quantities of HCl. Introduction of NaCl, KCl or NH<sub>4</sub>Cl as supporting electrolytes were found to cause electrode potential instability during capacitance-potential measurements and consequently were avoided. Similar potential instabilities were observed from measurements performed in electrolytes with pH >7 after titration with either NaOH or KOH. Typical capacitance-potential measurements for single crystal n-HfS<sub>2</sub> in 0.01M HCl pH 20 are shown in Figure 1 over the frequency range 20kHz to 100Hz. Lines at each measurement frequency can be seen to converge to a common point on the potential axis, suggesting the presence of a defect-free n-HfS<sub>2</sub>/electrolyte interfacial region. Similar frequency dependent lines were found for all measurements over the pH range 0 to 7. These

observations were in agreement with the frequency dependent dielectric constant associated with the photoelectrode space charge region<sup>17</sup>. As a consequence, however, donor densities for n-HfS<sub>2</sub> could not be obtained.

The dependency of n-HfS<sub>2</sub>  $V_{fb}$  on electrolyte pH is summarized in Figure 2. The observed 55.9mV shift in  $V_{fb}$  per unit change in electrolyte pH was consistent with the influence of an oxide layer at the interfacial region. Evidence for oxide layers on n-ZrS<sub>2</sub> has already been reported<sup>16</sup> using X-ray photoelectron spectroscopy techniques.

Capacitance potential plots for n-HfS<sub>2</sub> in 0.1M K<sub>4</sub>Fe(CN)<sub>6</sub>/K<sub>3</sub>Fe(CN)<sub>6</sub> electrolyte at pH 7 are summarized in Figure 3 as a function of measurement frequency. Extrapolation of capacitance data to the potential axis gave a  $V_{fb}$  of 0.77V vs. SCE. It is probable that the iron metal center of these cyanide complexes do not directly adsorb onto the photoelectrode surface because of the complete and stable ligand shell which surrounds them<sup>17</sup>. The PEC current-potential characteristics for n-HfS<sub>2</sub> in this Fe(CN)<sub>6</sub><sup>3-</sup>/Fe(CN)<sub>6</sub><sup>4-</sup> electrolyte under 100mW/cm<sup>2</sup> ELH illumination is shown in Figure 4. Upon anodic bias the photocurrent rises slowly to about 0.47mA/cm<sup>2</sup> at the reversible potential for the redox couple present. This probably reflected slow kinetics for mediating photogenerated electron holes across the interfacial region. Photopotentials for n-HfS<sub>2</sub> in this redox electrolyte at pH 7 were typically found to be around -350 to -390mV. This compares to a difference between  $V_{fb}$  at this pH and the redox potential of electroactive species being  $\approx 1V$ . The n-HfS<sub>2</sub> donor density could not be directly obtained from Mott-Schottky plots performed here in aqueous solution. However, previous frequency independent impedance-admittance studies performed by us<sup>14</sup> using similarly grown n-HfS<sub>2</sub>, performed in acetonitrile based non-aqueous electrolytes, indicated that a low donor density ( $3.4 \times 10^{14} \text{ cm}^{-3}$ ) was present. This would consequently suggest that the energy difference between the n-HfS<sub>2</sub> Fermi level and conduction band as  $\approx 0.29V$ , thereby implying that the maximum attainable photopotential from this photoanode as  $\approx 0.7V$ . In anodic biased regions small residual dark currents were evident although no visible layer of elemental sulfur was observed.

Capacitance-potential plots for n-HfS<sub>2</sub> in aqueous 0.1M FeCl<sub>2</sub>/FeCl<sub>3</sub> at pH 0 performed as a function of frequency are summarized in Figure 5, where  $V_{fb}$  values were found to be -0.38V vs. SCE. Again, frequency dependent capacitance values were observed. The PEC current-potential curve for a n-HfS<sub>2</sub> photoanode with and without 100mW/cm<sup>2</sup> ELH illumination in the above redox electrolyte, is



shown in Figure 6. Saturation current densities were found to be  $\approx 3\text{mA/cm}^2$ . At biased photoelectrode potentials negative of 0.15V vs. SCE, cathodic currents became evident due to  $\text{Fe}^{3+}$  reduction. Such cathodic currents, for example, were found absent in 0.1M  $\text{FeCl}_2$  at pH 0. The open-circuit photopotential obtained from n-HfS<sub>2</sub> in the above  $\text{Fe}^{3+}/\text{Fe}^{2+}$  redox electrolyte was found to be in the range -380 to -420mV. These photopotentials were similar to our previous observations above for this photoelectrode in  $\text{Fe}(\text{CN})_6^{3-}/\text{Fe}(\text{CN})_6^{4-}$ . However, in principle the maximum achievable photopotential for n-HfS<sub>2</sub> in the  $\text{FeCl}_3/\text{FeCl}_2$  redox electrolyte was  $\approx 1.1\text{V}$ , which compare to 0.7V for the hexacyanide based complexes. This suggested that a higher recombination rate for photogenerated minority carriers may be present, or that fast electron transfer to  $\text{Fe}^{3+}$  species may be occurring at less positive potentials. The higher observed saturation current densities found with the  $\text{Fe}^{3+}/\text{Fe}^{2+}$  couple suggested, as expected, higher oxidation rates for  $\text{Fe}^{2+}$  compared to  $\text{Fe}(\text{CN})_6^{4-}$ . This can be interpreted as a higher hole captive cross section being present for  $\text{Fe}^{2+}$  ions compared to  $\text{Fe}(\text{CN})_6^{4-}$  at the n-HfS<sub>2</sub>/redox electrolyte interfacial regions<sup>18</sup>.

Capacitance-potential curves for n-HfS<sub>2</sub> in 1M KI at pH 3.5 are shown in Figure 7 as a function of measurement frequency.  $V_{fb}$  values of -0.58V vs. SCE were found. The PEC current-potential curve is shown in Figure 8. The saturation current density was found to be  $3\text{mA/cm}^2$ , similar to that found for the  $\text{Fe}^{3+}/\text{Fe}^{2+}$  couple discussed above, suggesting in both cases that the current was limited by the number of available photogenerated holes at the interface. Upon introducing 0.01M  $\text{I}_2$  to the 1M KI electrolyte, the observed open-circuit photopotential decreased to -115mV as a consequence of absorption losses and  $\text{I}_2$  reduction at potentials negative of 0.2V vs. SCE, as shown in Figure 9. The band energy scheme for n-HfS<sub>2</sub> in aqueous electrolyte as a function of pH, derived from the above results, is shown in Figure 10.

#### CONCLUSION

The van der Waals surface of single crystal n-HfS<sub>2</sub> photoanodes showed relatively small dark currents. Photopotentials realized for redox electrolytes containing  $\text{Fe}^{3+}/\text{Fe}^{2+}$  and  $\text{Fe}(\text{CN})_6^{3-}/\text{Fe}(\text{CN})_6^{4-}$  couples were in the -400mV range and dependent on photoelectrode surface quality and the presence of reducible redox species. While the donor density of n-HfS<sub>2</sub> single crystals was expected low (on the order  $10^{14}\text{cm}^{-3}$ ), this would make the potential difference between the Fermi level and conduction band as 0.29V, thereby substantially decreasing

the maximum realizable photopotentials from these photoanodes. Highest anodic saturation current densities were  $\approx 3\text{mA/cm}^2$ .  $V_{fb}$  values varied 55.9mV/pH unit, as observed for oxide covered semiconductors.

The PEC properties of n-HfS single crystals studied here in  $\text{Fe}^{3+}/\text{Fe}^{2+}$ ,  $\text{Fe}(\text{CN})_6^{3-}/\text{Fe}(\text{CN})_6^{4-}$  and iodide containing electrolytes were found similar to observations made by other workers<sup>16</sup> on n-ZrS<sub>2</sub>. However, observed photocurrents obtained from n-HfS<sub>2</sub> were lower reflecting the larger band gap of this material.

#### ACKNOWLEDGEMENT

This work was supported in part by the Office of Naval Research.

#### REFERENCES

1. J. A. Wilson and A. D. Yoffee, *Adv. Phys.*, 18, 193 (1969).
2. E. Mooser, Ed., *Physics and Chemistry of Materials with Layered Structures*, Reidel, Dordrecht, Boston, MA 1976.
3. R. B. Murray, R. A. Bromley and A. D. Yoffee, *J. Phys. C. Solid State Phys.*, 5, 746 (1972).
4. L. F. Mattheiss, *Phys. Rev.*, B8, 3719 (1973).
5. H. Tributsch, *J. Electrochem. Soc.*, 128, 1261 (1981).
6. H. Tributsch, *Faraday Discuss. Chem. Soc.*, 70, 190 (1981).
7. M. Abramovich, H. Tributsch and O. Gorochoy, *J. Electroanal. Chem.*, 153, 115 (1983).
8. M. Abramovich and H. Tributsch, *J. Electroanal. Chem.*, 138, 121 (1982).
9. H. Tributsch, *Appl. Phys.*, 23, 61 (1980).
10. F. R. Gamble and T. H. Geballe, *Treatise on Solid State Chemistry*, Vol 3, Plenum Press, NY 1976.
11. G. V. Subbarao and J. C. Tsang, *Mater. Res. Bull.*, 9, 921 (1974).
12. M. S. Whittingham, U.S. Patent 4,040,917 (1977).
13. B. G. Yacobi, F. W. Boswell and J. M. Corbett, *J. Phys. C. Solid State Phys.*, 12, 2189 (1979).
14. K. W. Semkow, N. U. Pujare and A. F. Sammells, *J. Electrochem. Soc.*, 135, 327 (1988).
15. K. W. Semkow, N. U. Pujare and A. F. Sammells, *J. Electrochem. Soc.*, 135, (in press) (1988).
16. N. Chandra, J. K. Leland and A. J. Bard, *J. Electrochem. Soc.*, 134, 76 (1987).
17. F. Gordon and W. P. Gomes, *J. Phys., D. Appl. Phys.*, 11, L63 (1978).
18. S. Roy Morrison, *Electrochemistry at Semiconductor and Oxidized Metal Electrodes*, Plenum Press, NY 1980.

# LIST OF FIGURES

## Figure No.

- 1 Mott-Schottky plots for n-HfS<sub>2</sub> electrode in 0.01M HCl (pH = 2).
- 2 Dependence of the flat-band potential of n-HfS<sub>2</sub> on pH.
- 3 Mott-Schottky plots for n-HfS<sub>2</sub> electrode in 0.1M K<sub>4</sub>Fe(CN)<sub>6</sub> and 0.1M K<sub>3</sub>Fe(CN)<sub>6</sub> (pH = 7).
- 4 i-V curve for n-HfS<sub>2</sub> electrode in 0.1M K<sub>4</sub>Fe(CN)<sub>6</sub> + 0.1M K<sub>3</sub>Fe(CN)<sub>6</sub> at pH = 7. 100mW/cm<sup>2</sup> ELH illumination. Scan rate 25mV/sec. Photopotential -350mV.
- 5 Mott-Schottky plots for n-HfS<sub>2</sub> electrode in 0.1M FeCl<sub>2</sub> and 0.1M FeCl<sub>3</sub> (pH = 0).
- 6 i-V curve for n-HfS<sub>2</sub> electrode in 0.1M FeCl<sub>2</sub> + 0.1M FeCl<sub>3</sub> at pH = 0. 100mW/cm<sup>2</sup> ELH illumination. Scan rate 5mV/sec. Photopotential -280mV.
- 7 Mott-Schottky plots for n-HfS<sub>2</sub> electrode in 1.0M KI (pH = 3.5).
- 8 i-V curve for n-HfS<sub>2</sub> electrode in 1.0M KI at pH = 3.5. 100mW/cm<sup>2</sup> ELH illumination. Scan rate 30mV/sec. Photopotential -320mV.
- 9 i-V curve for n-HfS<sub>2</sub> electrode in 1.0M KI + 0.01M I<sub>2</sub> at pH = 3.5. 100mW/cm<sup>2</sup> ELH illumination. Scan rate 30mV/sec. Photopotential -115mV.
- 10 Band scheme for n-HfS<sub>2</sub> single crystal.

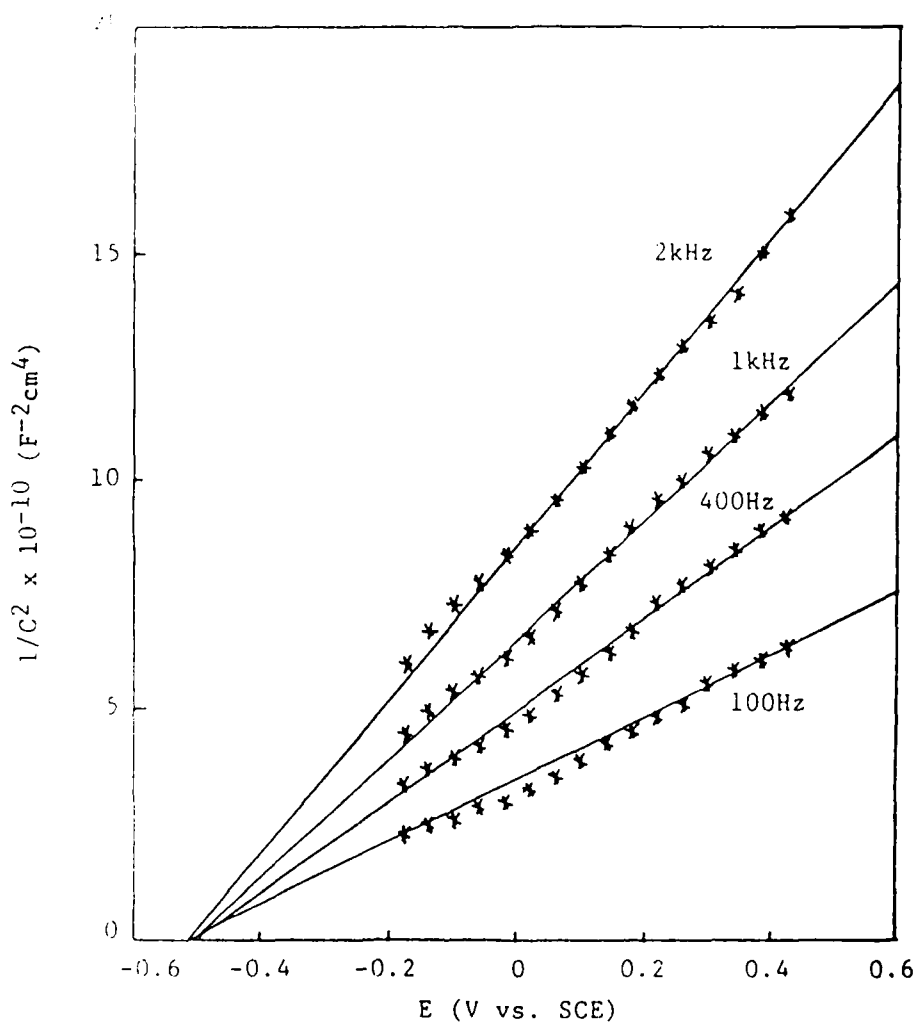


Figure 1.

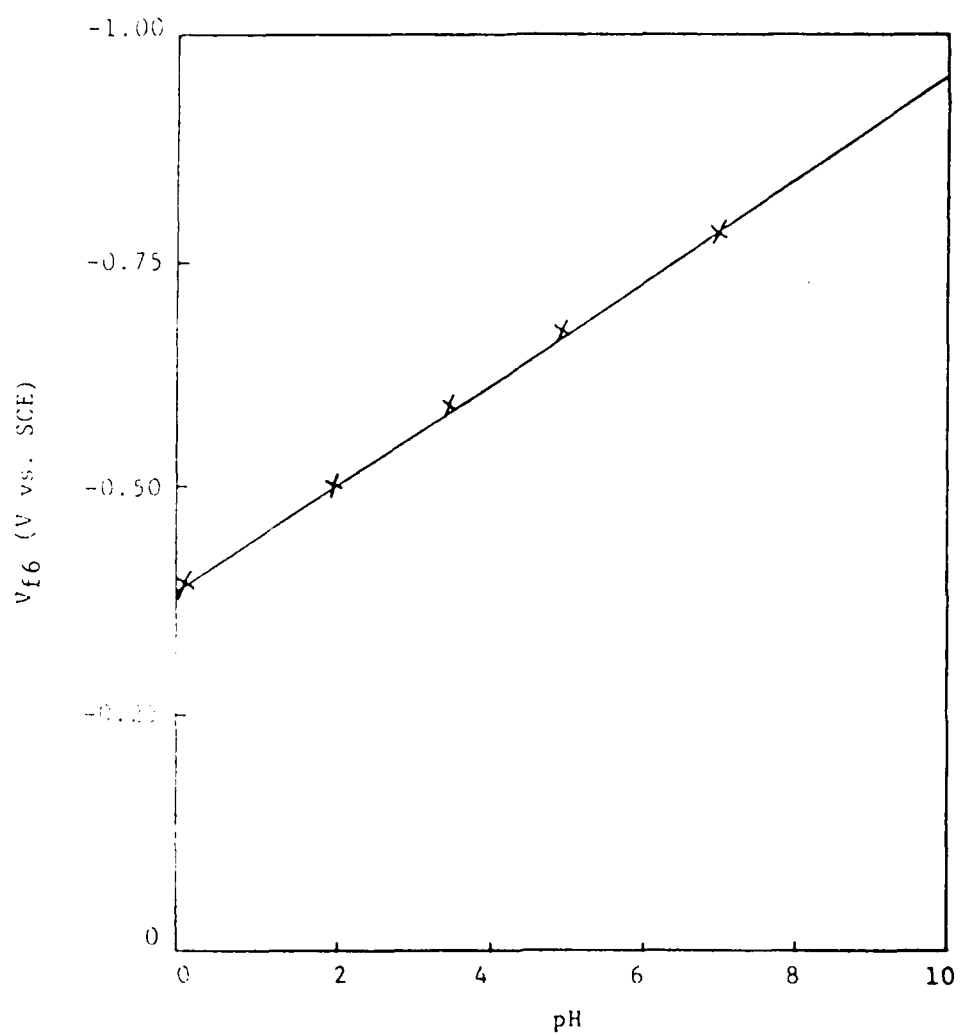


Figure 2.

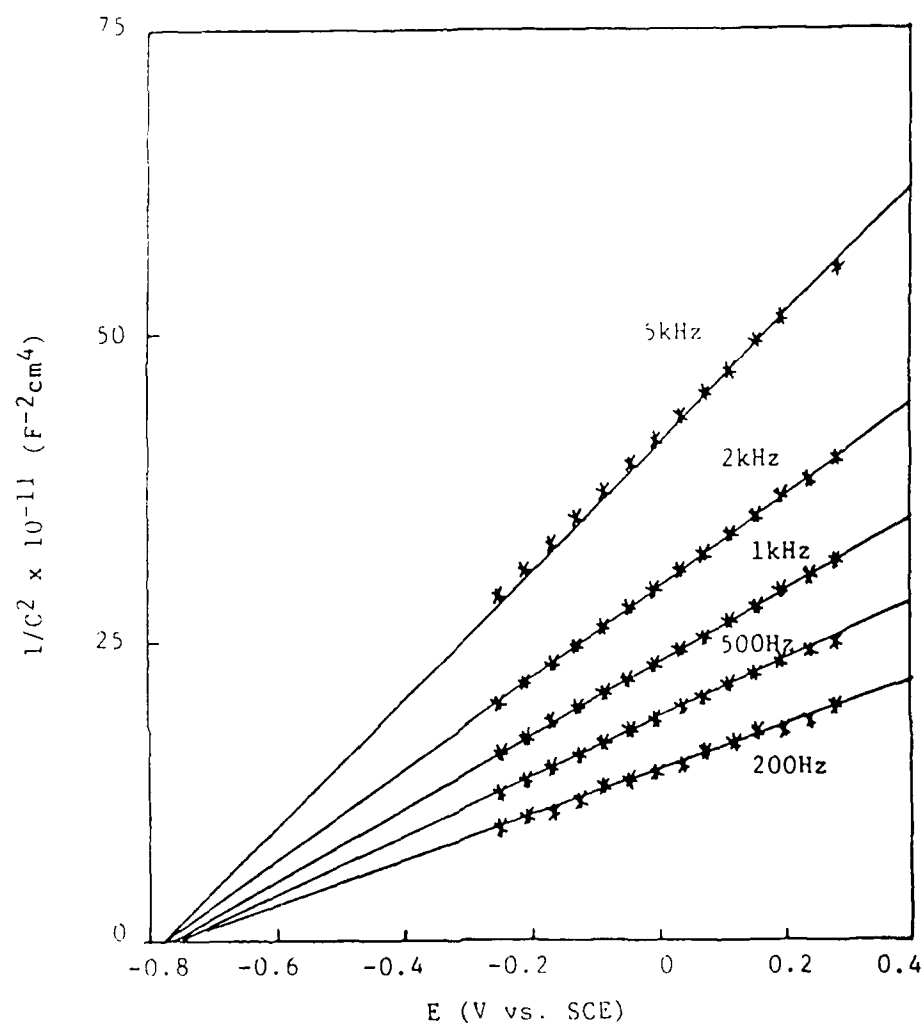


Figure 3.

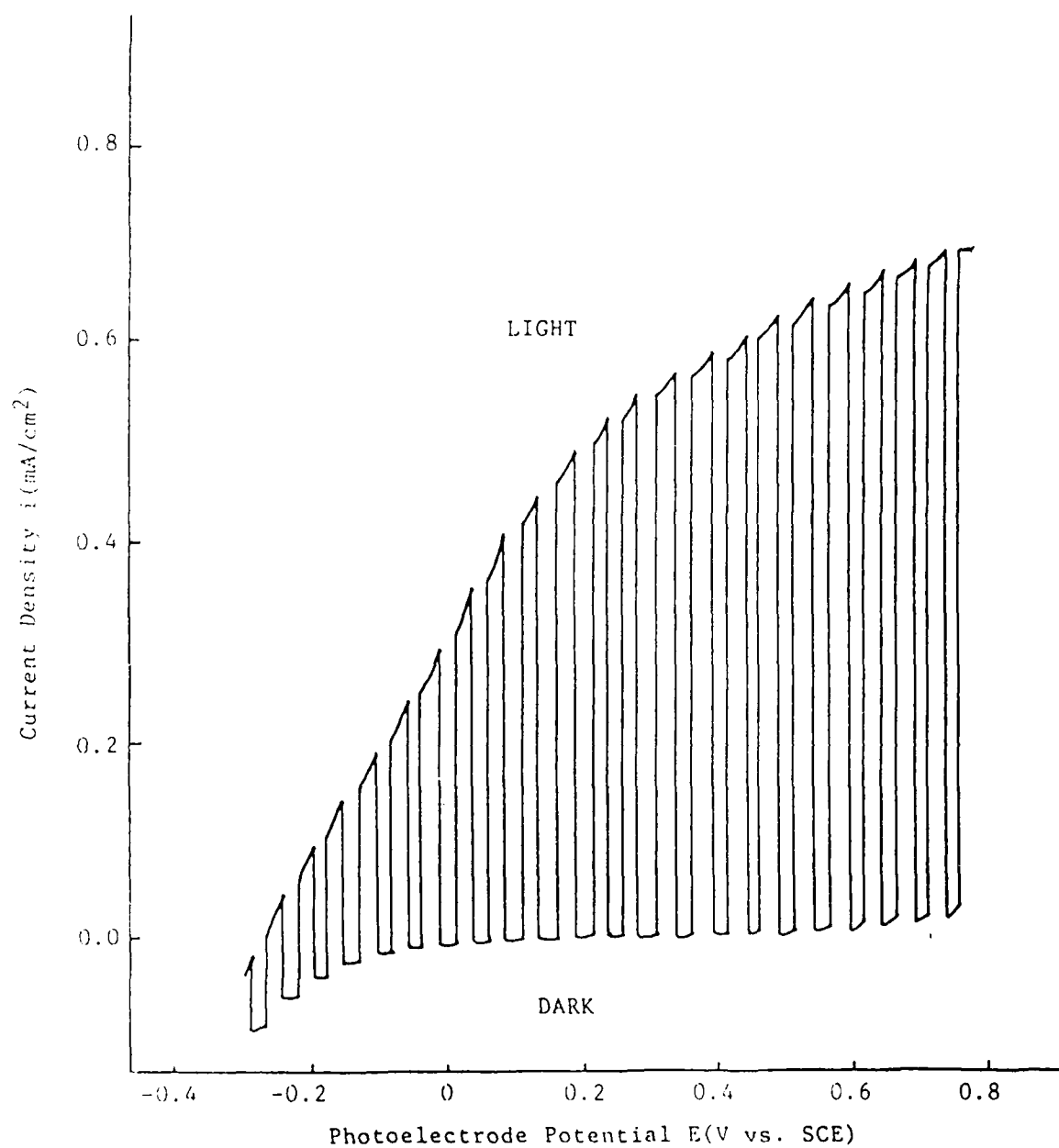


Figure 4.

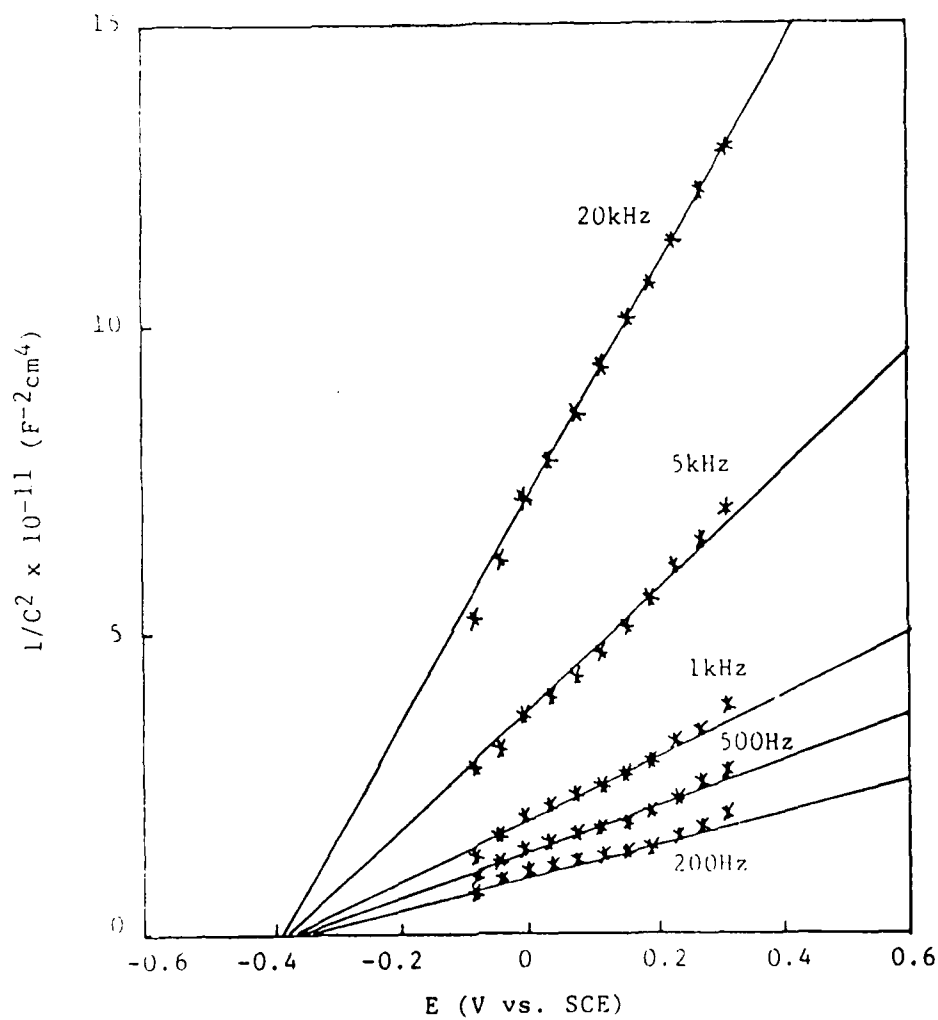


Figure 5.



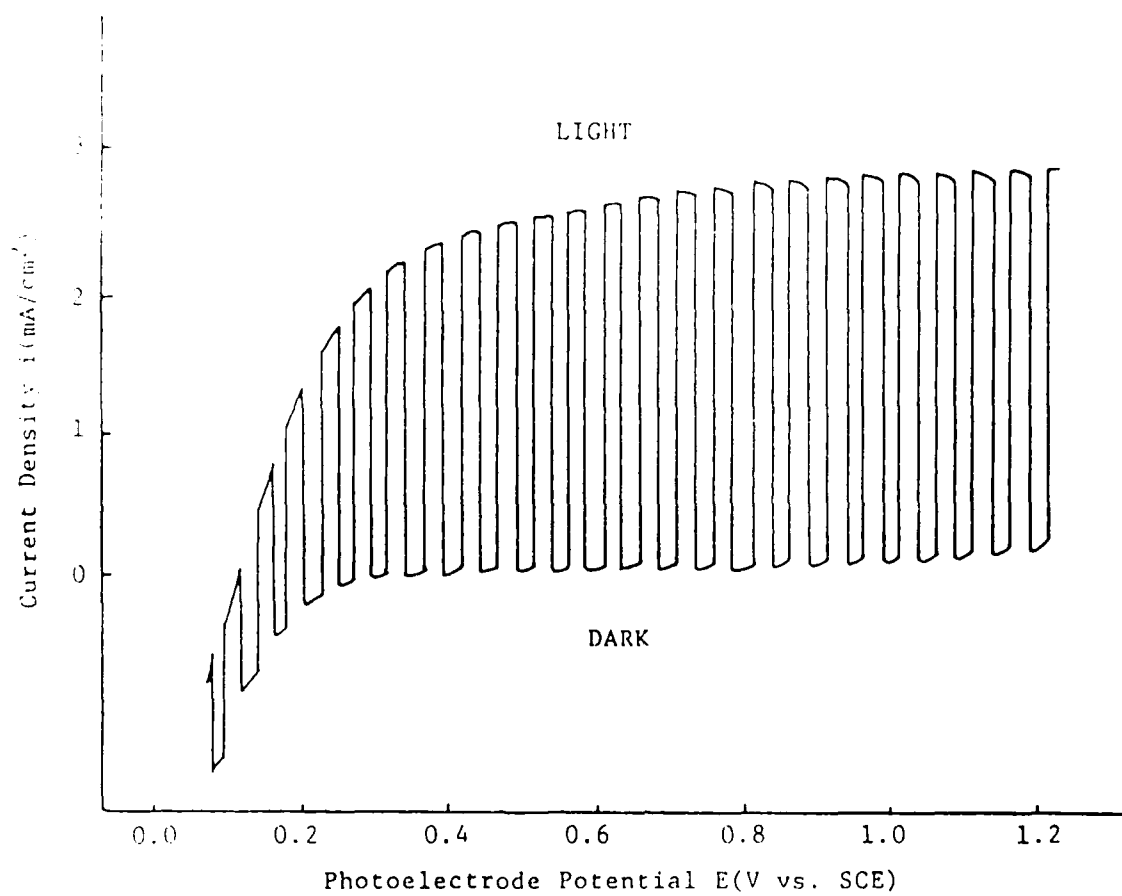


Figure 6.

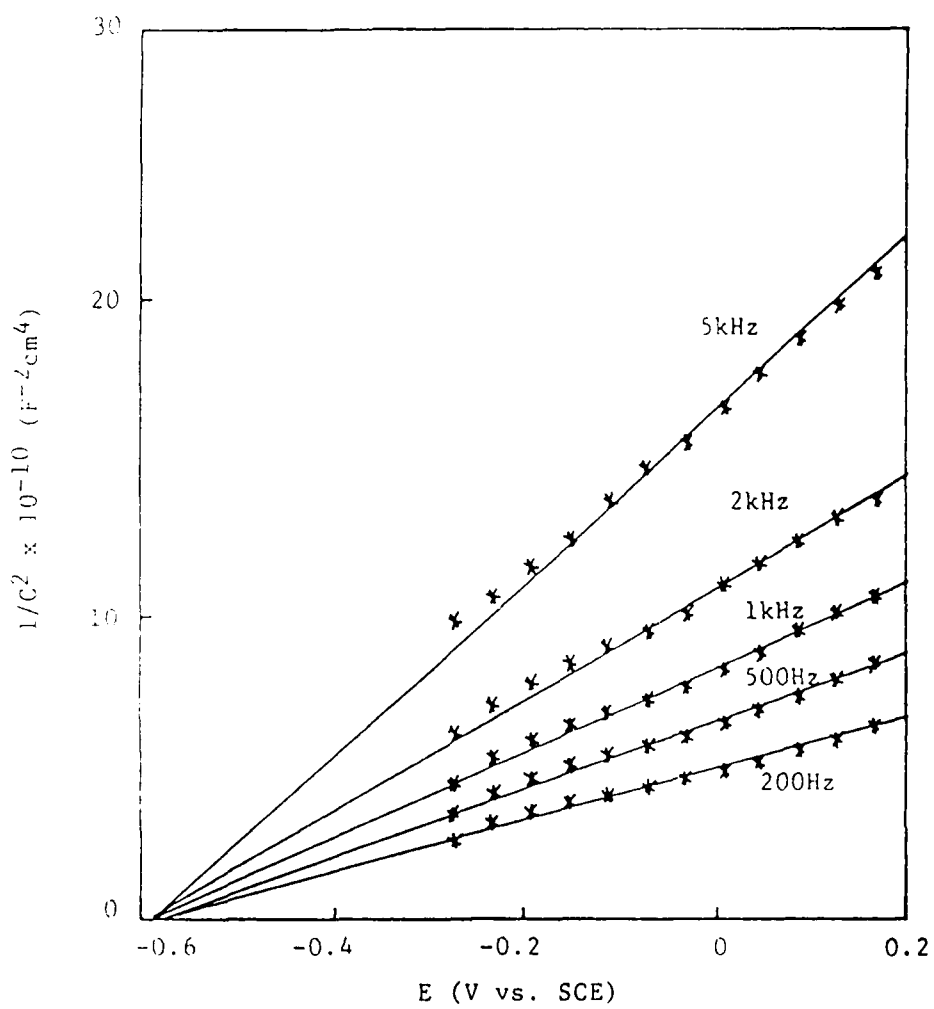


Figure 7.

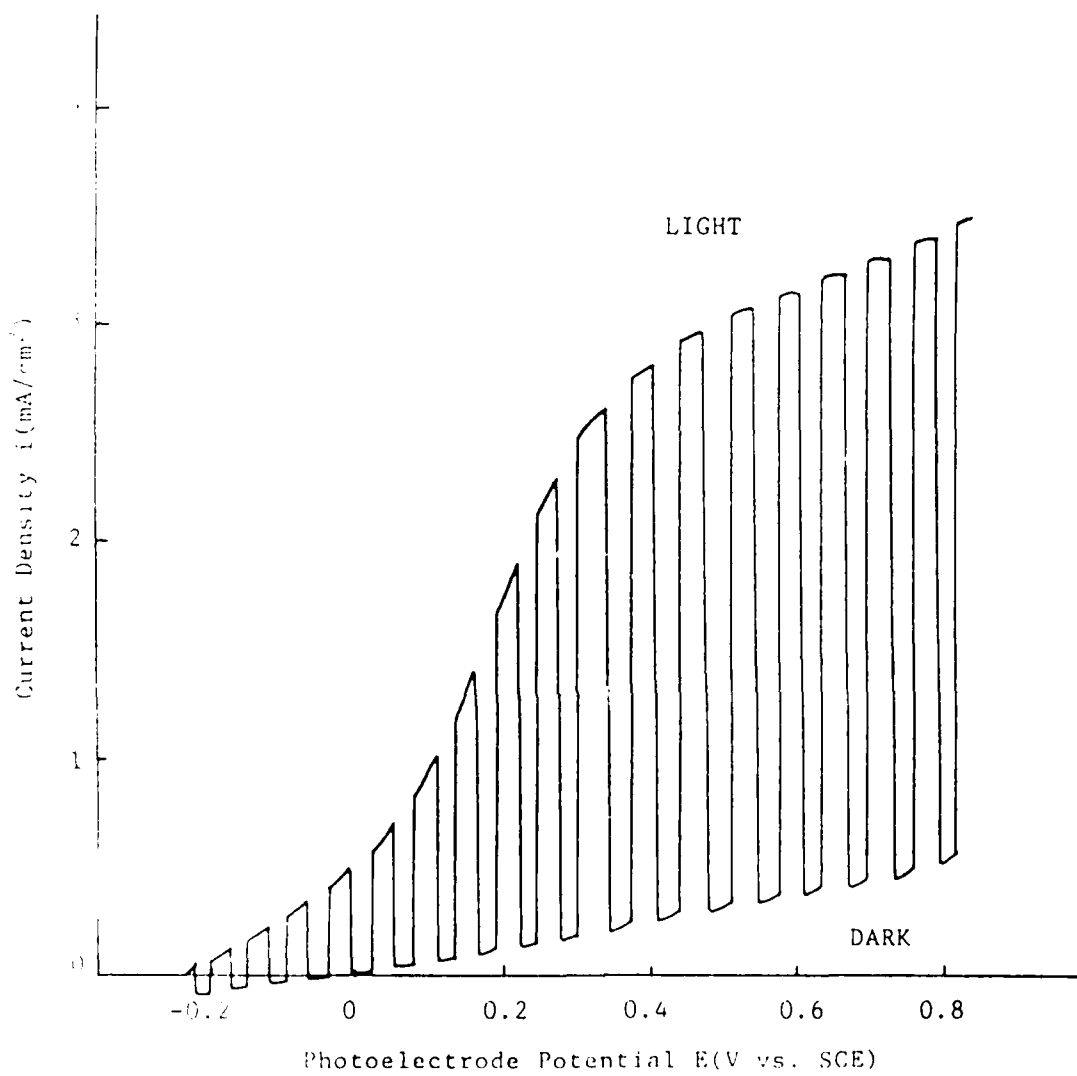


Figure 8.

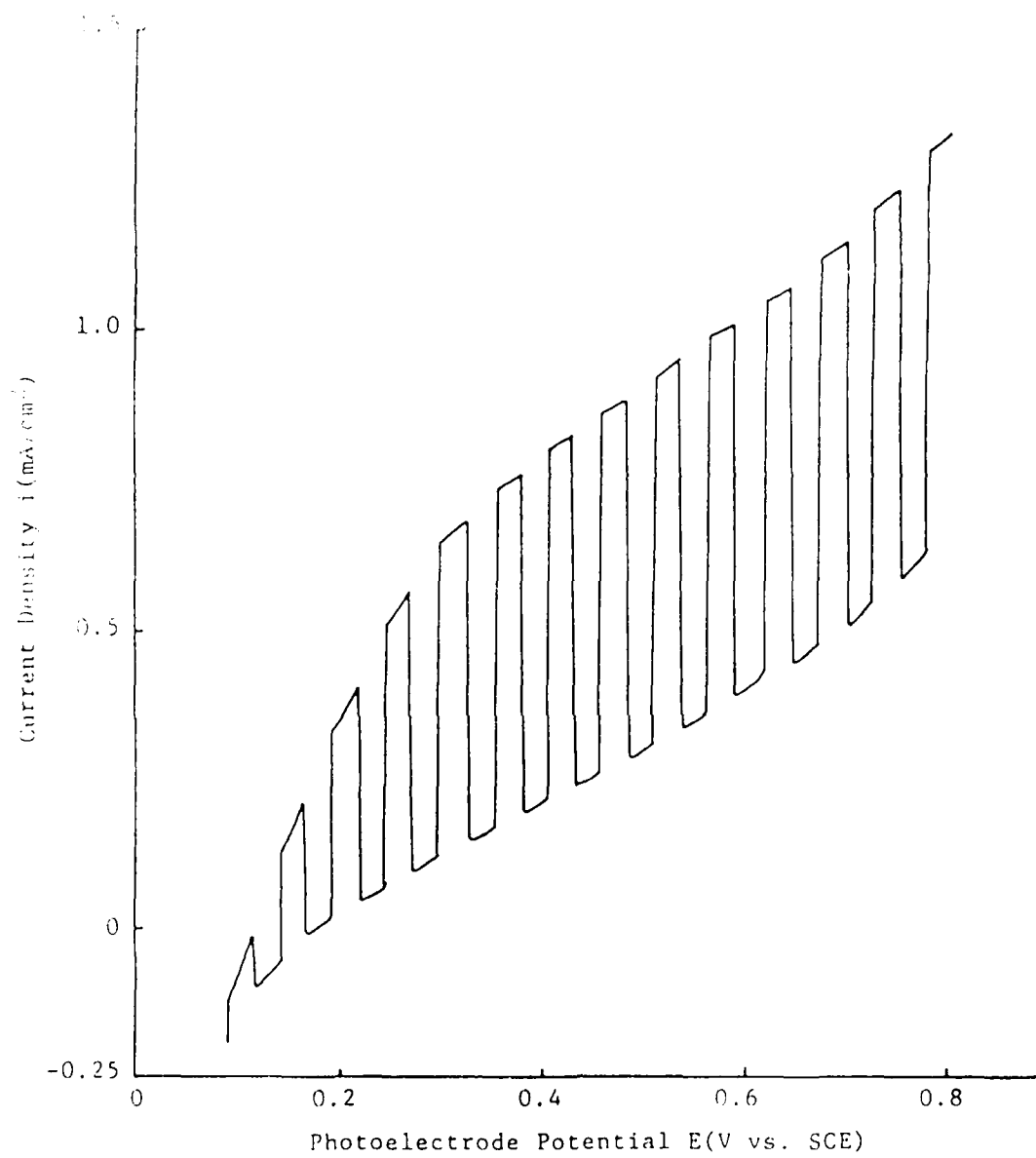


Figure 9.

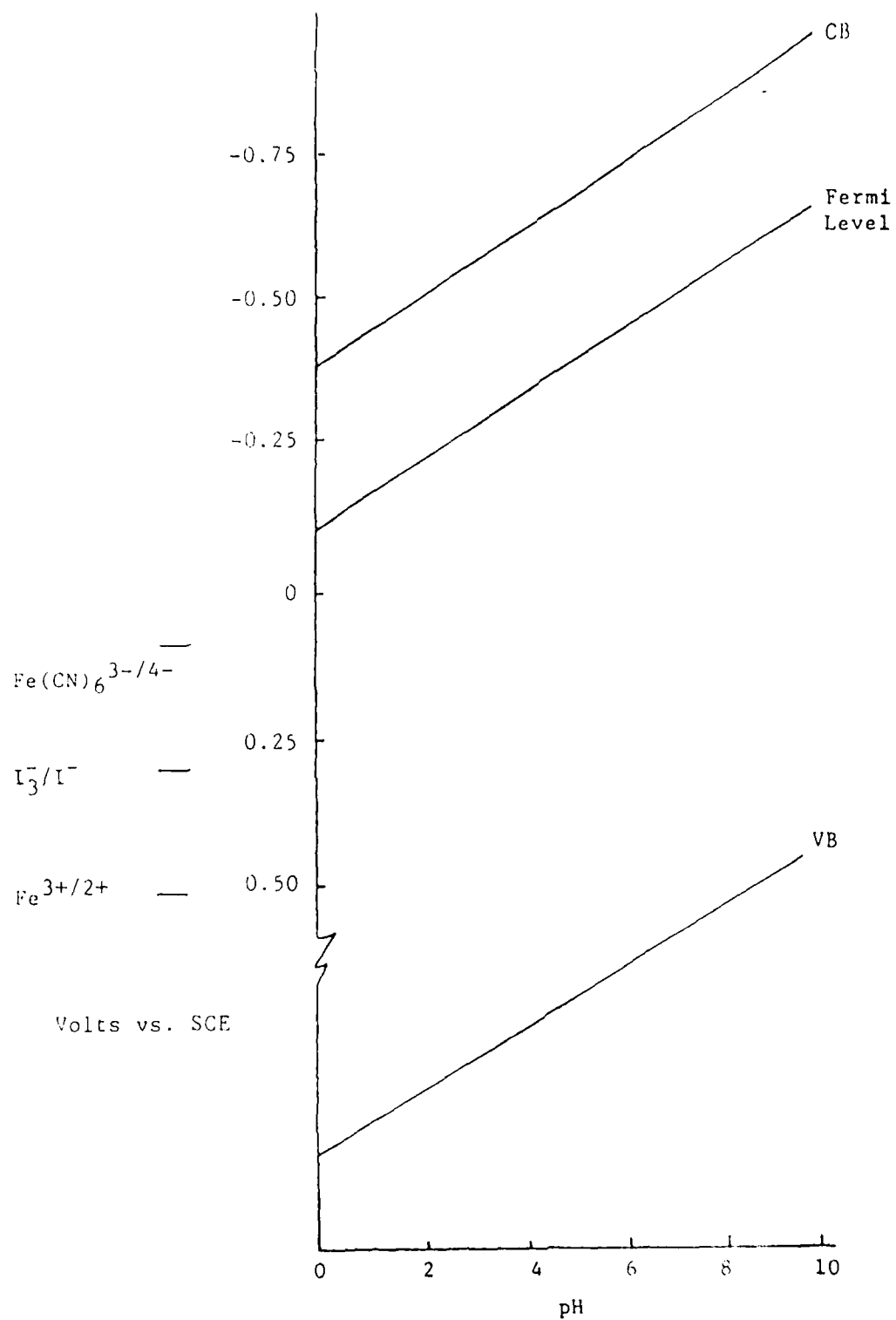


Figure 10.

SECURITY CLASSIFICATION OF THIS PAGE (When Data Entered)

REPORT DOCUMENTATION PAGE		READ INSTRUCTIONS BEFORE COMPLETING FORM
1. REPORT NUMBER 5	2. GOVT ACCESSION NO.	3. RECIPIENT'S CATALOG NUMBER
4. TITLE (and Subtitle) Transient Laser-Induced Photoelectrochemical Measurements at p-InP/Solid Polymer Electrolyte Interface		5. TYPE OF REPORT & PERIOD COVERED Technical Aug. 1987 - May 1988
7. AUTHOR(s) Ronald L. Cook, Robert C. MacDuff and Anthony F. Sammells		6. PERFORMING ORG. REPORT NUMBER
9. PERFORMING ORGANIZATION NAME AND ADDRESS Eltron Research, Inc. 4260 Westbrook Drive Aurora, IL 60504		8. CONTRACT OR GRANT NUMBER(s) N00014-86-C-0128
11. CONTROLLING OFFICE NAME AND ADDRESS Office of Naval Research/Chemistry Program		10. PROGRAM ELEMENT, PROJECT, TASK AREA & WORK UNIT NUMBERS
14. MONITORING AGENCY NAME & ADDRESS (if different from Controlling Office) Above		12. REPORT DATE May 1988
		13. NUMBER OF PAGES 25
		15. SECURITY CLASS. (of this report) Unclassified
		15a. DECLASSIFICATION/DOWNGRADING SCHEDULE
16. DISTRIBUTION STATEMENT (of this Report) Approved for public release, distribution unlimited.		
17. DISTRIBUTION STATEMENT (of the abstract entered in Block 20, if different from Report) Approved for public release, distribution unlimited.		
18. SUPPLEMENTARY NOTES Submitted: Journal of the Electrochemical Society		
19. KEY WORDS (Continue on reverse side if necessary and identify by block number) transient photocurrent measurements, indium phosphide, solid polymer electrolytes		
20. ABSTRACT (Continue on reverse side if necessary and identify by block number) Laser-induced photocurrent transient measurements at p-InP/solid polymer electrolyte (SPE) interface were performed as a function of both introduced redox couple within the polymer matrix (methylviologen) and dispersed platinum at the interfacial region. Poly(ethylene oxide)/poly(ethylene glycol) (PEO/PEG) mixtures were used as the SPE in this work. Platinum was found to enhance electron transfer across this interface ( $\tau = 3.57\mu\text{s}$ for p-InP/Pt vs. $5.12\mu\text{s}$ for p-InP). However, methylviologen present in the polymer was not found an effective electron acceptor but appeared responsible for introducing recombination		

DD FORM 1 JAN 73 1473

EDITION OF 1 NOV 65 IS OBSOLETE  
1/N 0107- LR 014-6601

Unclassified

SECURITY CLASSIFICATION OF THIS PAGE (When Data Entered)

sites at the interfacial region. Here, two segment decay curves were observed with only the slower decay rate being dependent upon potential. Results from this work suggest that further improvements in electrocatalysis at this interface will be necessary for promoting efficient minority carrier transfer from the semiconductor to polymer immobilized redox species proximate to the interface.

# TRANSIENT LASER-INDUCED PHOTOELECTROCHEMICAL MEASUREMENTS

## AT p-InP/SOLID POLYMER ELECTROLYTE INTERFACE

Ronald L. Cook\*, Robert C. MacDuff and  
Anthony F. Sammells\*

Eltron Research, Inc.  
Aurora, Illinois 60504

### ABSTRACT

Laser-induced photocurrent transient measurements at p-InP/solid polymer electrolyte (SPE) interface were performed as a function of both introduced redox couple within the polymer matrix (methylviologen) and dispersed platinum at the interfacial region. Poly(ethylene oxide)/poly(ethylene glycol) (PEO/PEG) mixtures were used as the SPE in this work. Platinum was found to enhance electron transfer across this interface ( $\tau = 3.57\mu\text{s}$  for p-InP/Pt vs.  $5.12\mu\text{s}$  for p-InP). However, methylviologen present in the polymer was not found an effective electron acceptor but appeared responsible for introducing recombination sites at the interfacial region. Here two segment decay curves were observed with only the slower decay rate being dependent upon potential. Results from this work suggest that further improvements in electrocatalysis at this interface will be necessary for promoting efficient minority carrier transfer from the semiconductor to polymer immobilized redox species proximate to the interface.

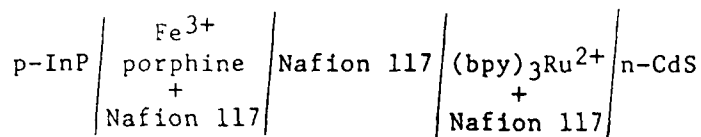
\*Electrochemical Society Active Member

Key Words: transient photocurrent measurements, indium phosphide,  
solid polymer electrolytes

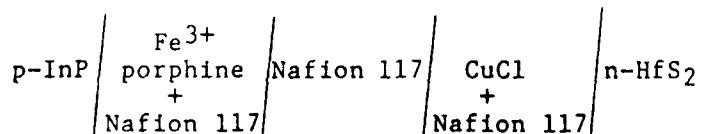


## INTRODUCTION

Solid polymer electrolyte (SPE)/photoelectrode interface provide an approach for the photoelectrochemical (PEC) conversion and storage of redox species incorporated in close proximity of this interfacial region. In general, lower recombination rates for photogenerated carriers might be expected at such interface<sup>1,2</sup> compared to junctions between polycrystalline semiconductors and solid electrolytes where high surface state populations are found resulting in low overall photoactivity<sup>3</sup>. Furthermore, SPE/photoelectrode interface can provide a strategy for protecting illuminated semiconductors from photocorrosion effects. We have previously reported on the preliminary PEC performance of solid-state SPE cells<sup>1,2</sup> where photopotentials in excess of 1V were reported<sup>1</sup> with typical SPE cell configurations investigated including:



$p\text{-InP/PEO, NaSCN, Na}_2\text{S, S/n-CdS}$



In this latter cell the van der Waal layers present in single crystal  $n\text{-HfS}_2$  would also be available for the reversible intercalation of copper redox species resident at the interfacial region, thereby providing, in principle, some storage capacity within the photoanode material itself.

A number of other solid-state SPE PEC cells have also been investigated<sup>4-6</sup> by other workers, with most experimental effort to this time being directed towards device fabrication. Results on the cell  $n\text{-Si, Pt, ppy/PEO/Pt, ITO}$ <sup>5</sup> (where ppy = polypyrrole and PEO = poly(ethylene oxide)), have suggested that overall device efficiency may be limited by not only the low PEO ionic conductivity, but also by surface recombination of photogenerated carriers present at the interfacial region, and consequent low efficiency for minority carrier transfer across the semiconductor polymer electrolyte junction.

Although a number of SPEs may be considered for this interfacial region, including  $\text{Ag}^+/\text{poly(ethylene sulfide)}$ <sup>7</sup>,  $\text{Li}^+/\text{poly(ethylene succinate)}$ <sup>8</sup> and  $\text{Li}^+/\text{poly(N-methylaziridine)}$ <sup>9</sup>, the most promising candidate materials for this

application appear to be PEO<sup>9</sup> and polyphosphazenes possessing etheric side groups<sup>10</sup>. The linear poly[(alkoxy)phosphazenes] incorporating LiCF<sub>3</sub>SO<sub>4</sub> have demonstrated ionic conductivities of  $7.5 \times 10^{-5} \text{ ohm}^{-1}\text{cm}^{-1}$  at 55°C. The ionic conductivity of PEO can be improved at temperatures closer to ambient by the introduction of poly(ethylene glycol) PEG<sup>11</sup> (mole fraction 0.6). This appears to be a result of the consequent partial dissolution of the crystalline PEO phases together with plasticization of its amorphous form, giving an SPE with an ionic conductivity of  $4 \times 10^{-4} \text{ ohm}^{-1}\text{cm}^{-1}$  at 55°C.

One technique which appears promising for providing mechanistic information on relative rates of minority carrier reaction pathways at illuminated semiconductor/electrolyte interface, is the application of laser-induced time-resolved photocurrent measurements<sup>12-18</sup>. This technique has also been previously used by us when investigating p-InP/aqueous electrolyte interface<sup>19-21</sup>. One feature of time-resolved photocurrent measurements is that information on kinetic parameters associated with minority carrier recombination and interfacial electron transfer may be obtained directly. This compares to steady-state photocurrent measurements where recombination and interfacial electron transfer rates can only be indirectly estimated using modeling procedures.

In this manuscript we discuss results obtained using laser induced time resolved photocurrent measurements as a probe for investigating kinetics associated with photogenerated carriers present at solid-state p-InP/PEO,PEG interface. The aim of this study is directed towards gaining insight into those physical parameters which lead to efficient minority carrier transfer to redox species immobilized in the polymer electrolyte matrix. Reduction of both the interfacial charge transfer resistance and that of the polymer electrolytes are the most direct routes to improving efficiencies for solid-state PEC/polymer storage cells.

## EXPERIMENTAL

A schematic of the experimental arrangement used in this work for performing laser-induced time-resolved photocurrent measurements on p-InP/SPE interface is shown in Figure 1. The excitation source was a PAR Model 2100 tunable dye laser, utilizing a TEA nitrogen laser for excitation of a grazing incidence dye laser. The pertinent features of the laser pulse are a pulse width of 1ns (FWHM) and a pulse energy of 30μJ, giving a nominal power output by the dye laser of 25kW throughout the tuning range. The laser dye used was rhodamine 6G,

which gave a maximum laser intensity when excited, to 588.19nm. The PEC cell used in this study consisted of a p-InP working electrode ( $0.10\text{cm}^2$  area) and a large ( $\approx 2\text{cm}^2$ ) indium tin oxide (ITO) counter electrode. The SPE was initially applied as a mixture of PEO(1.0g), PEG(1.52g) and  $\text{LiCF}_3\text{SO}_3$ (1.11g) in 20ml acetonitrile<sup>8</sup> to both p-InP and ITO. These two half-cells were then permitted to dry in air for 1 hour followed by a subsequent dry under vacuum overnight. Both electrodes were then pressed together and heated to  $55^\circ\text{C}$  under  $\text{N}_2$  using the experimental arrangement shown in Figure 2. A variable DC bias between the counter and working electrode was used to control the overall cell potential. The working p-InP photoelectrode potential for liquid junction cells used for comparative purposes in this study, was measured with respect to a SCE reference electrode via a high impedance digital voltmeter (Hewlett Packard 3478A). Transient photocurrents were recorded as a working electrode voltage drop across a 200 ohm resistor. The potential was directly introduced into a PAR Model 162 Boxcar Averager possessing an EG&G Model 165 Gated Integrator. Signal processing was triggered by a simultaneous fiber optics pulse from the tunable dye laser, and consequently could record the photocathode current response to the laser pulse without any appreciable delay. The time range over which the boxcar averager measured the signal could be set between 50ms and 100ns. The output of this system was a time resolved voltage analog of the transient current response, which was plotted on an X-Y recorder versus time. p-InP photocathodes  $\langle 100 \rangle$  were prepared from Zn doped p-InP (Crystacomm. Inc.) having a bulk doping density corresponding to  $N_D = 4 \times 10^{16}\text{cm}^{-3}$ . Contact to the p-InP wafer was made by sequential Au-Zn-Au vacuum deposition followed by annealing at  $475^\circ\text{C}$  under  $\text{H}_2$  for 2 min. Current collection was via a copper wire attached with silver epoxy (Epo-Tec) which was cured at  $150^\circ\text{C}$  for 1 hour. After appropriate insulation of both the current collector and photoelectrode ohmic contact regions with insulating epoxy (ChemGrip), the exposed photoelectrode front face was etched for 1 min. with concentrated HCl followed by a 3 min. etch with 6:1:1:1  $\text{HNO}_3:\text{HCl}:\text{CH}_3\text{COOH}:\text{HClO}_4$ .

#### RESULTS AND DISCUSSION

At illuminated photoelectrode/electrolyte junctions photogenerated minority carriers can be consumed by recombination either within the semiconductor bulk or at the semiconductor/electrolyte interface or transferred to an acceptor species in the electrolyte. This latter process can occur directly from the

photoelectrode conduction band or via surface states. Transient measurements of either photopotentials<sup>22</sup>, photocurrents<sup>16</sup> or photoluminescence<sup>23</sup> following pulsed laser illumination have been effective for probing minority carrier kinetics as a function of bulk<sup>24</sup> and surface semiconductor<sup>21,22</sup> modification. For transient photocurrent measurements, where information concerning charge transfer kinetics can be obtained, the transient photocurrent has been shown to be dominated by resistive and capacitive elements within the PEC cell<sup>13,16</sup>. Previous work has also shown that time dependency of the transient photocurrent decay signal can be modeled using an equivalent circuit for the PEC cell<sup>16</sup>. Tau ( $\tau$ ), the parameter characterizing time dependency for the photocurrent decay is given by:

$$\tau = (R_{\text{circuit}} \cdot C_{\text{circuit}}) \quad (1)$$

Analysis of  $\tau$  values in terms of various physical parameters can be accomplished by representing the cell as a series of resistive and capacitive elements. Figure 3 shows an equivalent circuit with RC elements representing various physical parameters in the cell. We have included in this representation RC elements corresponding to both carrier recombination at the semiconductor/electrolyte interface and Faradaic impedance. The Faradaic impedance consists of the charge transfer resistance  $R_{\text{ct}}$  and the resistive capacitive Warburg impedance elements  $R_2$  and  $C_2$ . However, a number of assumptions can be made to simplify the overall circuit to that shown in Figure 3B. For low light intensities the number of electrons reaching the surface can be smaller than the surface coverage of electrolyte molecules<sup>25</sup> so that the Warburg impedance associated with mass transfer limitations can be neglected. For semiconductor/electrolyte junctions  $C_{\text{sc}} \ll C_{\text{dl}}$  and thus the contribution of  $C_{\text{dl}}$  to the cell capacitance is small. Finally, the etch treatment used in this work can form a thin tunnelable oxide barrier which can passivate intra-band surface states.

For a pulsed RC circuit the current-time behavior can be given by<sup>26</sup>:

$$I(t) = I_F + (I_1 - I_F)e^{-t/\tau} \quad (2)$$

where  $I(t)$  is the current at time  $t$ ,  $I_F$  and  $I_1$  are the final and initial currents respectively,  $t$  is the time and  $\tau$  is the decay rate. For the p-InP/electrolyte system the photocurrent decayed to 0, so  $I_F = 0$  and the equation becomes:

$$I_t = I_1 e^{-t/\tau} \quad (3)$$

Rearranging and taking the natural log of both sides of equation (3) gives

$$\ln \frac{I(t)}{I_i} = -t/\tau \quad (4)$$

Plotting  $\ln \frac{I(t)}{I_i}$  vs.  $t$  allows one to obtain  $1/\tau$  from the slope. The decay rate  $\tau = RC$  for the simplified circuit is given by:

$$\tau = C_{sc}(R_{sc} + R_{ct} + R_{soln} + R_m) \quad (5)$$

Representative transient photocurrent decay spectra for respectively p-InP/SPE and p-InP/aq  $K_2SO_4$  interface are compared in Figure 4A and B, in the absence of any redox couple within the electrolyte. As evident from these results, the photocurrent decay response were similar.

For electron transfer from the conduction band to an acceptor molecule in an electrolyte the rate of electron transfer can be given by<sup>27</sup>:

$$i = i_0[\exp(-\eta_{sc}q/kt)-1] \quad (6)$$

where  $i$  is the current density,  $i_0$  is the exchange current density,  $\eta_{sc}$  the overvoltage when it appears across the semiconductor space charge region,  $q$  the charge on the electron and  $k$  the Boltzman constant. When the potential of the electron acceptor species ( $E^\circ_{redox}$ ) is significantly different than the potential of the conduction band edge ( $E^\circ_c$ )  $i_0$  and thus  $i$  can be extremely small. Thus, for efficient charge transfer to occur  $E^\circ_{redox} \approx E^\circ_c$  for p-InP  $E^\circ_c \approx 0.55V$  vs. NHE at pH 7<sup>27</sup>.

In the anhydrous polymer electrolyte PEO,PEG,LiCF<sub>3</sub>SO<sub>3</sub> the only reducible species within the voltage window of the PEO,PEG polymer would appear to be Li<sup>+</sup> (Li<sup>+</sup> + e<sup>-</sup> → Li<sup>0</sup>  $E^\circ = -3.03V$ ). It can be anticipated that for p-InP/PEO,PEG, LiCF<sub>3</sub>SO<sub>3</sub> cells with no impurities present in the polymer matrix, photocurrents would be negligible due to the large energy difference between  $E^\circ_{Li^+/Li}$  and  $E^\circ_c$ . Thus, molecular species with redox energies isoenergetic with the p-InP conduction band must be intentionally added to the SPE to permit transient photocurrent decay measurements.

For preliminary work on the p-InP/PEO,PEG,LiCF<sub>3</sub>SO<sub>3</sub> interface ≈1% water was added to the polymer to provide a suitable acceptor species for the photogenerated electrons. Here water reduction to give surface bound hydrogen was expected (e.g. p-InP + H<sub>2</sub>O + e → p-InP(H) + G.<sup>-</sup>). At the low laser pulse intensities present (neutral density filters were used to reduce laser intensity so that the voltage drop across the 200 ohm resistor was less than 25mV), only a small fraction of surface water would be necessary to permit electron transfer. For p-InP/PEO,PEG,LiCF<sub>3</sub>SO<sub>3</sub>/ITO cells, transient photocurrent decay spectra

were obtained at every 100mV between 0 to -600mV (vs. ITO). Due to variations in optical orientation, laser intensity due to dye breakdown, reflective losses and differences in electrode/polymer electrolyte contact quality, photocurrent analysis using absolute values can make comparison between different p-InP/SPE interface difficult.

To aid analysis of photocurrent-time results the photocurrent decay with respect to time was normalized to the peak current. Figure 5 and 6 show respectively the natural logarithm of the normalized photocurrent ( $\ln(I(t)/I_{\text{peak}})$ ) for the p-InP/polymer electrolyte junction at -0.1V and -0.3V. For these cells a single exponential decay of the photocurrent transient was observed at the p-InP/polymer electrolyte junction. From the slope of the curves in Figures 5 and 6, photocurrent decay rate constants ( $\tau$ ) could be obtained. The  $\tau$  values for the p-InP/PEO,PEG junction are given in Table 1 along with  $\tau$  values previously obtained at p-InP/aqueous  $K_2SO_4$  interfaces<sup>23</sup> (pH 6.9), where an increasing cathodic bias led to smaller  $\tau$  values.

Previous examination of transient photocurrent response at semiconductor electrolyte junctions has shown that the decay rate  $\tau$  is determined largely by cell RC elements<sup>12-18</sup>. For p-type photocathodes the application of an increasingly cathodic applied bias would result in larger space charge widths and consequently smaller space charge capacitances. This has been observed for transient photocurrent measurements in previous work<sup>21</sup> at p-InP/aqueous electrolyte interface. For carefully prepared semiconductor surfaces it has also been shown that  $1/\tau^2$  vs. applied bias plots should be linear<sup>16,21</sup>. Furthermore, since  $\tau=RC$ , such plots are analogous to Mott-Schottky plots. Figure 7 shows  $1/\tau^2$  as a function of applied bias for the p-InP/PEO,PEG, $LiCF_3SO_3$ /ITO cell. Here  $1/\tau^2$  was found linear with applied bias in the voltage range investigated. These results show that kinetics for transient photocurrent decay are dominated by the RC time constant of the semiconductor/polymer electrolyte cell and that such control is essentially identical to that observed at aqueous electrolyte/semiconductor junctions<sup>16,21</sup>.

By varying the value of the measurement resistor ( $R_m$ ) and plotting the value of  $\tau$  obtained at each value of  $R_m$ , an estimate of the cell resistance can be obtained. Figure 8 shows the results of such a plot for the SPE cell at 65°C at -0.5V vs. ITO. Under these conditions a cell resistance of 95 $\Omega$  was obtained. This value is about three times larger than that obtained in the cell p-InP/aqueous  $K_2SO_4$  (pH 6.9)/Pt( $\approx 35\Omega$ ). Lower cell resistances could be obtained by either reducing the thickness of the polymer electrolyte or increasing the temperature at which

the measurements were performed. However, this made the cell more susceptible to shorting during measurement. Previous work has shown that for n-Si/PEO(KI/I<sub>2</sub>) junctions significant improvements in the magnitude of the photocurrent could be realized by incorporating polypyrrole and platinum onto the surface of the n-Si electrode<sup>10</sup>. It is thought that this procedure lowers the activation energy for charge transfer to acceptor species in the polymer electrolyte. Since high activation energies lead to large charge transfer resistances, which lowers the overall solar conversion efficiency, it was of interest to see if similar procedures could also improve charge transfer at the p-InP/SPE interface. For p-InP however, it was found that pyrrole could not be polymerized onto the p-InP surface due to oxidation of the latter over the potential range necessary for pyrrole polymerization (-0.8V vs. SCE). Consequently, platinum was selected as the p-InP surface modification to be evaluated for promoting electron transfer across the p-InP/SPE interfacial region. Recent work by us has shown that  $\tau$  is sensitive to the nature of the metal deposited onto the electrode surface<sup>21</sup>. It was observed that in aqueous electrolyte faster decay rates (lower  $\tau$  values) were obtained for p-InP surface modified with platinum than for lead. In fact  $\tau$  values could be correlated with exchange current densities found for the bulk metals<sup>21</sup>.

Table 2 and Figure 9 summarize results from transient photocurrent measurements for the cell p-InP/Pt/PEO,PEG,LiCF<sub>3</sub>SO<sub>3</sub>/ITO. From cells of this configuration a single exponential decay was found and  $1/\tau^2$  was found to be linear with applied bias. These results show that the PEC deposition of Pt at the p-InP/polymer electrolyte interface does not significantly introduce new RC elements (such as deleterious mid-gap surface states) into the solid-state PEC cell. However, since cell resistance for p-InP(Pt)/PEO,PEG cells were close to those for p-InP/PEO,PEG (160 $\Omega$  for the p-InP/Pt/PEO,PEG cells), and since the electrodeposited Pt is not likely to introduce a change in  $C_{sc}$ <sup>21</sup>, the lower  $\tau$  values obtained for the p-InP/Pt/polymer junction suggest that some measure of improvement in the electron transfer rate has been achieved.

To achieve some electrical storage capacity in these cells it is a necessary requirement that a reversible redox couple be present in the polymer matrix. To examine the effects of intentionally introduced redox couples on the transient photocurrent decay response we have examined p-InP/PEO,PEG,LiCF<sub>3</sub>SO<sub>3</sub>/ITO with methylviologen as the redox species. Methylviologen (1,1'-dimethyl-4,4'

bipyridium)(2+),  $MV^{2+}$  has previously been shown to be an effective electron acceptor from the uncatalyzed p-InP/aqueous electrolyte interface<sup>28</sup>. Figure 10 shows a typical transient photocurrent decay spectrum for the cell p-InP/ $MV^{2+}$ , PEO, PEG,  $LiCF_3SO_3$ /ITO (.1g  $MV^{2+}$  in 20ml  $CH_3OH$  containing 1g PEO + 1.52g PEG + 1.11g  $LiCF_3SO_3$ ). For all cells fabricated and potentials investigated over the voltage range 0 to -800mV vs. ITO, a two segment exponential decay was observed.  $\tau$  Values for the initial fast segment were essentially constant as the voltage was changed from -0.1V to -0.6V vs. ITO (ave. value = 3.3 $\mu$ s) whereas the slower segment varied with applied potential.

Previous work has suggested that surface traps and/or recombination centers may be responsible for observed fast decay by the photocurrent transient<sup>12,13,16</sup>. Adsorbed ionic acceptors such as  $S^{2-}$  have been shown to increase the surface recombination velocity on CdS by three orders of magnitude<sup>9,23</sup>. Under open-circuit conditions, where the rate bulk and surface recombination determine the rate of decay of transient photopotential response, slower decay was observed on native  $TiO_2$  than on sionized  $TiO_2$ <sup>24</sup>. Thus, the faster decay observed here on p-InP may be due, in part, to  $MV^{2+}$  induced surface traps or recombination centers. The slower segment appears to be RC controlled since  $\tau$  decreases with increasing cathodic bias and plots of  $1/\tau^2$  are linear (Figure 11). When differences in series resistance are taken into account (210 $\Omega$  for methylviologen cell vs. 95 $\Omega$  for PEO, PEG,  $LiCF_3SO_3$  alone), the  $\tau$  values at a given applied bias are quite similar (210 $\Omega$ /95 $\Omega$   $\cdot$  3.41 $\mu$ s = 7.62 $\mu$ s). These results suggest that, at least in the case of the p-InP/PEO, PEG interface, simple addition of a redox couple known to possess good electron transfer kinetics<sup>28,29</sup> at the semiconductor/aqueous electrolyte junction does not necessarily lead to similar behavior at the semiconductor/polymer electrolyte junction. Furthermore, such redox couples may also induce surface states leading to increased surface recombination velocities at the semiconductor/polymer electrolyte junction. Transient photocurrent measurements following short laser pulses may give some insight into how such interfacial modifications can lead to higher solar energy conversion efficiencies at semiconductor/polymer junctions.

#### CONCLUSIONS

Measurement of the transient photocurrent response of p-InP/polymer electrolyte junctions have shown in a similar manner to p-InP/aqueous electrolyte junctions, that the photocurrent decay rate is dominated by the RC time constant of the cell.



Thus, modifications to the interfacial structure at the p-InP/polymer junction can be expected to result in changes in  $\tau$ . For the p-InP/polymer electrolyte system investigated in this work it was shown that photoelectrochemically deposited platinum can enhance electron transfer across the semiconductor/polymer electrolyte interface. However, simple inclusion of redox reagents having known good electron transfer kinetics at semiconductor/aqueous electrolyte junction, may not result in similar kinetics at the semiconductor/polymer electrolyte junctions. For efficient minority carrier transfer to the polymer bound acceptor, more complex interfacial structures incorporating electrodeposited metal or electrically conducting polymers between the semiconductor and redox species may be necessary.

#### ACKNOWLEDGEMENT

This work was supported in part by the Office of Naval Research.

# REFERENCES

1. A. F. Sammells and S. K. Schmidt, J. Electrochem. Soc., 132, 520 (1985).
2. A. F. Sammells and P. G. P. Ang, J. Electrochem. Soc., 131, 617 (1984).
3. P. G. P. Ang and A. F. Sammells, Photoeffects at Semiconductor/Electrolyte Interfaces, A. J. Nozik, Ed., Am. Chem. Soc. Symp., Series 146, 387-99, Washington D.C. (1981).
4. T. Skotheim and I. Lundstrom, J. Electrochem. Soc., 129, 895 (1982).
5. T. A. Skotheim and O. Inganas, J. Electrochem. Soc., 132, 2117 (1985).
6. T. Skotheim, Appl. Phys. Lett., 38, 712 (1981).
7. D. F. Shriver, B. L. Papke, M. A. Ratner, R. Dupon, T. Wen and M. Brodwin, Solid State Ionics, 5, 83 (1981).
8. D. F. Shriver, R. Dupon and M. Stainer, Extended Abstracts Electrochem. Soc., 83, Number 490, San Francisco (1983).
9. M. Armand, Solid State Ionics, 10, 745 (1983).
10. P. M. Blonsky and D. F. Shriver, J. Am. Chem. Soc., 106, 6854 (1984).
11. J. Kelly, J. R. Owen and B. C. H. Steele, J. Electroanal. Chem., 168, 467 (1984).
12. Z. Harzion, D. Huppert, S. Gottesfeld and N. Croitoru, J. Electroanal. Chem., 150, 571 (1983).
13. Z. Harzion, N. Croitoru and S. Gottesfeld, J. Electrochem. Soc., 128, 551 (1981).
14. T. Sakata, E. Janata, W. Jaegermann and H. Tributsch, J. Electrochem. Soc., 133, 339 (1986).
15. W. Jaegermann, J. Phys. Chem., 88, 5309 (1984).
16. R. H. Wilson, T. Sakata, T. Kawai and K. Hashimoto, J. Electrochem. Soc., 132, 1082 (1985).
17. W. Jaegermann, T. Sakata, E. Janata and H. Tributsch, J. Electroanal. Chem., 189, 65 (1985).
18. S. Prybyla, W. S. Struve and B. A. Parkinson, J. Electrochem. Soc., 131, 1587 (1984).
19. R. L. Cook, P. F. Dempsey and A. F. Sammells, J. Electrochem. Soc., 133, 1821 (1986).
20. R. L. Cook, P. F. Dempsey and A. F. Sammells, J. Electrochem. Soc., 133, 2287 (1986).
21. R. L. Cook, R. C. MacDuff and A. F. Sammells, J. Electrochem. Soc., (submitted).
22. P. V. Kamat and M. A. Fox., J. Phys. Chem., 87, 59 (1983).
23. M. Evenor, D. Huppert and S. Gottesfeld, J. Electrochem. Soc., 133, 296 (1986).
24. K. Bitterling, F. Willig and F. Decker, J. Electroanal. Chem., 228, 29 (1987).

FD-302 (Rev. 11-27-70)

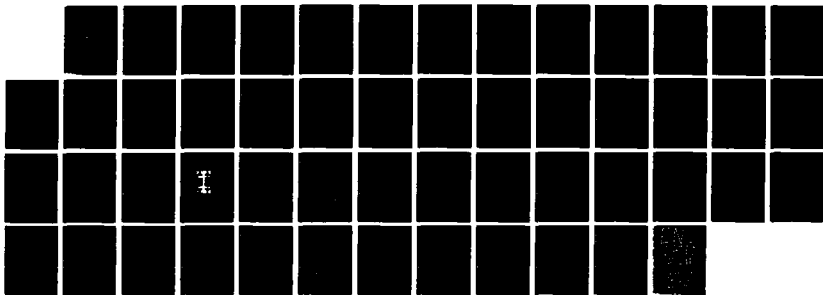
PHOTOINTERCALATING SEMICONDUCTOR/SOLID ELECTROLYTE  
JUNCTIONS FOR STORAGE A (U) ELTRON RESEARCH INC AURORA  
IL A F SAMMELLS 31 MAY 88 N00014-86-C-0128

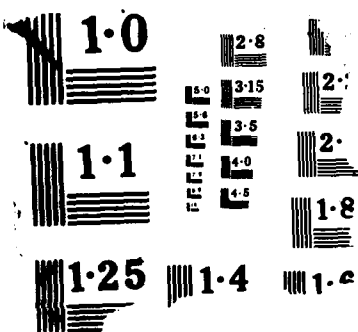
2/2

UNCLASSIFIED

F/G 7/6

NL





25. S. Prybyla, W. S. Struve and B. A. Parkinson, J. Electrochem. Soc., 131, 1587 (1984).
26. T. L. Floyd, Principles of Electronic Circuits, Charles E. Merrill Publ. Co., Columbus, OH pp. 407-445 (1981).
27. S. R. Morrison, "Electrochemistry at Semiconductor and Oxidized Metal Electrodes", Plenum Press, NY pp. 79-113 (1988).
28. A. B. Bocarsly, D. C. Bookbinder, R. W. Dominey, N. S. Lewis and M. S. Wrighton, J. Am. Chem. Soc., 103, 3683 (1980).
29. D. C. Bookbinder, N. S. Lewis, M. G. Bradley, A. B. Bocarsly and M. S. Wrighton, J. Am. Chem. Soc., 101, 7721 (1979).

TABLE 1

Photocurrent decay rate constants for p-InP at aqueous and polymer electrolyte junctions.

Applied Bias <sup>a</sup>	$\tau(\mu\text{s})$		$1/\tau^2(10^{-5}\mu\text{s}^{-2})$	
	H <sub>2</sub> O	PEO/PEG	H <sub>2</sub> O	PEO/PEG
-0.1	4.91	5.82	.042	.0295
-0.2	3.83	5.30	.068	.0356
-0.3	3.41	5.12	.086	.0381
-0.4	3.07	4.85	.106	.0425
-0.5	2.64	4.69	.143	.0455
-0.6	2.52	4.50	.157	.0494

<sup>a</sup> vs. SCE in aqueous electrolyte, vs. ITO in polymer electrolyte.

TABLE 2

Photocurrent decay rate constants for p-InP/Pt/PEO,PEG,LiCF<sub>3</sub>SO<sub>3</sub>/ITO cell configurations.

Bias	$\tau(\mu\text{s})$	$1/\tau^2(10^{-5}\mu\text{s}^{-2})$
-0.1	3.732	.0718
-0.2	3.645	.0757
-0.3	3.567	.0786
-0.4	3.497	.0821
-0.5	3.402	.0864
-0.6	3.343	.0893
VITO	TITO	

TABLE 3

Photocurrent decay rate constants for the cell  
p-InP/PEO,PEG,LiCF<sub>3</sub>SO<sub>3</sub>,MV<sup>2+</sup>/ITO at 65°C and R<sub>m</sub> = 200Ω.

Applied Bias	$\tau^a$ (μs)		$1/\tau^2 (10^{-5} \mu s^{-2})$
	FD	SD	
-0.1	3.38	9.64	0.0108
-0.2	3.42	8.31	0.0145
-0.3	3.31	7.63	0.0172
-0.4	3.35	6.86	.0213
-0.5	3.40	6.26	.0255
-0.6	3.41	5.82	.0295

<sup>a</sup>FD = fast decay, SD = slow decay

# FIGURE CAPTIONS

- Figure 1. Schematic diagram for laser induced time resolved measurements performed on p-InP/SPE interface in this work.
- Figure 2. Schematic of cell used in obtaining time resolved photocurrent measurements on cells of configuration p-InP/PEO,PEG/ITO.
- Figure 3. a) Equivalent circuit for photoelectrochemical cell.  
b) Simplified circuit.
- Figure 4. a) Transient photocurrent spectra for the cell p-InP/PEO,PEG,LiCF<sub>3</sub>SO<sub>3</sub>/ITO at 65°C. Bias = 0.3V. R<sub>m</sub> = 200Ω.  
b) Transient photocurrent response for p-InP in K<sub>2</sub>SO<sub>4</sub>. pH = 6.9 following 1ns laser pulse.
- Figure 5. Plot of the normalized natural log of photocurrent response as a function of time for the cell p-InP/PEO,PEG,LiCF<sub>3</sub>SO<sub>3</sub>/ITO at 65°C and applied bias of -0.1V. R<sub>m</sub> = 200Ω.
- Figure 6. Plot of the normalized natural log of photocurrent response as a function of time for the cell p-InP/PEO,PEG,LiCF<sub>3</sub>SO<sub>3</sub>/ITO at 65°C and applied bias of -0.3V. R<sub>m</sub> = 200Ω.
- Figure 7. Reciprocal of the square of the measured decay constant  $\tau$  as a function of applied bias for the cell p-InP/PEO,PEG, LiCF<sub>3</sub>SO<sub>3</sub>/ITO at 65°C. R<sub>m</sub> = 200Ω.
- Figure 8. Plot of  $\tau$  as a function of load resistance for the cell p-InP/PEO,PEG,LiCF<sub>3</sub>SO<sub>3</sub>/ITO at 65°C and a bias of -0.5V vs. ITO.
- Figure 9. Reciprocal of the square of the measured decay constant  $\tau$  plotted as a function of applied bias for the cell p-InP/Pt/PEO,PEG,LiCF<sub>3</sub>SO<sub>3</sub>/ITO at 65°C. R<sub>m</sub> = 200Ω.
- Figure 10. Plot of the normalized natural log of the photocurrent response as a function of time for the cell p-InP/PEO,PEG, LiCF<sub>3</sub>SO<sub>3</sub>,MV<sup>2+</sup>/ITO at 65°C and an applied bias of -0.3V (vs. ITO). R<sub>m</sub> = 200Ω.
- Figure 11. Reciprocal of the square of the measured decay constant  $\tau$  as a function of applied bias for the cell p-InP/MV<sup>2+</sup>,PEO,PEG, LiCF<sub>3</sub>SO<sub>3</sub>/ITO at 65°C. R<sub>m</sub> = 200Ω.



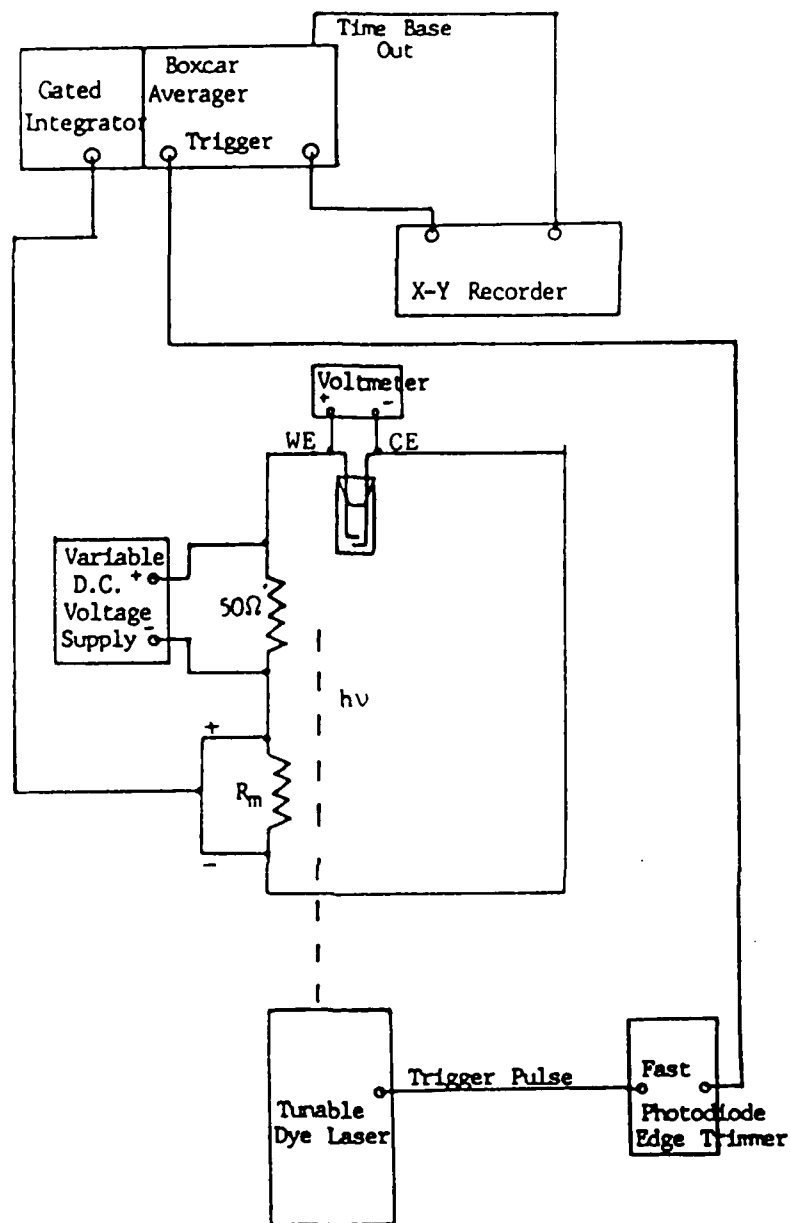


Figure 1.

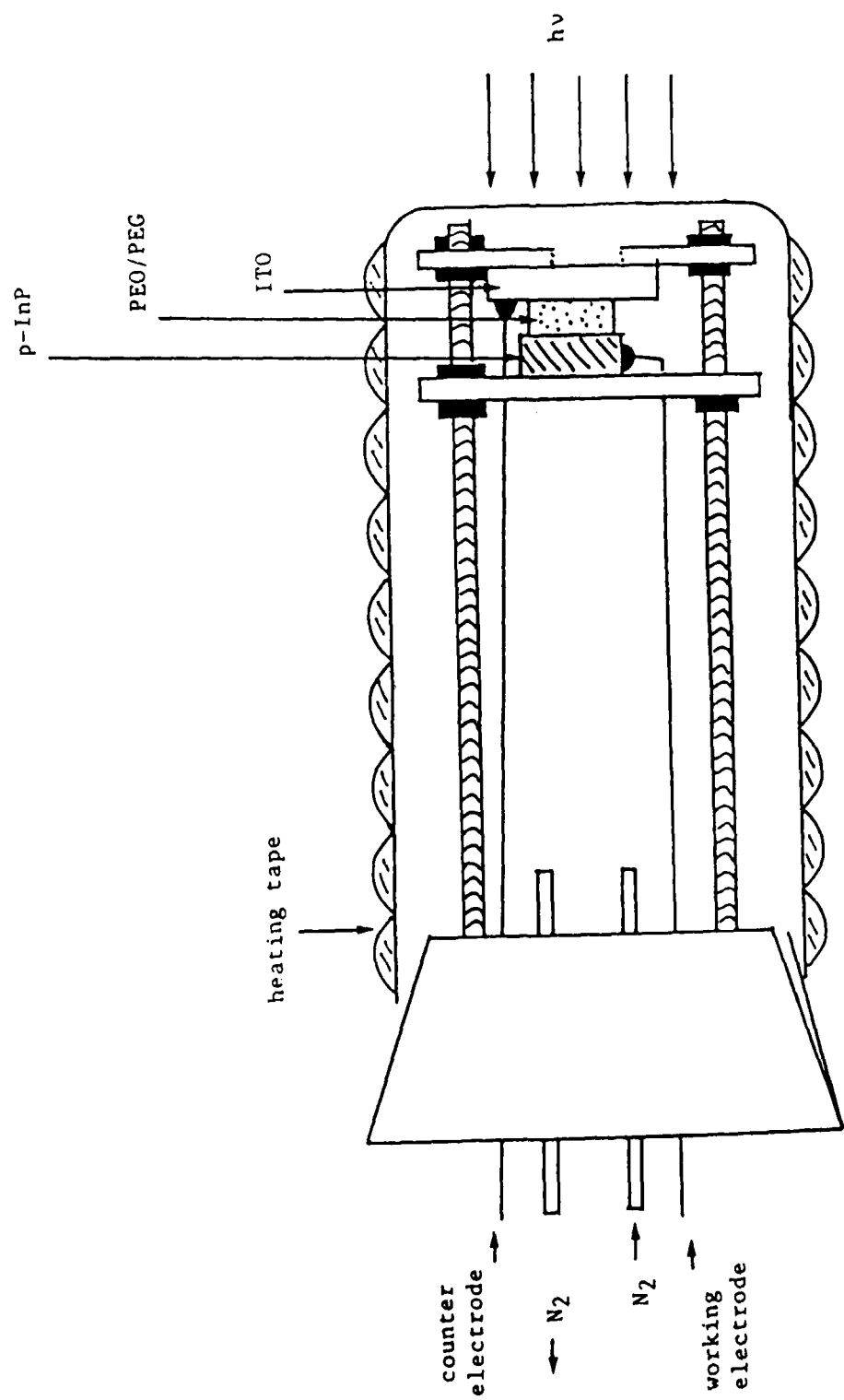


Figure 2.

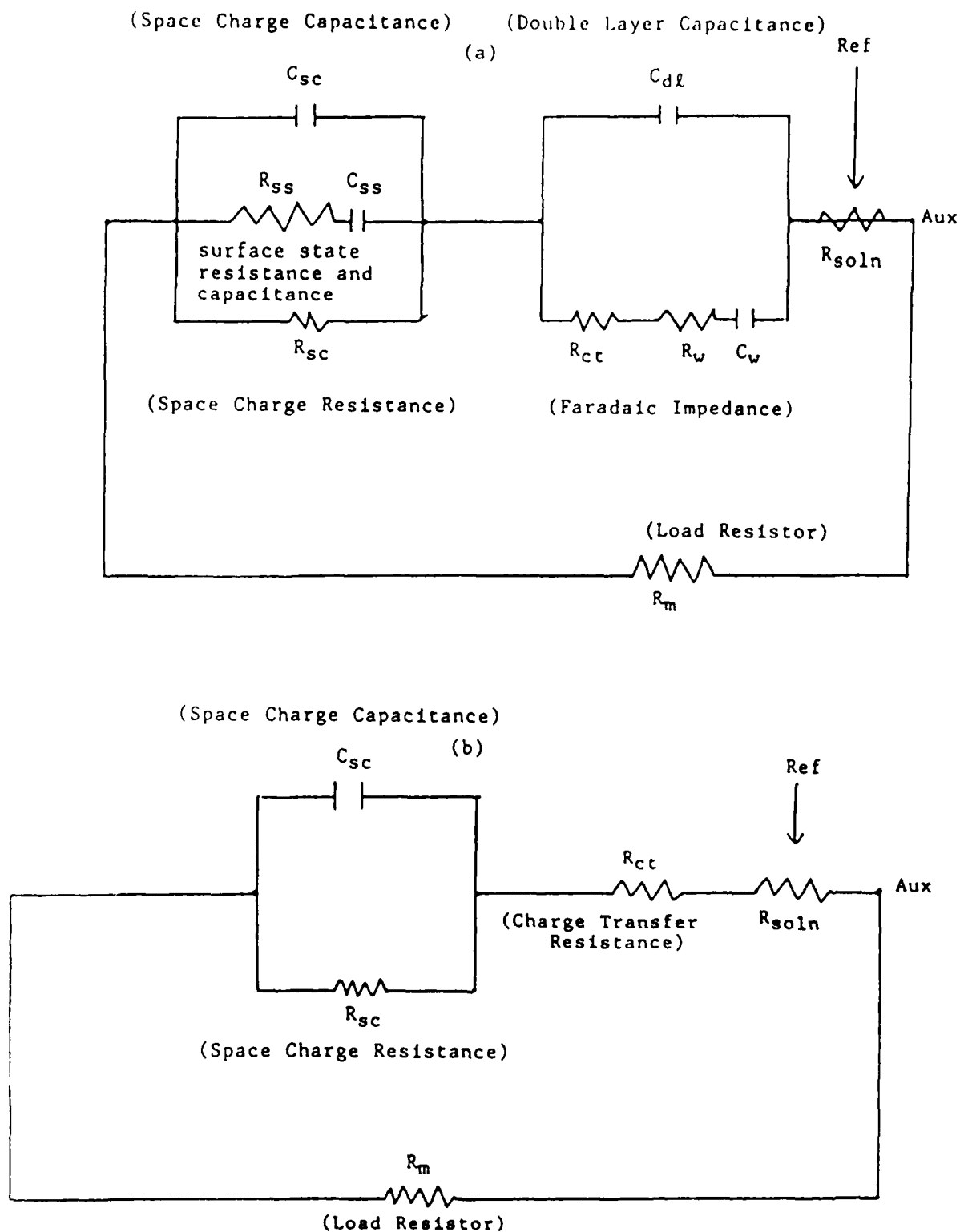


Figure 3.

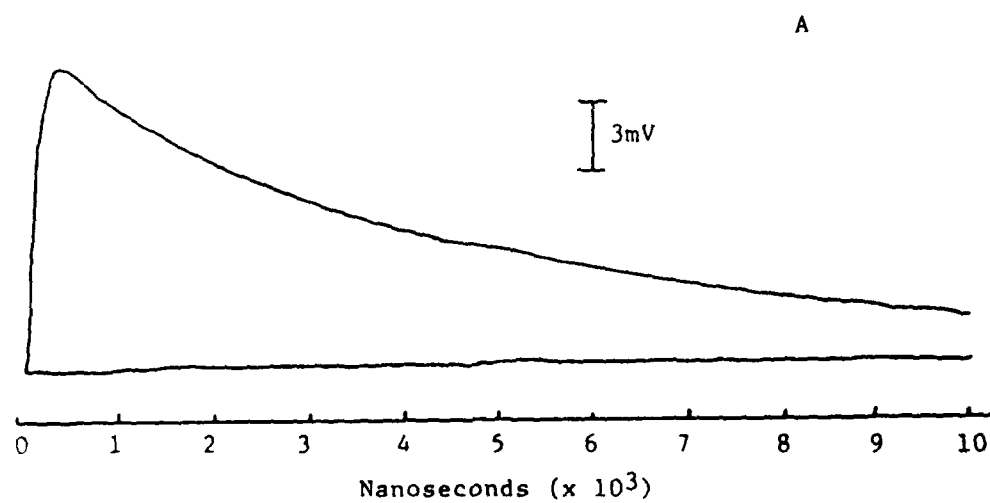


Figure 4A.

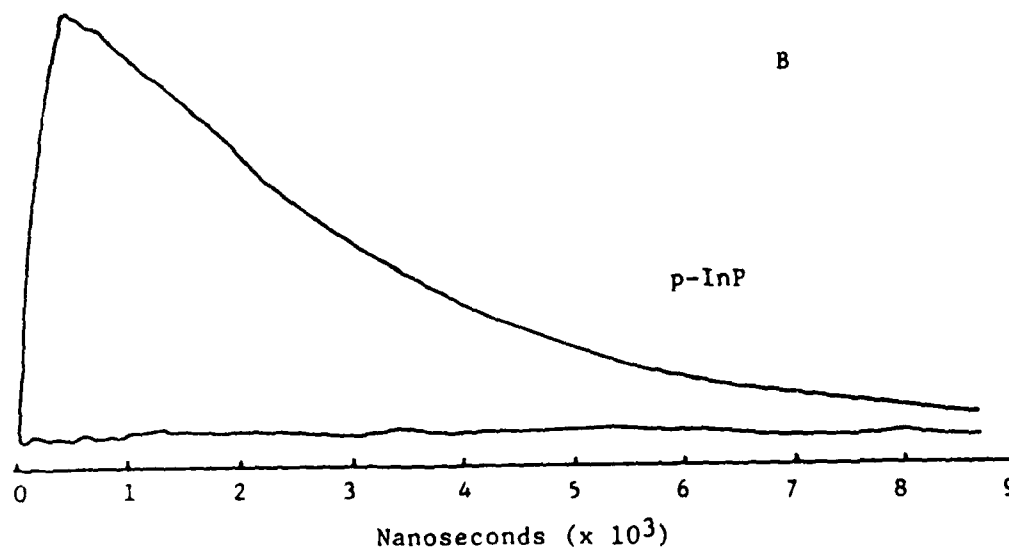


Figure 4B.

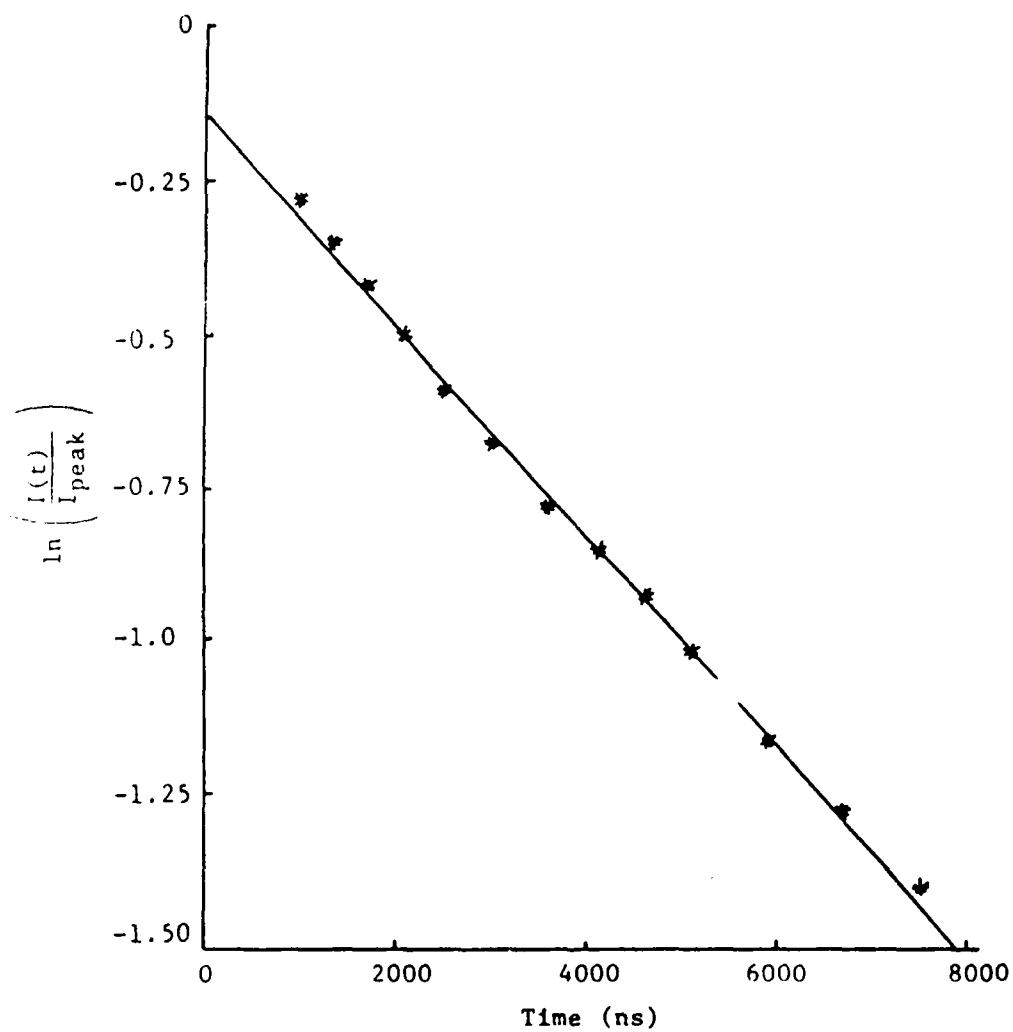


Figure 5.

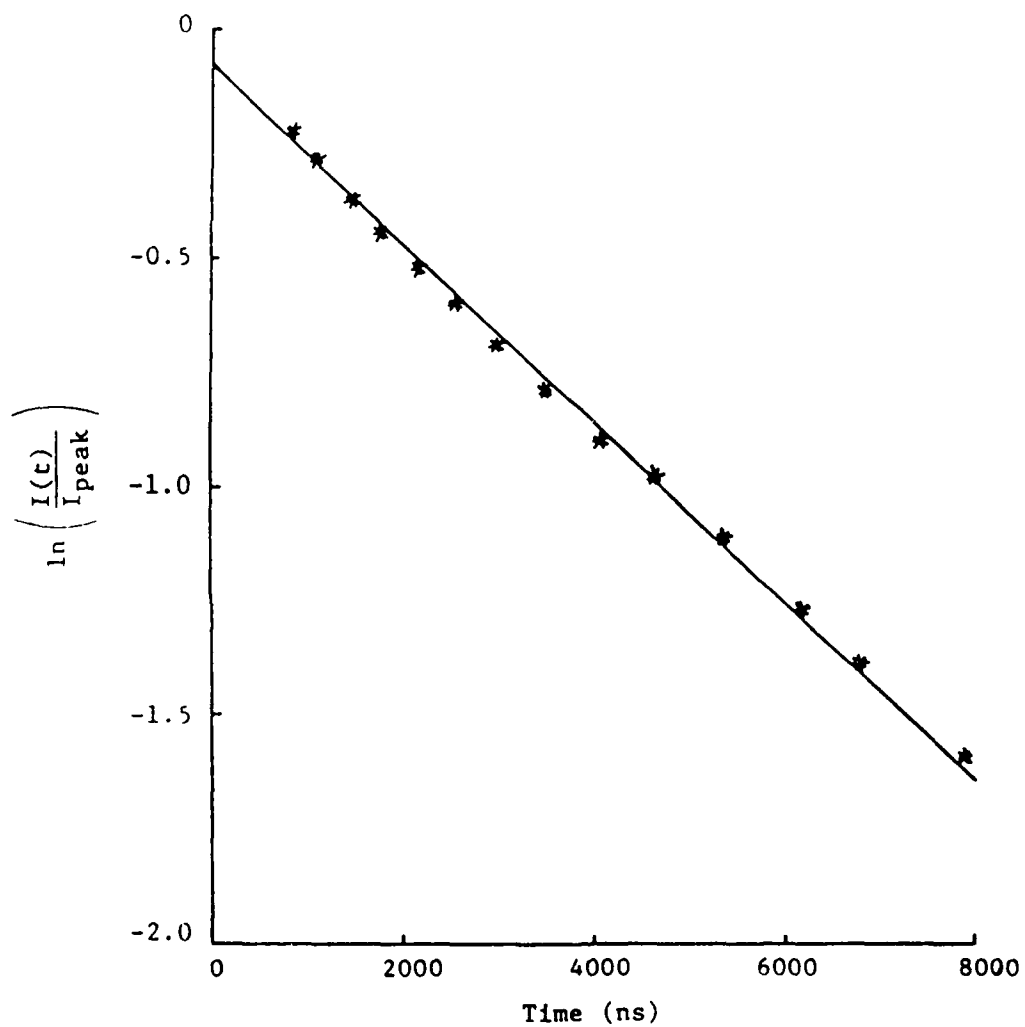


Figure 6.

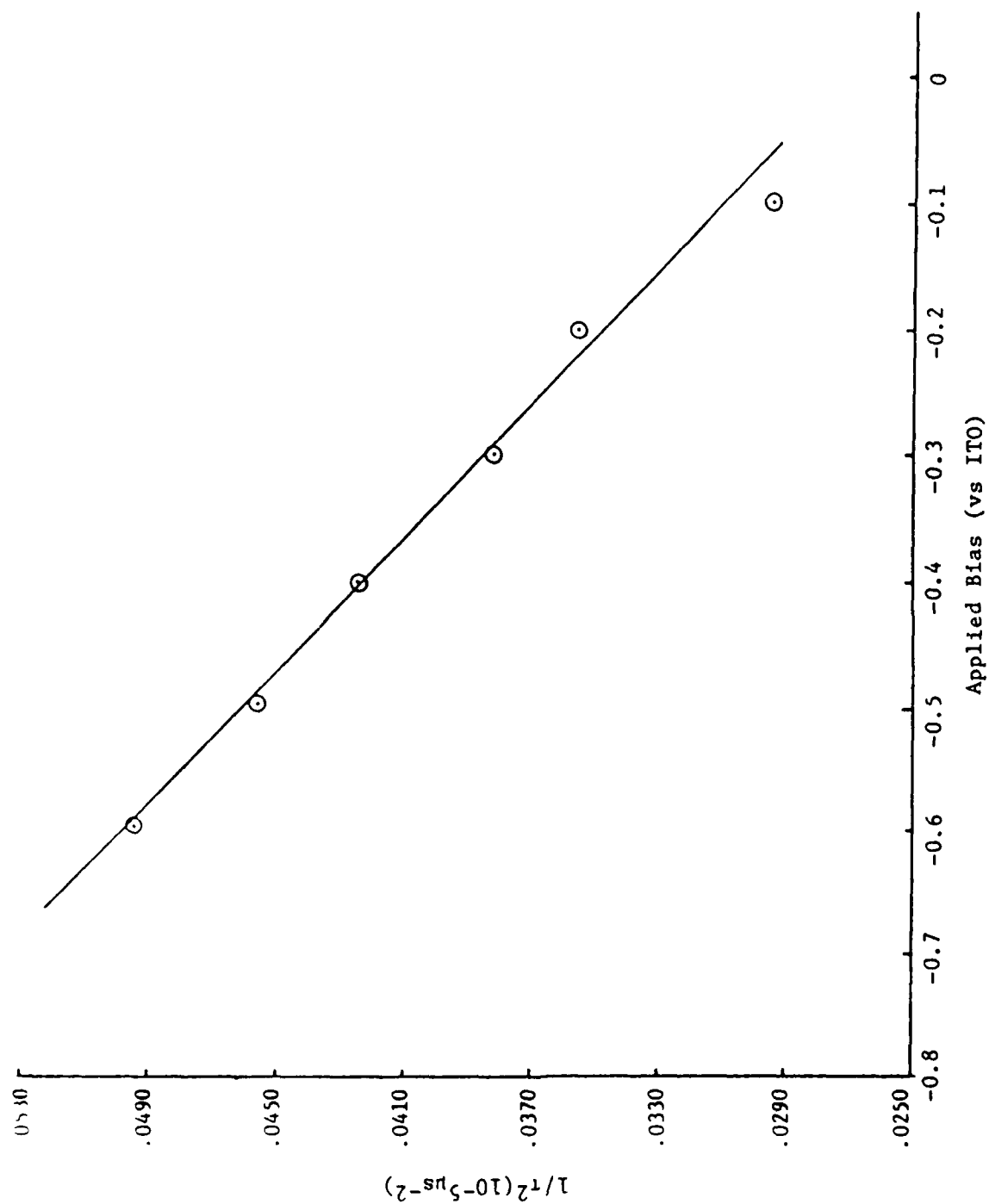


Figure 7.

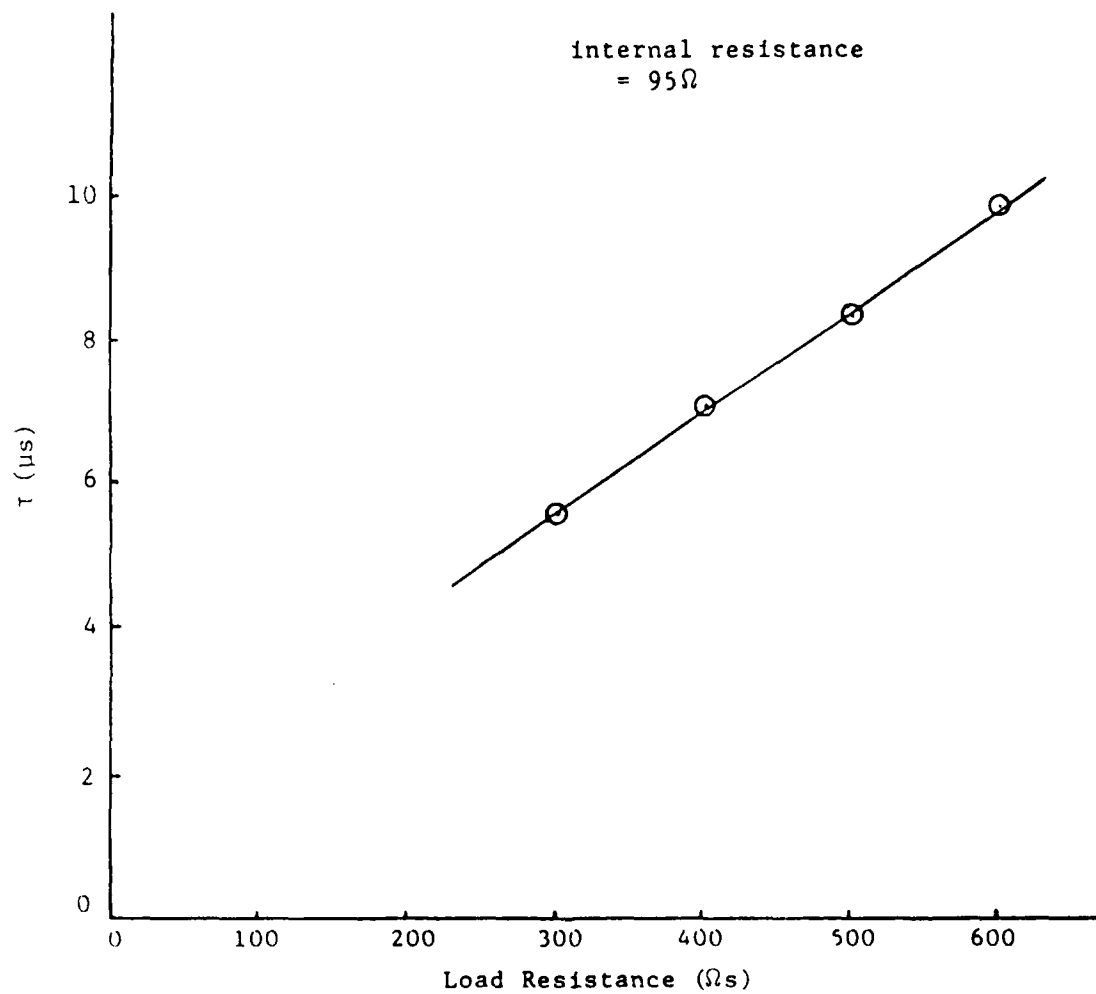


Figure 8.



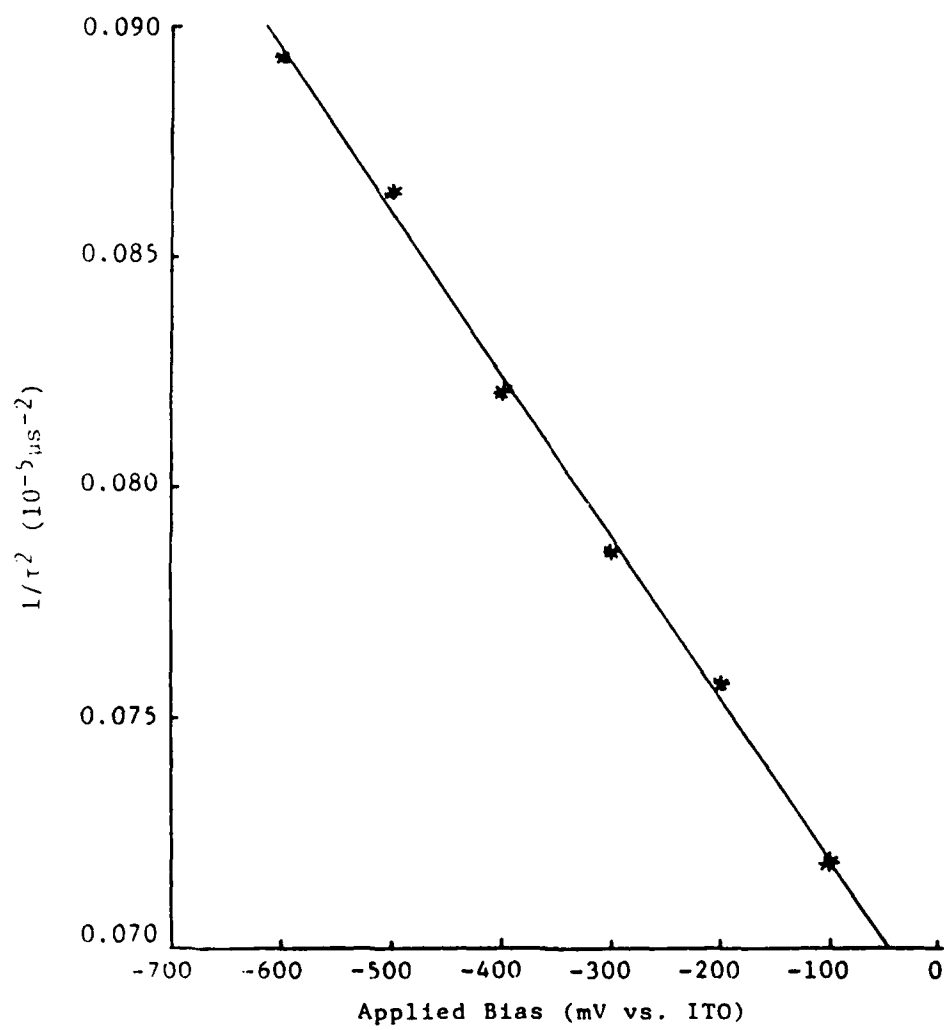


Figure 9.

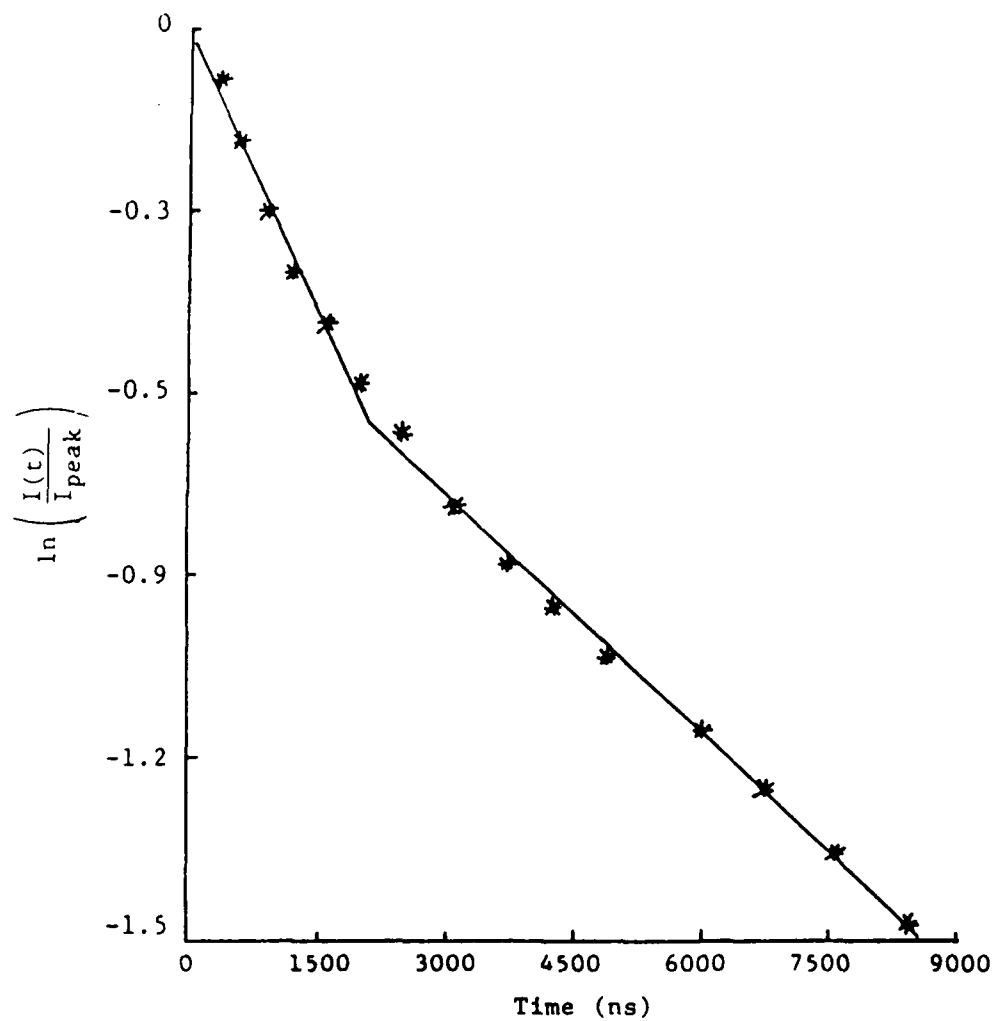


Figure 10.

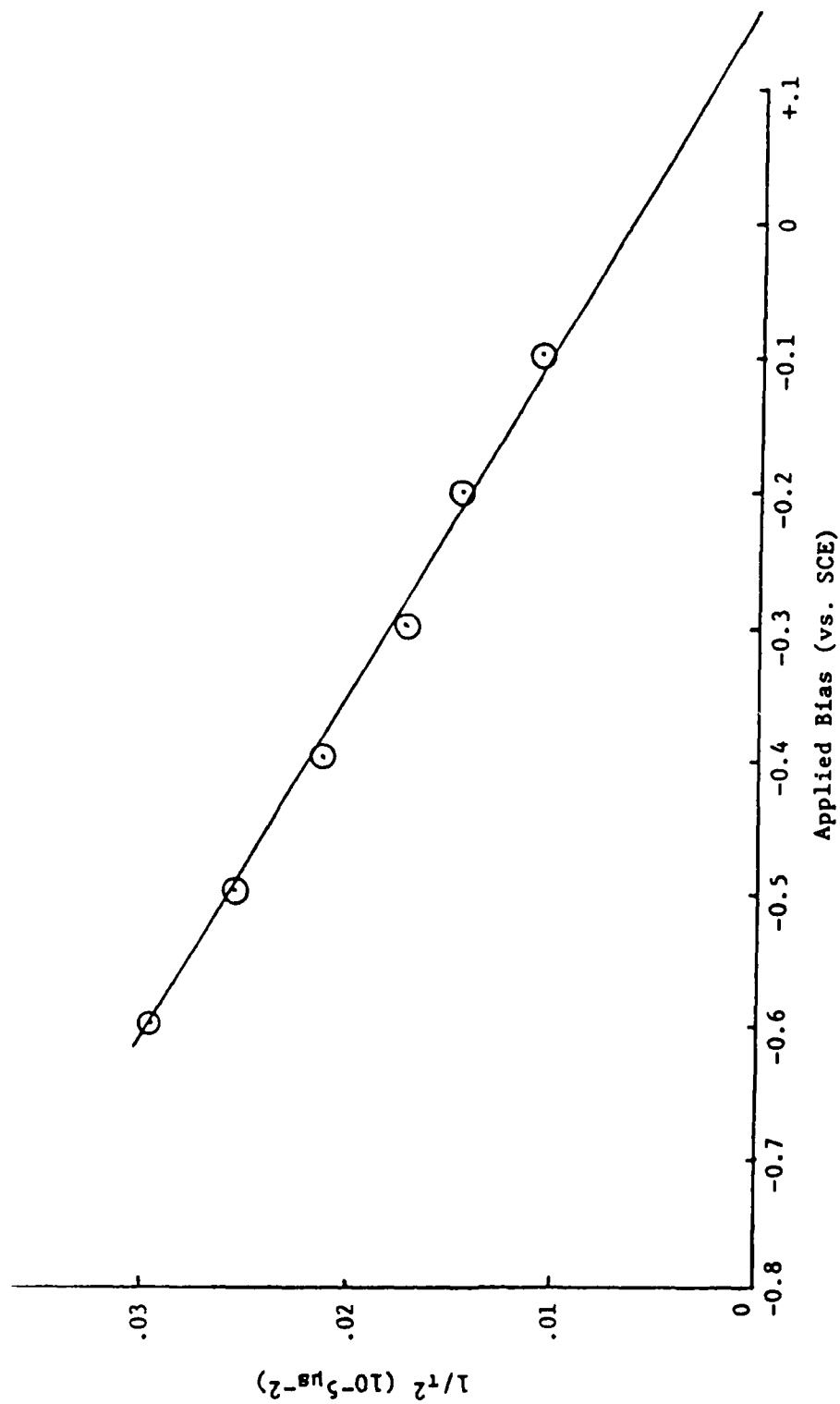


Figure 11.

SECURITY CLASSIFICATION OF THIS PAGE (When Data Entered)

REPORT DOCUMENTATION PAGE		READ INSTRUCTIONS BEFORE COMPLETING FORM
1. REPORT NUMBER 6	2. GOVT ACCESSION NO.	3. RECIPIENT'S CATALOG NUMBER
4. TITLE (and Subtitle) Organophosphine-Transition Metal Complexes as Selective Surfaces for the Reversible Detection of Sulfur Dioxide on SAW Devices		5. TYPE OF REPORT & PERIOD COVERED Technical Aug. 1987 - May 1988
		6. PERFORMING ORG. REPORT NUMBER
7. AUTHOR(s) R. L. Cook, R. C. MacDuff and A. F. Sammells		8. CONTRACT OR GRANT NUMBER(s) N00014-86-C-0128
9. PERFORMING ORGANIZATION NAME AND ADDRESS Eltron Research, Inc. 4260 Westbrook Drive Aurora, IL 60504		10. PROGRAM ELEMENT, PROJECT, TASK AREA & WORK UNIT NUMBERS
11. CONTROLLING OFFICE NAME AND ADDRESS Office of Naval Research/Chemistry Program		12. REPORT DATE May 1988
		13. NUMBER OF PAGES 18
14. MONITORING AGENCY NAME & ADDRESS (if different from Controlling Office)  Above		15. SECURITY CLASS. (of this report)  Unclassified
		15a. DECLASSIFICATION/DOWNGRADING SCHEDULE
16. DISTRIBUTION STATEMENT (of this Report)  Approved for public release, distribution unlimited.		
17. DISTRIBUTION STATEMENT (of the abstract entered in Block 20, if different from Report)  Approved for public release, distribution unlimited.		
18. SUPPLEMENTARY NOTES  Accepted for publication in Analytica Chimica Acta.		
19. KEY WORDS (Continue on reverse side if necessary and identify by block number)  surface acoustic wave devices, organotransition metal complexes, sulfur dioxide detection		
20. ABSTRACT (Continue on reverse side if necessary and identify by block number) Some organotransition metal complexes, $Mn(OPPh_3)_4I_2(SO_2)$ and $Cu(PBz_3)_2Sph$ , were identified as candidate coatings for the detection of sulfur dioxide on piezoelectric crystal sensors. The complex $Mn(OPPh_3)_4I_2(SO_2)$ binds $SO_2$ to form $Mn(OPPh_3)_4I_2(SO_2)$ and can be used as a coating for an integrating piezoelectric sensor. Regeneration of the initial complex can be accomplished by placing the coated piezoelectric sensor under vacuum for 4h. In comparison, the complex, $Cu(PBz_3)_2Sph$ , was found to act as a reversible coating for the detection of $SO_2$ on piezoelectric crystal sensors in the range of 10-1000ppm $SO_2$ .		

ORGANOPHOSPHINE-TRANSITION METAL COMPLEXES AS SELECTIVE SURFACES

FOR THE REVERSIBLE DETECTION OF SULFUR DIOXIDE ON SAW DEVICES

Ronald L. Cook, Robert C. MacDuff and A. F. Sammells\*

Eltron Research, Inc.  
Aurora, IL 60504

SUMMARY

Some organotransition metal complexes,  $\text{Mn}(\text{OPPh}_3)_4\text{I}_2(\text{SO}_2)$  and  $\text{Cu}(\text{PBz}_3)_2\text{SPh}$ , were identified as candidate coatings for the detection of sulfur dioxide on piezoelectric crystal sensors. The complex  $\text{Mn}(\text{OPPh}_3)_4\text{I}_2(\text{SO}_2)$  binds  $\text{SO}_2$  to form  $\text{Mn}(\text{OPPh}_3)_4\text{I}_2(\text{SO}_2)$  and can be used as a coating for an integrating piezoelectric sensor. Regeneration of the initial complex can be accomplished by placing the coated piezoelectric sensor under vacuum for 4h. In comparison, the complex,  $\text{Cu}(\text{PBz}_3)_2\text{SPh}$ , was found to act as a reversible coating for the detection of  $\text{SO}_2$  on piezoelectric crystal sensors in the range of 10-1000ppm  $\text{SO}_2$ .

There are several incentives for the direct detection of  $\text{SO}_2$  under ambient conditions. These include potential leakage from pressurized lithium/ $\text{SO}_2$  electrochemical cells in close proximity to sensitive electronics, the direct monitoring of  $\text{SO}_2$  containing effluents and, of course, the measurement of atmospheric  $\text{SO}_2$ .

Sulfur dioxide enters the atmosphere as a by-product of ore smelting, power generation and internal combustion engines. Sulfur dioxide, along with nitrous oxides, are the primary source of acid rain contributing to the deterioration of vegetation soils and lakes[1,2]. In plants,  $\text{SO}_2$  has been shown to inhibit  $\text{CO}_2$  fixation, block starch hydrolysis, break down chlorophyll containing cells, and induce early foliage loss[3]. Vegetation damage via destruction of localized leaf tissue has been reported at concentrations as low as 2-3ppm  $\text{SO}_2$ [4]. In people, both acute and chronic toxicity of  $\text{SO}_2$  has been reported[4]. Sulfur dioxide is also suspected to cause mutagenic effects as well as lung tumors and several types of cancer. For these reasons there has been considerable research pursued towards developing methods of sulfur dioxide detection.

One method, which has shown considerable promise in recent years, is the use of coated quartz crystals as sorption detectors[5]. Application of a voltage to the quartz crystal causes the crystal to oscillate at a given frequency. The quartz crystal frequency will be sensitive to the substance mass "sorbed" onto its surface. When the Surface Acoustic Wave (SAW) crystal is coated with a material selective for adsorption of an analyte of interest, consequent frequency changes will be related to the analyte mass via the equation[6,7]

$$\Delta f = (k_1 + k_2) f_o^2 h \rho' - k_2 f_o^2 h \left( \frac{4\mu'}{v_r^2} \left( \frac{\lambda' + \mu'}{\lambda' + 2\mu'} \right) \right) \quad (1)$$

where  $\Delta f$  is the change in SAW resonant frequency due to a perturbation of the

Rayleigh wave velocity by the coating,  $k_1$  and  $k_2$  are material constants for the SAW crystal,  $f_0$  is the unperturbed resonant frequency,  $h$  the coating thickness,  $\rho$ , the film density,  $V_r$  the unperturbed Rayleigh wave velocity,  $\lambda'$  the Lamé' constant and  $\mu'$  the modulus of the coating. For typical organic polymer films equation 1 can be simplified to:

$$\Delta f \approx (k_1 + k_2) f_0^2 h \rho' \quad (2)$$

Since  $h\rho'$  is mass per unit area, the SAW device frequency shift depends primarily on mass changes of the coating on the surface of the SAW crystal. The sensitivity of piezoelectric crystal sensors possessing selective surfaces can be high, with detection limits being estimated[8] as  $\approx 10^{-12}$ g. Selective substrates for this application should possess both high sensitivity and selectivity to a single analyte. They should also ideally be chemically reversible and stable.

In recent years a number of coatings have been identified for  $SO_2$  detection on piezoelectric bulk wave crystal based sensors[9-13]. These have included organic amines typified by triethanolamine[9,12] ( $SO_2$  detection limit 10ppb-30ppm), N,N,N',N'-tetrakis(2-hydroxypropyl)ethylenediamine[9] (10ppb-30ppm), ethylenedinitrilotetraethanol[11a] (1-10ppm) and styrene-dimethylaminopropyl maleimide copolymer 1:1[11b] (5-200ppm). Additionally, coated SAW devices have also been evaluated for  $SO_2$  detection[13]. These coatings have in common a tertiary nitrogen atom containing three organic groups attached to the nitrogen (i.e.  $N(CH_2R)_3$ ). Presumably a Lewis acid-Lewis base reaction between the nitrogen atom and the  $SO_2$  molecule is responsible for the sensitivity of amine-based coatings. The above coatings are, however, sensitive to a variety of oxidizing gases. Consequently, there are strong incentives to identify new coatings strategies which might permit greater manipulation of their eventual selectivity via, for example, changing coordinating ligands to a given metal center.

Here we wish to report a new class of  $\text{SO}_2$  sensitive coating compatible for incorporating onto piezoelectric crystals based upon organophosphine-transition metal complexes. The advantages of transition metal complexes as sites for  $\text{SO}_2$  adsorption are mainly those associated with the ability to change reactivity of small molecules with the transition metal site by varying either the transition metal or the ligands in the coordination sphere. Thus, selectivity for a given molecule, for example  $\text{SO}_2$ , might be adjusted by changes in either coordinating ligand or metal center. As ligands in the metal coordination sphere, phosphines and organophosphines are frequently studied due to their possessing both a wide range of basicities and imparting influence on overall stereochemistry. It appears that organophosphines having high electron donating abilities (i.e.  $\text{PCy}_3$  where Cy = cyclohexyl) can lead to strong  $\text{SO}_2$  binding in  $\text{Cu}(\text{PR}_3)_2\text{SPh}$  complexes[14]. Strong binding of  $\text{SO}_2$  to a  $\text{Cu}(\text{PR}_3)_2\text{SPh}$  complex can lead to high sensitivity and slow reversibility. By judicious choice of the ligand basicity it may be possible to optimize both sensitivity and reversibility of organophosphine transition metal complexes towards  $\text{SO}_2$  detection. Such complexes may, by virtue of the relative ease with which the steric and electronic properties of the phosphorus ligands can be changed, lead to piezoelectric  $\text{SO}_2$  sensors with high selectivity and sensitivity.

## EXPERIMENTAL

### Apparatus

A schematic of the experimental arrangement used in this work is shown in Figure 1. A 52MHz ST quartz crystal utilizing a dual SAW delay line oscillator configuration was used in this work (Figure 2) (Microsensor Systems, Inc.). One delay line was covered with the chemically sensitive reagent, while the second delay line served as a reference. The frequencies of the two delay line oscillators were mixed to provide a measured frequency equal to the difference



between the two oscillator frequencies, which was measured with a CT-90 frequency counter (Ramsey Electronics, Inc.). The SAW device was enclosed in a teflon chamber utilizing 1/16" stainless steel tubing for introduction and exhaust of the appropriate gases. Calibrated flowmeters (Gilmont) were used to meter sulfur dioxide (Matheson 1000ppm, in N<sub>2</sub>) and nitrogen (pre-purified, Matheson) into a mixing chamber at a constant rate prior to introduction of the gas stream into the SAW device. A gas flow rate of 60mlmin<sup>-1</sup> was used in all experiments. The majority of measurements were performed at ambient temperature.

#### Reagents

Reagent grade chemicals were used without any further purification. Copper (II) acetate, manganese (II) iodide, thiophenol and tribenzyl phosphine were purchased from Alfa and triphenylphosphine oxide was purchased from Strem Chemicals. The preparations of both the copper and manganese complexes were carried out using standard Schlenk techniques under a nitrogen atmosphere to avoid oxidation of reactants or reaction products.

#### Synthetic Procedures

(CuSPh)<sub>n</sub>[14]: Benzenethiol (3.7ml in 60ml of methanol) was added to cupric acetate (3.6g in 30ml distilled water) with stirring. A yellow precipitate formed immediately which was filtered and thoroughly washed with H<sub>2</sub>O, CH<sub>3</sub>OH, benzene and ether. The precipitate was then dried in vacuo overnight.

Cu(PBz)<sub>2</sub>SPh[14]: Polymeric cuprous mercaptide (1.54g) prepared in the previous step was suspended in 30ml of chloroform. Tribenzyl phosphine (5.0g) was then added to the (CuSPh)<sub>n</sub>-chloroform mixture. Within 30 min. following phosphine addition the chloroform solution became clear and colorless. Precipitation of Cu(PBz<sub>3</sub>)<sub>2</sub>SPh was accomplished by addition of 200ml of n-heptane and recrystallized from CHCl<sub>3</sub>/n-heptane before use in the SAW experiments.

Mn(OPPh<sub>3</sub>)<sub>4</sub>I<sub>2</sub>(SO<sub>2</sub>)<sub>2</sub>[15]: Anhydrous manganese II iodide (2.77g) and tri-phenylphosphine oxide (10g) were stirred together for 7 days in 100ml of propylacetate. The resulting tan suspension was then saturated with gaseous SO<sub>2</sub> after which it became orange. This was stirred for an additional 2 days, filtered, and the resulting Mn(OPPh<sub>3</sub>)<sub>4</sub>I<sub>2</sub>(SO<sub>2</sub>)<sub>2</sub> crystals recrystallized from toluene.

#### Crystal Coating

A chloroform solution of Cu(PBz<sub>3</sub>)<sub>2</sub>SPh or a methanol solution of Mn(OPPh<sub>3</sub>)<sub>4</sub>I<sub>2</sub>(SO<sub>2</sub>)<sub>2</sub> was applied to one side of the SAW device using a 10ul syringe. Several applications were necessary to achieve a coating which provided a frequency difference of 100,000 ± 5000 Hz. Before exposure to SO<sub>2</sub>, the modified crystal was dried under nitrogen for 2h.

#### RESULTS AND DISCUSSION

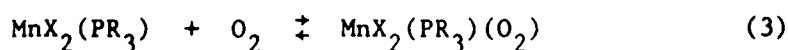
The manipulation of both steric and electronic ligand properties in the coordination sphere of transition metal complexes can lead to enhanced metal center reactivity to small molecules. An example of such reactivity enhancement by varying ligands in the coordination sphere would be the oxidative addition of CH<sub>3</sub>I to Ir(CO)(Cl)(PR<sub>3</sub>)<sub>2</sub> giving Ir(CO)(Cl)(PR<sub>3</sub>)<sub>2</sub>(CH<sub>3</sub>)(I)[16]. On varying R from p-ClC<sub>6</sub>H<sub>4</sub> to p-CH<sub>3</sub>C<sub>6</sub>H<sub>4</sub> and CH<sub>3</sub>OC<sub>6</sub>H<sub>4</sub> relative rates for CH<sub>3</sub>I oxidative addition to Ir(CO)(Cl)(PR<sub>3</sub>)<sub>2</sub> increased from 1 to 40 to 90 respectively[16]. For complexes of transition metals possessing organophosphine ligands, it is recognized that changing phosphorus ligand substituents can give rise to marked changes in the behavior of the respective transition metal complexes[17]. In recent years quantitative measurements of electronic and steric properties for PR<sub>3</sub>, P(OR)<sub>3</sub> and PX<sub>3</sub> groups have been discussed[17] permitting manipulation of transition metal reactivity. It has been shown that the

frequency of the  $A_1$  carbonyl stretching frequency of  $Ni(CO)_3L$  ( $L$  = phosphine) could be predicted to within  $\pm 0.3\text{cm}^{-1}$  via the equation[17]:

$$\nu = 2056.1 + \sum_{i=1}^3 \chi_i$$

where  $\nu$  is the  $A_1$  carbonyl stretching frequency in  $Ni(CO)_3$  and  $\chi_i$  is the contribution to the base stretching frequency ( $2056.1\text{cm}^{-1}$ ) by each substituent group attached to the phosphorus ligand in the  $Ni(CO)_3L$  complex. This relationship, measuring the ability of phosphine to modify electron density at transition metal centers, can be used to select substituents to give desired changes in ligand basicity and thus reactivity towards a given chemical species. The steric requirements of phosphine ligands are determined by measurements of the apex angle of a cylindrical cone centered  $2.28\text{\AA}$  from the center of the phosphorus atoms, which just touches the van der Waals radii of the outermost atoms of the substituent groups[17]. Angle measurement (termed cone angle) can be achieved using space filling CPK molecular models[17] (Ealing Corp.). From such an approach cone angles of  $87^\circ$  to  $212^\circ$  were obtained.

An example of both steric and electronic control modification induced by organophosphine ligands can be seen in the reversible oxygen addition reaction [18,19]:



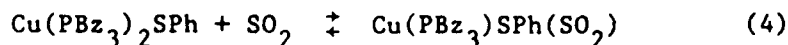
When  $R = n-C_4H_9$  the reaction is reversible[18]. However, when  $R = CH_2CH_2CN$ , a substituent whose steric requirements are identical to  $n-C_4H_9$ ,  $O_2$  will not bind to the organophosphine complex[19]. On going from  $R = n-C_4H_9$  to  $R = CH_2CH_2CN$  the phosphine group becomes more efficient at removing electron density from the Mn metal center. Furthermore, the oxygen affinity of  $MnX_2PR_3$  complexes increases in the order[18]  $PPh_3$ (no affinity),  $PPh_2Bu^n$ ,  $P(Bu^n)_3$  suggesting that a higher electron density at the Mn atom results in greater  $O_2$  affinity. In the  $MnX_2PR_3$  complexes  $O_2$  would appear to act as a Lewis acid

accepting electron density from the Mn complex. Analogous behavior is observed for the reaction of  $\text{SO}_2$  with  $\text{Cu}(\text{PR}_3)_2\text{SPh}$  where  $\text{SO}_2$  binds directly as a Lewis acid to the coordinated  $\text{SPh}^-$  groups[14]. Here, a higher  $\text{SO}_2$  affinity is observed for  $\text{PR}_3 = \text{PCy}_3$  compared to  $\text{PR}_3 = \text{PBz}_3$  ( $\text{Bz} = \text{benzyl}$ ). Since  $\text{PCy}_3$  is more basic than  $\text{PBz}_3$ , the higher electron density on copper and consequently on sulfur in the  $\text{SPh}^-$  group, the more strongly bound the  $\text{SO}_2$  molecule.

Such control of small molecule binding at transition metal centers via the rational selection of steric and electronic parameters of phosphine ligands has prompted us to examine the use of organophosphine-transition metal complexes as selective sites for  $\text{SO}_2$  detection on piezoelectric sensors. The first complex identified was trans-bis(sulfur dioxide)tetrakis(triphenylphosphine oxide)manganese (I)di-iodide ( $\text{Mn}(\text{OPPh}_3)_4\text{I}_2(\text{SO}_2)_2$  [15]. Previous work[15] has shown that when placed under vacuum for  $\approx 2\text{-}3\text{h}$  or when heated to  $129^\circ\text{C}$ , the  $\text{Mn}(\text{OPPh}_3)_4(\text{SO}_2)_2\text{I}_2$  complex loses one molecule of  $\text{SO}_2$  to give  $\text{Mn}(\text{OPPh}_3)_4(\text{SO}_2)\text{I}_2$ . Upon exposure of this latter complex to  $\text{SO}_2$  the bis(sulfur dioxide) complex is reformed.

Table 1 shows the device response for a  $\text{Mn}(\text{OPPh}_3)_4\text{I}_2(\text{SO}_2)$  coated SAW crystal, to 20ppm  $\text{SO}_2$  (in nitrogen) at a flow rate of  $60\text{mlmin}^{-1}$ . The  $\text{Mn}(\text{OPPh}_3)_4\text{I}_2(\text{SO}_2)_2$  coated SAW crystal was initially pretreated by subjecting it to vacuum ( $\approx 50\mu\text{m Hg}$ ) overnight to give the complex  $\text{Mn}(\text{OPPh}_3)_4\text{I}_2(\text{SO}_2)$ . Here it was observed that the  $\text{Mn}(\text{OPPh}_3)_4\text{I}_2(\text{SO}_2)$  coating could adsorb  $\text{SO}_2$  in a reproducible, quasi-reversible manner. Quasi-reversible in the sense that  $\text{SO}_2$  was removed from  $\text{Mn}(\text{OPPh}_3)_4\text{I}_2(\text{SO}_2)_2$  to give  $\text{Mn}(\text{OPPh}_3)_4\text{I}_2(\text{SO}_2)$  between experiments by subjecting the coated SAW crystal to a vacuum treatment. The reproducibility of  $\text{SO}_2$  adsorption under conditions evaluated (i.e.  $25^\circ\text{C}$  and  $60\text{mlmin}^{-1}$  flow rate for 20ppm  $\text{SO}_2$  in nitrogen) and the ability to regenerate the coating, suggests that  $\text{Mn}(\text{OPPh}_3)_4\text{I}_2(\text{SO}_2)$  coated SAW devices could be used as chemical dosimeters.

A second complex identified for this application was bis(tribenzylphosphine) copper(II)thiophenolate( $\text{Cu}(\text{PBz}_3)_2\text{SPh}$ )[14]. This compound, when exposed to  $\text{SO}_2$ , forms the  $\text{Cu}(\text{PBz}_3)_2\text{SPh}(\text{SO}_2)$  adduct in the solid state, which exhibits rapid equilibration[14] and good reversibility towards  $\text{SO}_2$ . The chemical behavior of these complexes with regard to  $\text{SO}_2$  binding suggested that coatings of these materials introduced onto the surface of piezoelectric crystals, would provide a promising new coating for  $\text{SO}_2$  detection. Table 2 summarizes results for  $\text{SO}_2$  detection using  $\text{Cu}(\text{PBz}_3)_2\text{SPh}$  coated SAW devices. Here, good reversibility and sensitivity to  $\text{SO}_2$  in the range 10-1000ppm was observed following an initial exposure of the complex to  $\text{SO}_2$ . In Figure 3 it can be seen that the coating response to  $\text{SO}_2$  was rapid and reached 90% of maximum signal after 90s. However, the signal did not fully recover to the initial background frequency. This behavior may be due to residual  $\text{SO}_2$  being retained in the  $\text{Cu}(\text{PBz}_3)_2\text{SPh}$  coating. Previous work has shown that the  $\text{Cu}(\text{PBz}_3)_2\text{SPh} + \text{SO}_2$  complex equilibrium lies to the right in the equation[14]:



At 20°C the equilibrium vapor pressure above a sample of  $\text{Cu}(\text{PBz}_3)_2\text{SPh}$  originally containing 0.63 mole of  $\text{SO}_2$  per mole  $\text{Cu}(\text{PBz}_3)_2\text{SPh}$  was only 1.8 torr[14]. This suggests that a significant fraction of  $\text{SO}_2$  in the  $\text{Cu}(\text{PBz}_3)_2\text{SPh}(\text{SO}_2)$  complex is tightly bound and not removed under vacuum. Thus, pretreatment of the  $\text{Cu}(\text{PBz}_3)_2\text{SPh}$  coating may be necessary to insure reproducibility during subsequent measurements. Furthermore, the complexes containing tightly bound  $\text{SO}_2$  will not be able to participate in the subsequent sorption of  $\text{SO}_2$ , thus decreasing the overall coating sensitivity. To test the hypothesis that  $\text{SO}_2$  was retained on the  $\text{Cu}(\text{PBz}_3)_2\text{SPh}$  coated SAW device, the coated crystal was subjected to a flow of pure  $\text{SO}_2$  for 5 minutes followed by a nitrogen purge for 2h. This sequence was performed in order to saturate non-reversible sites on the

$\text{Cu}(\text{PBz}_3)_2\text{SPh}$  coating. That  $\text{SO}_2$  was retained in this  $\text{Cu}(\text{PBz}_3)_2\text{SPh}$  coating was shown by the observation that the frequency difference between coated and uncoated oscillators was higher following the pure  $\text{SO}_2$ /nitrogen pretreatment. The higher baseline frequency obtained following the  $\text{SO}_2$ /nitrogen pretreatment was consistent with a fraction of the coating containing tightly bound  $\text{SO}_2$  in the  $\text{Cu}(\text{PBz}_3)_2\text{SPh}(\text{SO}_2)$  complex. This behavior was found reproducible when fresh  $\text{Cu}(\text{PBz}_3)_2\text{SPh}$  coatings were applied to clean SAW crystal surfaces. Thus, the coating following  $\text{SO}_2$  treatment probably contained both  $\text{Cu}(\text{PBz}_3)_2\text{SPh}(\text{SO}_2)$  and  $\text{Cu}(\text{PBz}_3)_2\text{SPh}$ . Following this pretreatment procedure the SAW device response was found to be quite reversible, recovering to >90% of the initial frequency difference within 2-3m (Figure 4). The  $\text{Cu}(\text{PBz}_3)_2\text{SPh}$  sensor response to  $\text{SO}_2$  was also found linear in the range 10-1000ppm  $\text{SO}_2$  (1000ppm,  $\Delta(\text{Hz}) = 530$ ; 100ppm,  $\Delta(\text{Hz}) = 350$ ; 10ppm,  $\Delta(\text{Hz}) = 190$ ). Below 10ppm the frequency change was not reproducible. However, it is not known at this time whether the 10ppm detection limit is an inherent limitation of the coating or of the SAW device configuration used.

To gain preliminary insight into the temperature dependency of the  $\text{Cu}(\text{PBz}_3)_2\text{SPh}$  coated SAW delay line, heating tape was wrapped around two feet of the incoming gas line to the SAW device. Response time and sensitivity were found to vary with temperature. At higher input gas temperatures ( $\approx 60^\circ\text{C}$ ) the total weight of  $\text{SO}_2$  adsorbed and thus the change in the SAW device difference frequency decreased. However, the response times for  $\text{SO}_2$  detection and the subsequent recovery to baseline were improved as temperature increased. Exposure of the  $\text{Cu}(\text{PBz}_3)_2\text{SPh}$  coating to room air over a 2-3 month period was not found to affect  $\text{SO}_2$  adsorption ability, suggesting that the complex is stable in air. However, in oxygen saturated  $\text{CHCl}_3$  the  $\text{Cu}(\text{PBz}_3)_2\text{SPh}$  complex shows decomposition. Presumably the phosphine becomes oxidized to the phosphine

oxide. For SAW devices coated with solutions of the oxidized copper complex, no  $\text{SO}_2$  sensitivity was observed. Exposure of the  $\text{Cu}(\text{PBz}_3)_2\text{SPh}$  coated SAW device to  $\text{O}_2$ ,  $\text{CO}_2$ ,  $\text{NH}_3$  or  $\text{CO}$  at 1000ppm showed difference frequency changes  $<20\text{Hz}$ . Response to 1000ppm  $\text{NO}_2$  was found variable with difference frequencies changing between 20 and 90Hz.

### CONCLUSIONS

The present work has shown that organophosphine transition metal complexes can be useful materials for  $\text{SO}_2$  detection on piezoelectric crystal sensors. Although several complexes, including  $\text{MnI}_2(\text{PPh}_3)[20]$ ,  $\text{Pt}(\text{PPh}_3)(\text{I})[21]$ , and  $\text{Ir}(\text{PPh}_3)_2(\text{CO})(\text{Cl})[22]$  are known to bind  $\text{SO}_2$ , only  $\text{Mn}(\text{OPPh}_3)_4\text{I}_2(\text{SO}_2)$  and  $\text{Cu}(\text{PBz}_3)_2\text{SPh}$  were investigated here as coatings sensitive to  $\text{SO}_2$ .  $\text{Cu}(\text{PBz}_3)_2\text{SPh}$  demonstrated both good sensitivity and reversibility towards  $\text{SO}_2$ . Future studies will address the effect of varying both the phosphorus ligands and the organic group attached to sulfur in order to optimize  $\text{Cu}(\text{PR}_3)_2\text{SR}'$  complexes as coatings for  $\text{SO}_2$  detection. In particular, less basic phosphorus ligands (i.e.  $\text{P}(\text{OPh})_3$ ) and organic thiols such as  $-\text{SC}_6\text{F}_5$  might be expected to give lower electron density at the sulfur atom. Since this would shift the equilibrium in equation (4) to the left on a  $\text{Cu}(\text{PR}_3)_2\text{SR}$  coated device, both higher sensitivity and faster response might be anticipated. The present approach may also be extended to the development of oxygen sensitive coatings. The complexes  $\text{Mn}(\text{NCS})_2(\text{PR}_3)$  ( $\text{R} = \text{Me, Et, Pr or Bu}$ ) have been shown to react with oxygen in the solid state to form  $\text{Mn}(\text{NCS})_2(\text{PR}_3)(\text{O}_2)$  adducts[18]. Reaction of dry  $\text{O}_2$  with the  $\text{Mn}(\text{NCS})_2(\text{PR}_3)$  complexes is both rapid and reversible.

This work was supported in part by the Office of Naval Research.

## REFERENCES

1. E. B. Cowling and R. A. Lindhurst, *Bioscience*, 31 (1981) 649.
2. E. B. Cowling, *Environ. Sci. Technol.*, 16 (1982) 110A.
3. B. D. Webster, U.S. Dept. Agric. Res. Serv., #24 (1971).
4. E. J. Calabrese, "Pollutants and High Risk Groups", Interscience, NY, 1976.
5. G. G. Guilbault, *Ion-Select. Electr. REv.*, 2 (1980) 3.
6. A. Snow and H. Wohltjen, *Anal. Chem.*, 56 (1984) 1411.
7. H. Wohltjen, *Sens. Actuators*, 5 (1985) 307.
8. A. W. Warner and C. D. Stockbridge, "The Measurements of Mass Using Quartz Crystal Resonators", *Symposium on Vacuum Microbalance Techniques*, Los Angeles, CA (1962).
9. K. H. Karmarker and G. G. Guilbault, *Anal. Chim. Acta.*, 71 (1974) 419.
10. K. H. Karmarker, L. M. Webber and G. G. Guilbault, *Anal. Chim. Acta.*, 81 (1976) 265.
11. a) J. Cheney, T. Norwood and J. Homolya, *Anal. Lett.*, 9(4) (1976) 361.  
b) M. W. Frechette and J. L. Fasching, *Environ. Sci. Technol.*, 7 (1973) 1135.
12. J. Cheney and J. Homolya, *Anal. Lett.*, 8 (1975) 175.
13. A. Bryant, L. Lee and J. Vetelino, "Proc. IEEE Ultrasonics Symp.", *IEEE Cat.*, 81CH1689-9 (1981) 1735.
14. P. G. Eller and G. J. Kubas, *J. Am. Chem. Soc.*, 99 (1977) 4346.
15. G. A. Gott et.al., *J. Chem. Soc., Chem. Commun.*, (1984) 1283.
16. P. Ugo et.al., *J. Am. Chem. Soc.*, 94 (1972) 7364.
17. A. Tolman, *Chem. REv.*, 77 (1977) 313.
18. C. A. McAuliffe et.al., *J. Chem. Soc., Dalton Trans.*, (1983) 2147.
19. H. Al-Khateeb and C. A. McAuliffe, *Inorg. Chim. Acta.*, 45 (1980) 195.
20. D. S. Barratt et.al., *J. Chem. Soc., Dalton Trans.*, (1985) 135.
21. M. R. Snow and J. A. Ibers, *Inorg. Chem.*, 12 (1973) 224.
22. S. J. LaPlaca and J. A. Ibers, *Inorg. Chem.*, 5 (1966) 405.



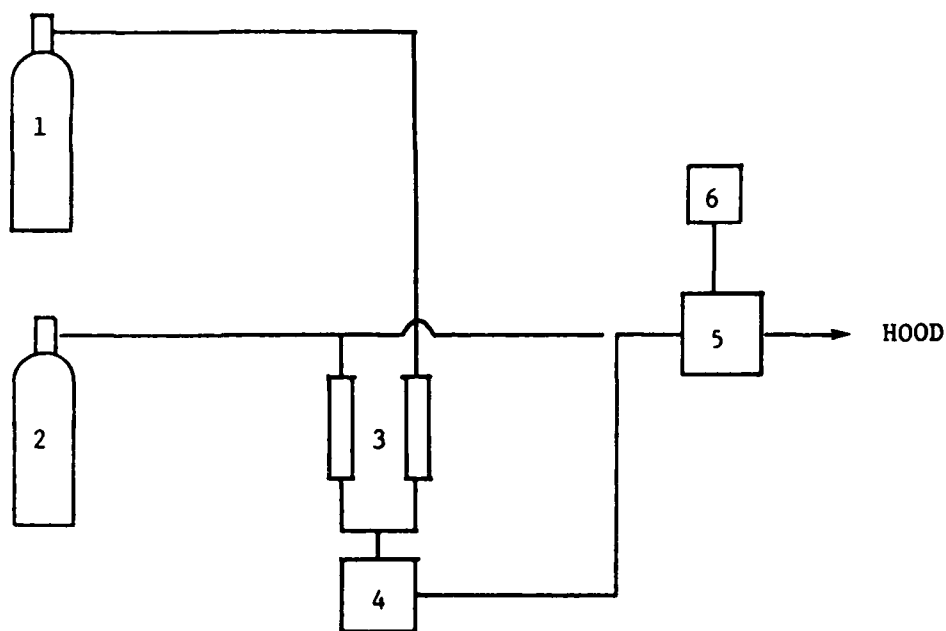


Figure 1. Schematic for experimental setup for SO<sub>2</sub> detection  
 (1) SO<sub>2</sub> source, 1000ppm SO<sub>2</sub>, (2) N<sub>2</sub> source,  
 (3) flowmeters, (4) gas mixing chamber,  
 (5) piezoelectric crystal sensor (6) digital  
 frequency counter.

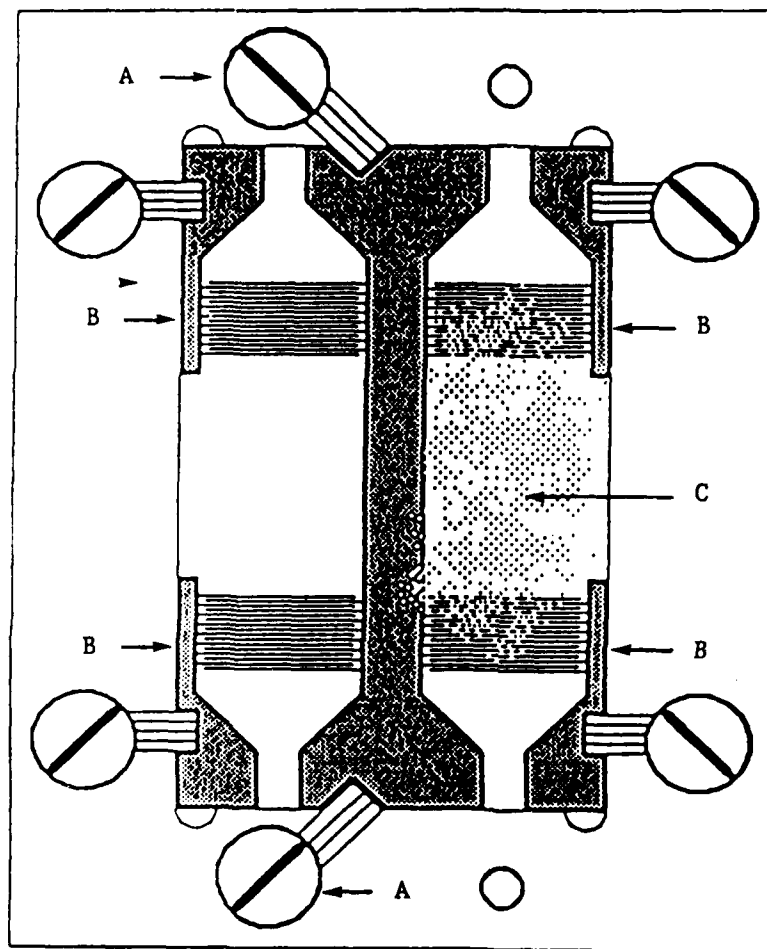


Figure 2. Schematic of 52MHz dual SAW delay line (Microsensor Systems, Inc.) with coatings of either  $\text{Mn}(\text{OPPh}_3)_4(\text{SO}_2)\text{I}_2$  or  $\text{Cu}(\text{PBz}_3)_2\text{SPh}$  on one of the delay lines. A = ground connection, B = gold bus bar pads, C = organophosphine transition metal complex coating.

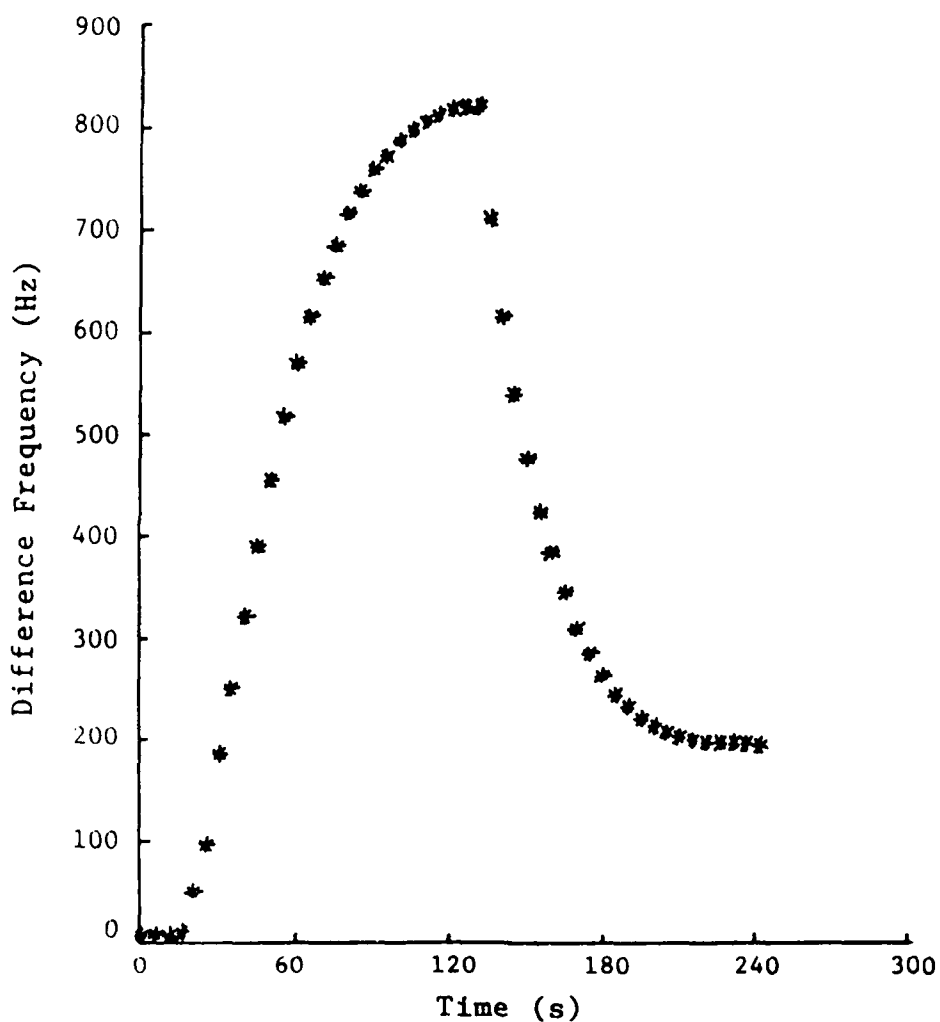


Figure 3. Device response of  $\text{Cu}(\text{PBz}_3)_2\text{SPh}$ -coated piezoelectric crystal to 1000ppm  $\text{SO}_2$ . Flow rate  $60\text{mlmin}^{-1}$ .  $T = 25^\circ\text{C}$ .

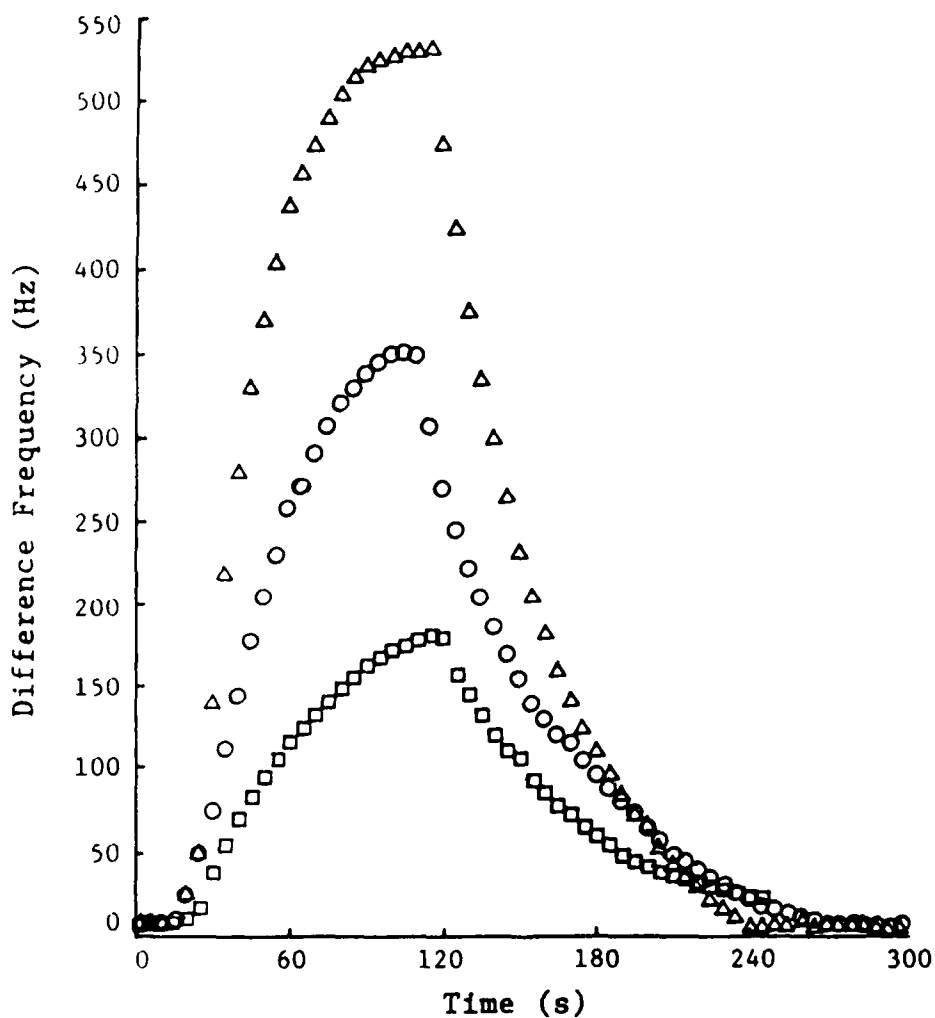


Figure 4. Change in crystal frequency as a function of  $\text{SO}_2$  concentration following pretreatment of  $\text{Cu}(\text{PBz}_3)_2\text{SPh}$  coating with pure  $\text{SO}_2$  for 5m, followed by 2h nitrogen purge. Flow rate =  $60\text{mlmin}^{-1}$ .  $T = 25^\circ\text{C}$ .  
 □ = 10ppm, ○ = 100ppm, Δ = 1000ppm.

TABLE 1

Response of  $\text{Mn(OPPh}_3)_4\text{I}_2(\text{SO}_2)$  coated  
SAW device to  $\text{SO}_2$  [a].

<u>Time Exposed (s)</u>	<u><math>\Delta(\text{Diff. Freq.})</math> (Hz)</u> [b]
10	44 ( $\pm 2$ )
20	228 ( $\pm 2$ )
30	350 ( $\pm 2$ )
40	476 ( $\pm 2$ )
50	623 ( $\pm 3$ )
60	758 ( $\pm 3$ )

[a] 20ppm  $\text{SO}_2$  in nitrogen gas. Flow rate =  $60\text{mlmin}^{-1}$ .  
T =  $25^\circ\text{C}$ .

[b] Ave. 3 experiments (S.D.)

TABLE 2

Response of  $\text{Cu}(\text{PBz}_3)_2\text{SPh}$  coated SAW device to  $\text{SO}_2$ [a].

<u><math>\text{SO}_2</math> conc.</u>	<u><math>\Delta(\text{Diff. Freq.})</math> (Hz)</u> [b]
10	190 ( $\pm 5$ )
100	350 ( $\pm 3$ )
1000	530 ( $\pm 3$ )

[a]  $\text{SO}_2$  mixed with  $\text{N}_2$  to give 10, 100, 1000ppm at a flow rate of  $60\text{mlmin}^{-1}$ .  $T = 25^\circ\text{C}$ .

[b] Ave. of 6 experiments (S.D.)

SECURITY CLASSIFICATION OF THIS PAGE (When Data Entered)

REPORT DOCUMENTATION PAGE		READ INSTRUCTIONS BEFORE COMPLETING FORM
1. REPORT NUMBER 7	2. GOVT ACCESSION NO.	3. RECIPIENT'S CATALOG NUMBER
4. TITLE (and Subtitle) Reversible SO <sub>2</sub> Detection Using a Multiple Reflecting Optical Waveguide Sensor		5. TYPE OF REPORT & PERIOD COVERED Technical Aug. 1987 - May 1988
7. AUTHOR(s) R. L. Cook, R. C. MacDuff and A. F. Sammells		6. PERFORMING ORG. REPORT NUMBER
9. PERFORMING ORGANIZATION NAME AND ADDRESS Eltron Research, Inc. 4260 Westbrook Drive Aurora, IL 60504		8. CONTRACT OR GRANT NUMBER(s) N00014-86-C-0128
11. CONTROLLING OFFICE NAME AND ADDRESS Office of Naval Research/Chemistry Program		10. PROGRAM ELEMENT, PROJECT, TASK AREA & WORK UNIT NUMBERS
14. MONITORING AGENCY NAME & ADDRESS (if different from Controlling Office)  Above		12. REPORT DATE May 1988
		13. NUMBER OF PAGES 14
		15. SECURITY CLASS. (of this report) Unclassified
		15a. DECLASSIFICATION/DOWNGRADING SCHEDULE
16. DISTRIBUTION STATEMENT (of this Report)  Approved for public release, distribution unlimited.		
17. DISTRIBUTION STATEMENT (of the abstract entered in Block 20, if different from Report)  Approved for public release, distribution unlimited.		
18. SUPPLEMENTARY NOTES  Submitted: Environmental Science and Technology		
19. KEY WORDS (Continue on reverse side if necessary and identify by block number)  sulfur dioxide detection, multiple reflecting optical waveguide sensor		
20. ABSTRACT (Continue on reverse side if necessary and identify by block number)  A multiple-reflecting optical waveguide has been investigated for the direct detection and measurement of gaseous SO <sub>2</sub> . This was achieved by monitoring the variation in light intensity at a silicon photodetector following interaction of multiple-reflected illumination with a Cu(PBz <sub>3</sub> )SPh coating on the surface of a long glass tube. Direct illumination along the tube axis cavity was avoided. Such changes in net transmitted illumination intensity along the tube axis were a consequence of color changes occurring in this complex associated with reversibly binding SO <sub>2</sub> . This was a result of absorption characteristic changes		

induced in laterally propagated internally reflected waves within the tube. This as yet unoptimized device, was able to reproducibly and reversibly detect between 100 and 1000ppm SO<sub>2</sub>.



REVERSIBLE SO<sub>2</sub> DETECTION USING A MULTIPLE  
REFLECTING OPTICAL WAVEGUIDE SENSOR

Ronald L. Cook, Robert C. MacDuff  
and Anthony F. Sammells\*

Eltron Research, Inc.  
4260 Westbrook Drive  
Aurora, IL 60504

## Abstract

A multiple-reflecting optical waveguide has been investigated for the direct detection and measurement of gaseous  $\text{SO}_2$ . This was achieved by monitoring the variation in light intensity at a silicon photodetector following interaction of multiple-reflected illumination with a  $\text{Cu}(\text{PBz}_3)\text{SPh}$  coating on the surface of a long glass tube. Direct illumination along the tube axis cavity was avoided. Such changes in net transmitted illumination intensity along the tube axis were a consequence of color changes occurring in this complex associated with reversibly binding  $\text{SO}_2$ . This was a result of absorption characteristic changes induced in laterally propagated internally reflected waves within the tube. This as yet unoptimized device, was able to reproducibly and reversibly detect between 100 and 1000ppm  $\text{SO}_2$ .

## Introduction

The harmful environmental consequences of sulfur dioxide emissions have been well documented over the last several years<sup>1-3</sup>. Sulfur dioxide enters the atmosphere as a by-product of ore smelting, power generation and internal combustion engines. Sulfur dioxide, together with nitrogen oxides, are primary sources of acid rain contributing to deterioration of vegetation in soils and lakes<sup>1,2</sup>. In plants, the presence of  $\text{SO}_2$  has been shown to inhibit  $\text{CO}_2$  fixation, block starch hydrolysis, and cause a breakdown of chlorophyll containing cells leading to early foliage loss. Vegetation damage via destruction of localized leaf tissue has been reported at concentrations as low as 2-3ppm  $\text{SO}_2$ <sup>4</sup>. In people, both acute and chronic toxicity of  $\text{SO}_2$  has been reported<sup>4</sup>. Sulfur dioxide is also suspected to cause mutagenic effects as well as lung tumors and several types of cancer<sup>4</sup>.

For the above reasons there has been considerable research pursued towards developing methods for sulfur dioxide detection<sup>5-8</sup>. One of the most frequently

employed methods is based upon the use of a Schiff type reaction<sup>5</sup> which involves stabilization of atmospheric sulfur dioxide in aqueous solutions as dichlorodisulfitomercurate (II) followed by colormetric estimation with acidified pararosaniline. However, major limitations of this method<sup>6</sup> include atmospheric oxidation of the dichlorodisulfitomercurate (II) solution at room temperature, the necessity for using relatively high concentrations of toxic mercuric chloride and the presence of interfering impurities in the pararosaniline dye. Improvements to this technique have included replacement of the tetrachloromercurate (II) adsorber with formaldehyde<sup>6</sup>, ethanedial<sup>7</sup>, and oxal-dihydroxamic<sup>8</sup>.

In recent years chemical gas sensors based upon the use of optical waveguides have been developed, and practical devices for ammonia detection in the parts per billion fabricated<sup>9</sup>. These devices consisted of a glass tube or rod coated with an organic dye. Interaction of the gas to be detected with the coating gave rise to modification of either the film adsorption coefficient or its refractive index. Such changes were detected by changes in the flux of internally multiply reflected light within the tube. The simplicity and ease of construction for such devices has encouraged us to develop an optical waveguide chemical sensor for SO<sub>2</sub>. In this communication we show that organophosphine transition metal complexes can serve as sensitive, selective and reversible coatings for the optical detection of SO<sub>2</sub> in the parts per million concentration range.

### Experimental

Apparatus. Figures 1 and 2 show schematics for the optical waveguide detection system. Sulfur dioxide (1000ppm, Matheson) and nitrogen were mixed to give SO<sub>2</sub> concentrations between 1000 and 100ppm, using a net flow rate through the optical waveguide assembly of 100ml/min. Direct illumination was

provided from an unfiltered 12V, 100 watt tungsten halogen lamp focused directly into the end of 4mm OD, 100cm long glass tube, the outside surface of which was initially spray coated with a 50µg/ml solution of  $\text{Cu}(\text{PBz}_3)_2\text{SPh}$ . Direct illumination down the open end of this tube was avoided via use of an opaque epoxy. This resulted in multiple reflections occurring along the glass walls of the tube. An EG&G VT1113B p on n silicon diode and an operational amplifier transimpedance circuit were used as the photodetection/amplification system. A voltage signal corresponding to variations in light intensity incident at the silicon photodiode was then traced using a Houston X-Y recorder.

Synthetic Procedures. Reagent grade chemicals copper (II) acetate, manganese (II) iodide, benzenethiol and tribenzylphosphine (Alfa) were used without further purification. The copper complex was prepared using standard Schlenk techniques under a nitrogen atmosphere.

$(\text{CuSPh})_n^{10}$ : Benzenethiol (3.7ml in 60ml of methanol) was added to cupric acetate (3.6g in 30ml distilled water) with stirring. A yellow precipitate formed immediately which was filtered and thoroughly washed with  $\text{H}_2\text{O}$ ,  $\text{CH}_3\text{OH}$ , benzene and ether. The precipitate was then dried overnight under vacuum.

$\text{Cu}(\text{PBz})_2\text{SPh}^{10}$ : Polymeric cuprous mercaptide (1.54g) prepared in the previous step was suspended in 30ml of chloroform. Tribenzyl phosphine (5.0g) was then added to the  $(\text{CuSPh})_n$ -chloroform mixture. Within 30 minutes following phosphine addition the chloroform solution became clear and colorless. Precipitation of  $\text{Cu}(\text{PBz}_3)_2\text{SPh}$  complex was accomplished by addition of 200ml of n-heptane. Fluffy white crystals were collected, filtered and washed with n-heptane followed by recrystallization from  $\text{CHCl}_3$ /n-heptane.

#### Results and Discussion

When light flux is internally reflected at the interface of an optically dense transparent medium (the walls of a glass tube) and a medium of lower

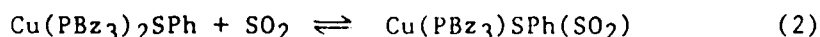
optical density (air), at angles greater than the critical angle, total internal reflection of the light flux can occur. For the glass-air interface Snell's Law predicts that the critical angle for total internal reflection is  $\approx 42^\circ$ . Superposition of reflected waves with incoming waves can result in formation of a non-propagating standing wave at the glass-air interface. The non-propagating standing wave (termed an evanescent wave) exhibits a slowly decaying electric field whose amplitude exponentially decreases with distance from the glass-air interface. It is known that the evanescent wave can be a sensitive probe of this interface<sup>11</sup> and, in principle, could be used to probe appropriately coated glass substrates which might be chemically sensitive to a given gaseous species. If  $\text{SO}_2$  were to chemically react with a coated glass substrate, thereby producing some modification of the films adsorption coefficient or refractive index, then changes in evanescent wave intensity might be expected related to  $\text{SO}_2$  concentration. For multiple reflections at glass-film interface the reflection coefficient,  $R$ , is given by<sup>12</sup>:

$$R^N = (1 - \alpha d e)^N \approx 1 - \alpha N d e \quad (1)$$

where  $\alpha$  is the film adsorption coefficient and  $d e$  is the effective film thickness. For  $N$  multiple reflections, small changes in either  $d e$  or  $\alpha$  can be amplified  $N$  times, enabling small changes in the films adsorption coefficient to be detected.

Ideally, the film coating present on the outside wall of the glass tube should possess high sensitivity, good selectivity, a fast response time, and be chemically reversible so that baseline recovery times are rapid. One class of compounds giving rise to color changes following adsorption of small molecules such as  $\text{O}_2$ ,  $\text{NO}$  or  $\text{SO}_2$  are organophosphine-transition metal complexes. There are many examples of organophosphine-transition metal complexes that bind  $\text{SO}_2$ <sup>10</sup>. One complex that undergoes a color change (white to yellow-orange) and reversibly

binds  $\text{SO}_2$  is  $\text{Cu}(\text{PBz}_3)_2\text{SPh}$  (bis(tribenzylphosphine)copper (II) thiophenolate). This complex exhibits rapid equilibria and good chemical reversibility towards  $\text{SO}_2$ <sup>10</sup> via:



The extent with which the above reaction can be directed to the right side of equation 2 is determined by the basicity of the phosphine ligand and the temperature<sup>10</sup>. Thus, by varying ligand substituents at the phosphorus and the temperature, the response time, sensitivity and recovery time of a  $\text{Cu}(\text{PR}_3)_2\text{SPh}$  coating can be manipulated. As a consequence, this complex appeared an ideal substrate for incorporation into the optical waveguide shown schematically in Figure 2.

Preliminary work to identify adsorption wavelengths over which this complex might be responsive when exposed to  $\text{SO}_2$  was performed by spraying a chloroform solution of  $\approx 100\mu\text{g}$   $\text{Cu}(\text{PBz}_3)_2\text{SPh}/\text{ml}$  onto two glass slides followed by placing them into separate sealed quartz cuvettes. Pure  $\text{SO}_2$  was then introduced into one cuvette wherein the  $\text{Cu}(\text{PBz}_3)_2\text{SPh}$  coating immediately turned yellow-orange. Using the second cuvette without  $\text{SO}_2$  as a blank, the adsorption spectrum in Figure 3 was obtained. The complex did not adsorb between 600 and 1000nm, but sharply increased adsorption was observed at wavelengths shorter than 500nm. The optical light source used was a focused 100W tungsten halide lamp and a blue enhanced PIN silicon photodiode with an integral infrared filter for detecting adsorption changes associated with  $\text{SO}_2$  reaction at the  $\text{Cu}(\text{PBz}_3)_2\text{SPh}$  coating. Figure 4 shows the optical waveguide response towards 1000ppm  $\text{SO}_2$  at room temperature. The system reached 90% of maximum response in  $\approx 6$  min. However, at room temperature full recovery of the signal back to the baseline was not observed. A similar response (i.e. 6 min. response time to 90% maximum signal and only partial baseline recovery) was observed when 500ppm  $\text{SO}_2$  was

passed over the waveguide detector (Figure 5) with the output signal being proportionally smaller.

To increase reversibility towards  $\text{SO}_2$  the detector assembly was heated to  $60^\circ\text{C}$ . Previous work with  $\text{Cu}(\text{PBz}_3)\text{SPh}(\text{SO}_2)$  has shown increased  $\text{SO}_2$  dissociation at higher temperatures<sup>10</sup>. Figure 6 shows the response of this optical waveguide sensor to respectively 1000, 500 and 100ppm  $\text{SO}_2$  at  $60^\circ\text{C}$ . These results show increased response time (90% maximum = 5 min.) and complete reversibility. A plot of  $\text{SO}_2$  concentration (ppm) as a function of the output voltage from the operational amplifier/photodiode detector circuit is shown in Figure 7. These results show linearity between detector response and  $\text{SO}_2$  concentration levels below  $\approx 750\text{ppm}$ . Above this value the detector response appeared to saturate. These results showed that detector response towards  $\text{SO}_2$  was linear below 500ppm  $\text{SO}_2$  with the line passing through the origin. Present detector limitations appear to be more related to optical focusing and electronics issues rather than inherent to the  $\text{SO}_2$  sensitive coating. Preliminary work performed using  $\text{SO}_2$  flow rates  $\approx 0.05\text{ml/min}$ . of 1000ppm  $\text{SO}_2$  in nitrogen and 100ml/min. nitrogen, gave a detectable signal to noise response for the estimated 0.5ppm  $\text{SO}_2$  present. These results suggest the present unoptimized optical  $\text{SO}_2$  detector may be capable of  $\text{SO}_2$  detection in the sub-ppm region. We have also evaluated the  $\text{Cu}(\text{PBz}_3)_2\text{SPh}$  coated optical waveguide device for selectivity. No response was found when exposed to respectively 5000ppm  $\text{CO}$ ,  $\text{CO}_2$ ,  $\text{NH}_3$ ,  $\text{Cl}_2$  and  $\text{NO}_2$ .

### Conclusions

The results presented here show that  $\text{Cu}(\text{PBz}_3)_2\text{SPh}$  coated multiple-reflecting optical waveguide devices can be used as effective reversible  $\text{SO}_2$  sensors. Most of the present limitations of this device are not inherent to the sensitive surface selected but more related to drift in the light source used and electronic noise.

### Acknowledgement

This work was supported in part by the Office of Naval Research.

### References

1. Cowling, E. B., Linthurst, R. A., Bioscience, 31(9), pp. 649-654 (1981).
2. Cowling, E. B., Environ. Sci., Technol., 16(2), pp. 110A-123A (1982).
3. Webster, B. D., U.S. Dept. Agric., Agric. Res. Serv., #24 (1971).
4. Calabrese, E. J., "Pollutants and High Risk Groups", Interscience, New York (1976).
5. West, P., Gaeke, G., Anal. Chem., 1816-1819 (1956).
6. Dasgupta, P. K., DeCesare, K., and Ullrey, J. C., Anal. Chem., 52, 1912-1922 (1980).
7. Irgum, K. and Lindgen, M., Anal. Chem., 57, 1330 (1985).
8. Paul, K. R. and Gupta, V. K., Atmospheric Environment, 17, 1773-1777 (1983).
9. Giuliani, J. F., Wohltjen, H. and Jarvis, N. L., Optics Lett., 8, 54-56 (1983).
10. Eller, P. G. and Kubas, G. J., J. Am. Chem. Soc., 99(13), pp. 4346-4351 (1977).
11. Harrick, N. J., "Internal Reflection Spectroscopy", Interscience Publ., Div. of J. Wiley and Sons, New York, 1967.
12. Giuliani, J. F., Bey, Jr., P. P., Wohltjen, H., Snow, A. and Jarvis, N. L. in "Proceedings of the International Conference on Solid-State Sensors and Actuators-Transducers '85", Boston MA. pp. 74-76, June 11-14, 1985.



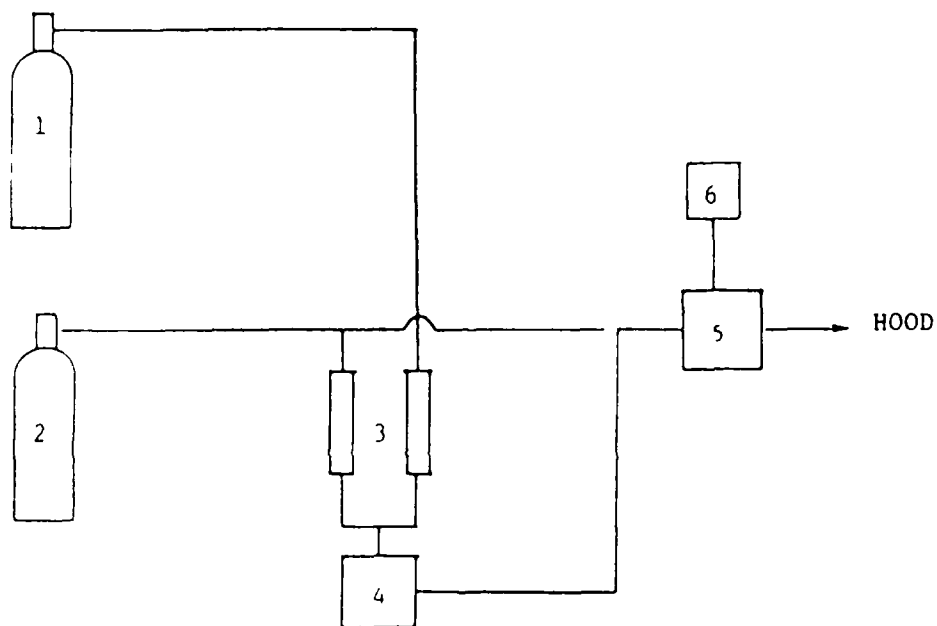


Figure 1. Schematic for experimental setup for  $\text{SO}_2$  detection.  
 (1)  $\text{SO}_2$  source, 1000ppm  $\text{SO}_2$ , (2)  $\text{N}_2$  source,  
 (3) flowmeters, (4) gas mixing chamber,  
 (5) optical wave guide chemical sensor,  
 (6) amplification electronics and X-Y recorder

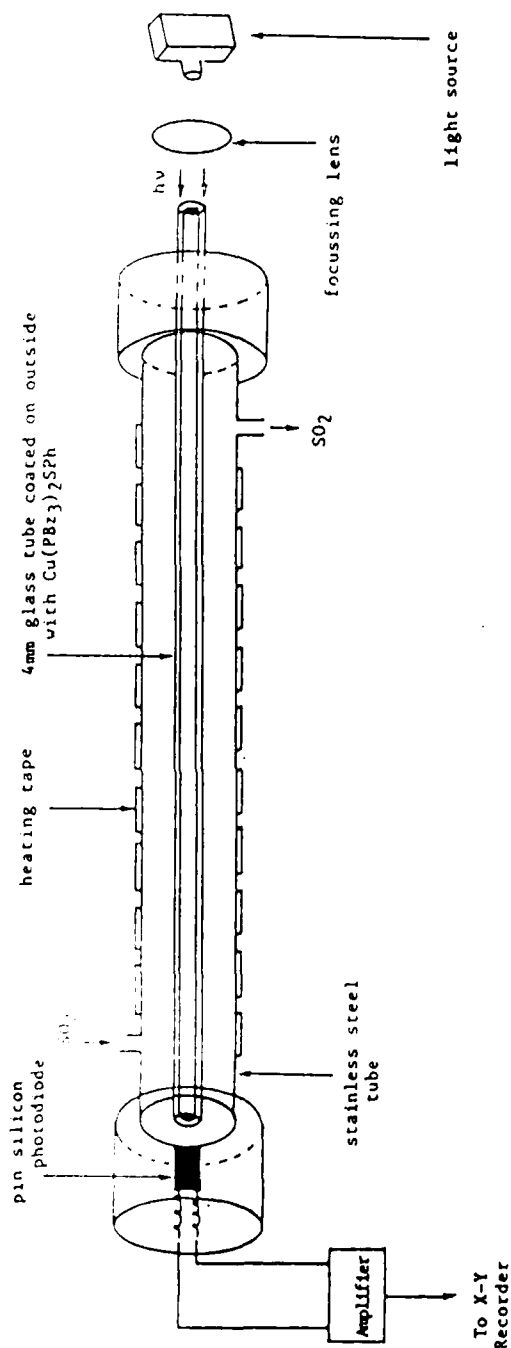


Figure 2. Schematic diagram for guided wavelength optical  $\text{SO}_2$  detector.

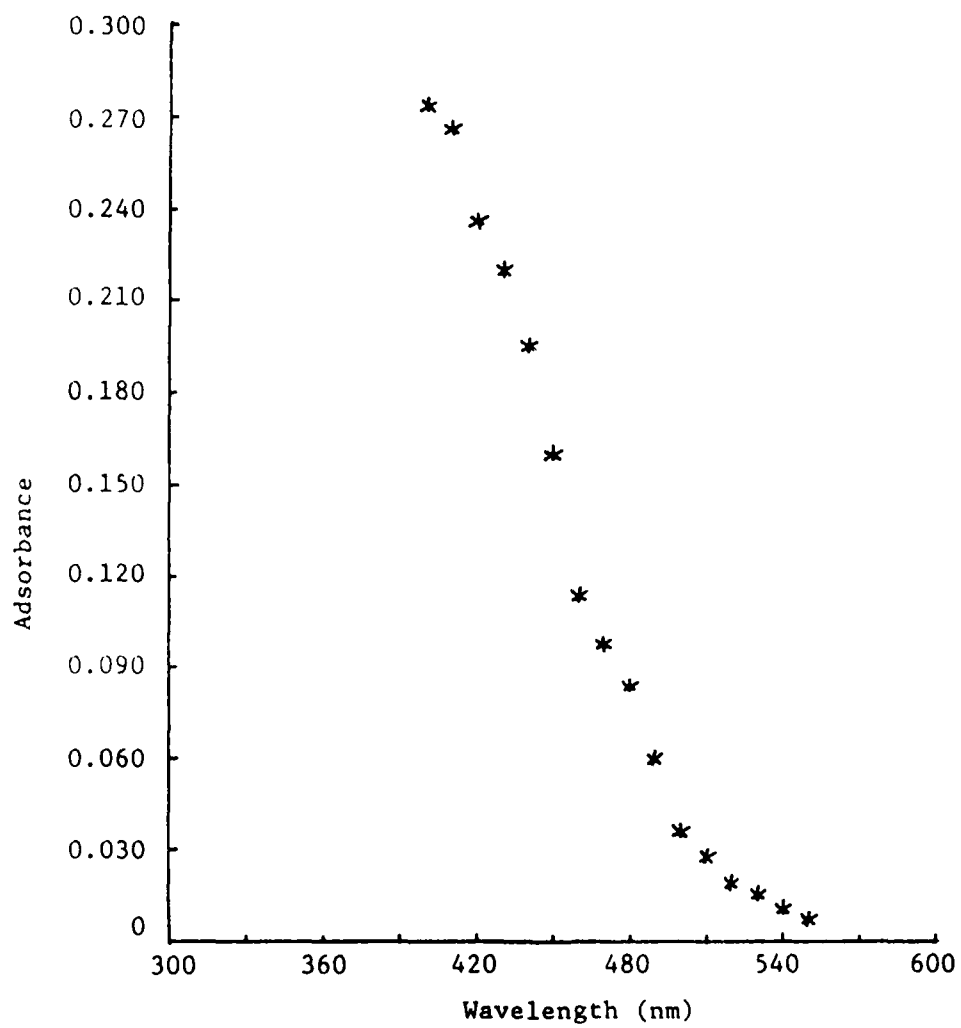


Figure 3. Adsorbance spectra for  $\text{Cu}(\text{PBz}_3)_2\text{SPh}(\text{SO}_2)$  sprayed onto a glass substrate.

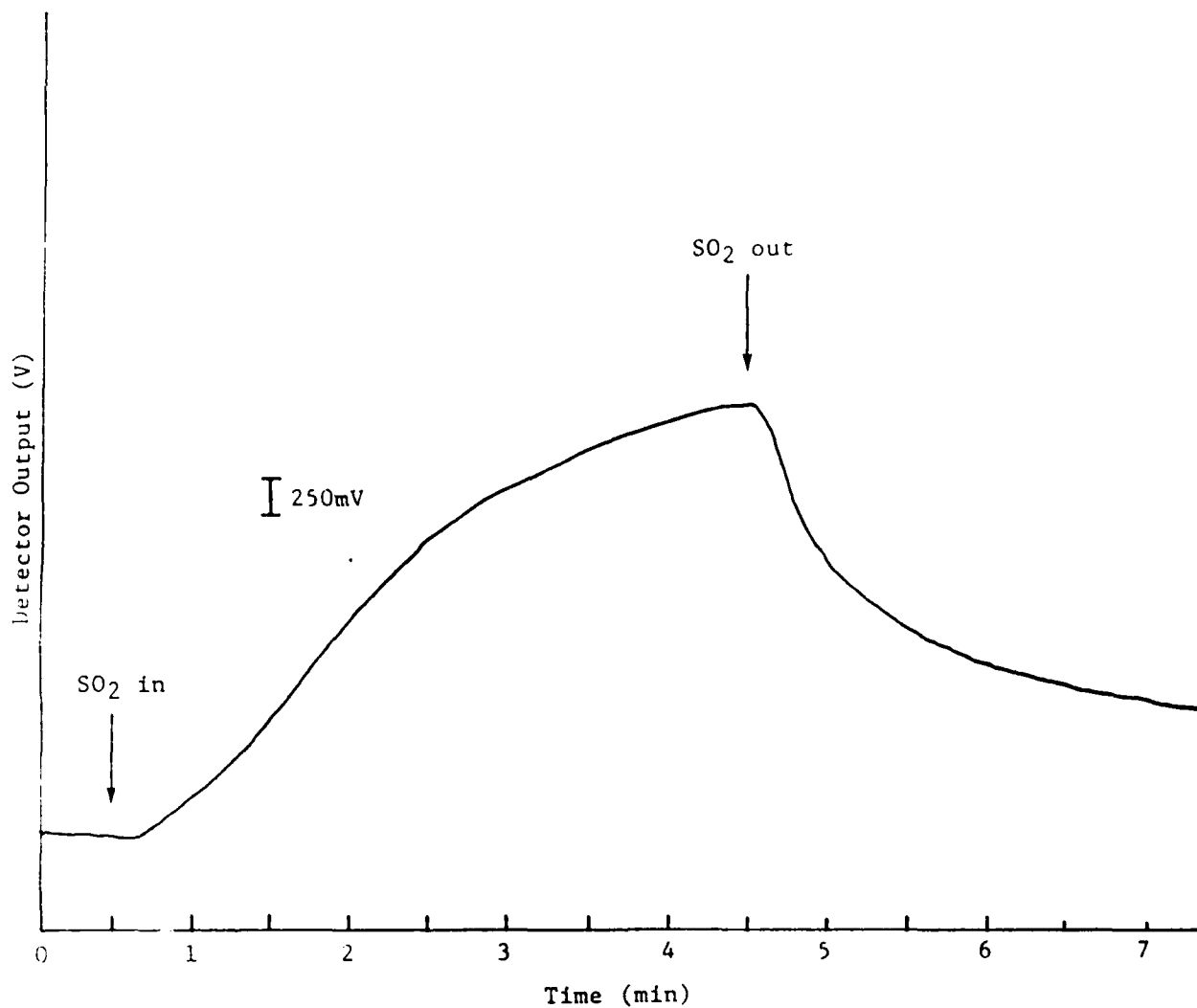


Figure 4. Optical waveguide chemical sensor response to 1000ppm SO<sub>2</sub> at 25°C.

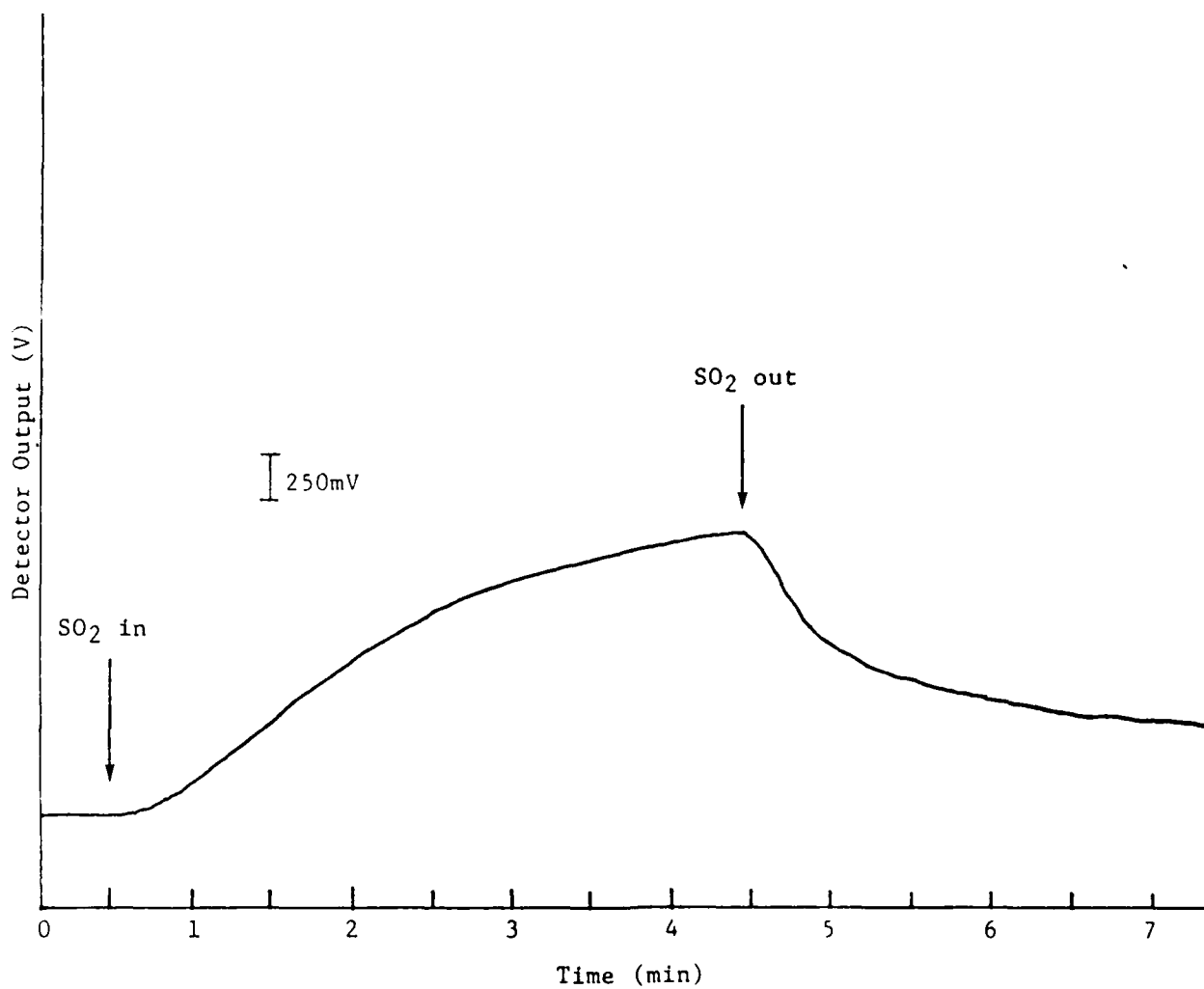


Figure 5. Optical waveguide chemical sensor response to 500ppm SO<sub>2</sub> at 85°C.

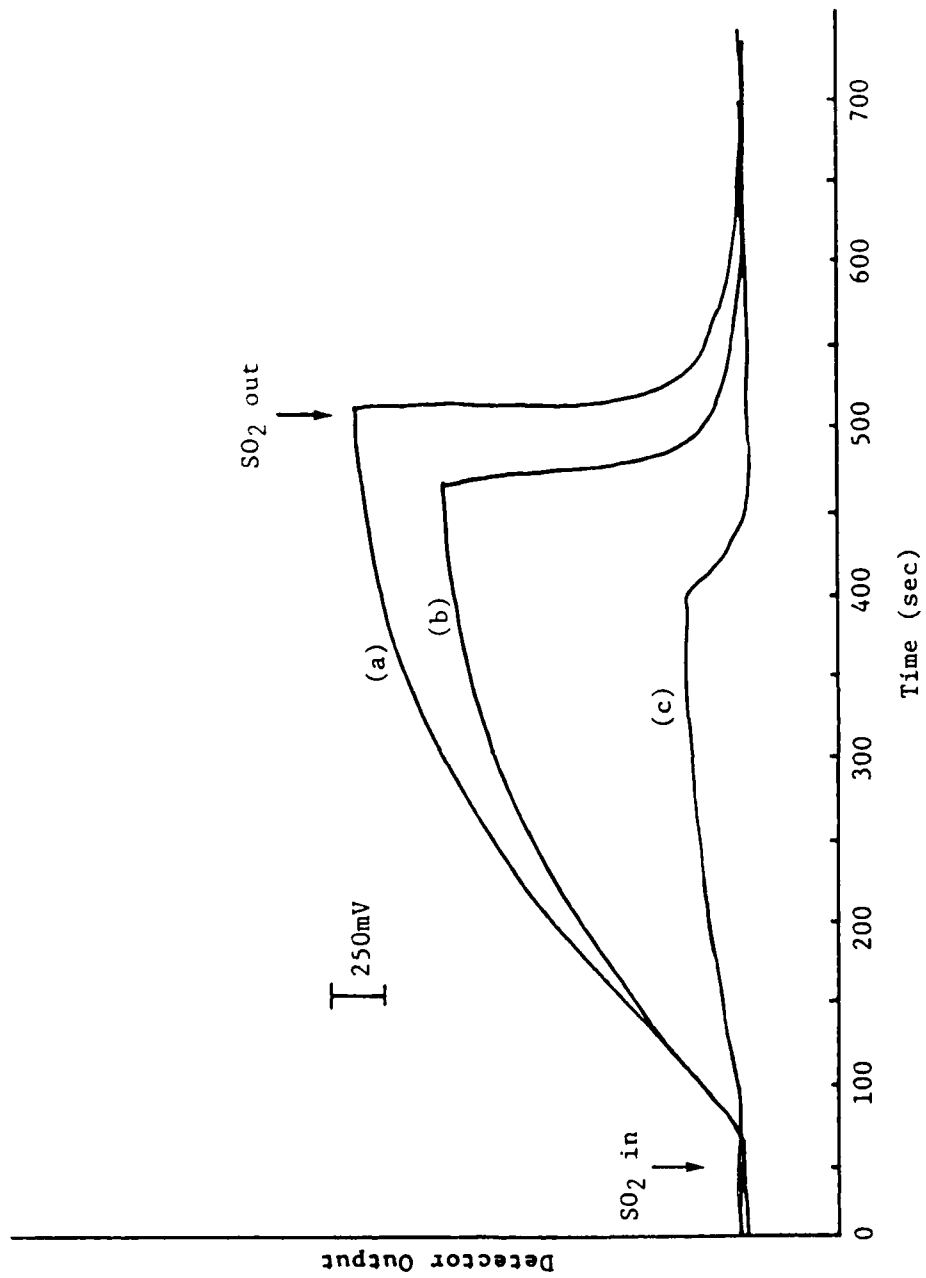


Figure 6. Optical waveguide chemical sensor response to SO<sub>2</sub>, (a) 1000ppm, (b) 500ppm, (c) 100ppm at 60°C.

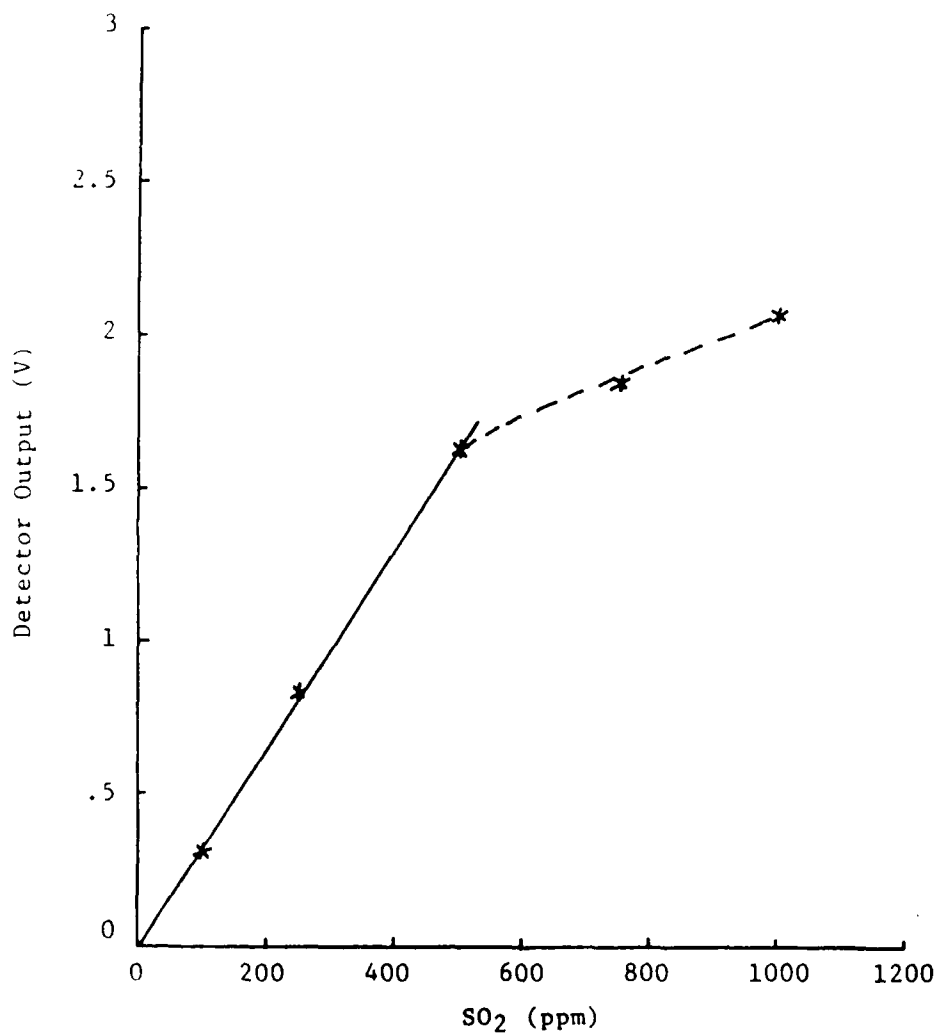


Figure 7. Plot of SO<sub>2</sub> concentration as a function of detector output voltage at 60°C.

END

DATED

FILM

8-88

Dtic